TRANSFORMATION ELECTROMAGNETICS/OPTICS FOR DESIGNING AND SCANNING ANTENNA ARRAYS

A Dissertation
Submitted to the Graduate Faculty
of the
North Dakota State University
of Agriculture and Applied Science

By

Dipankar Mitra

In Partial Fulfillment of the Requirements
for the Degree of
DOCTOR OF PHILOSOPHY

Major Department:
Electrical and Computer Engineering

May 2021

Fargo, North Dakota

North Dakota State University
Graduate School

Title

TRANSFORMATION ELECTROMAGNETICS/OPTICS FOR DESIGNING AND SCANNING ANTENNA ARRAYS

By

Dipankar Mitra

The Supervisory Committee certifies that this ***disquisition*** complies with North Dakota State University's regulations and meets the accepted standards for the degree of

DOCTOR OF PHILOSOPHY

SUPERVISORY COMMITTEE:

Benjamin D. Braaten, Ph.D.
Chair

Jacob Glower, Ph.D.

Ivan T. Lima, Ph.D.

Jeffery W. Allen, Ph.D.

Mijia Yang, Ph.D.

Approved:

May 18, 2021
Date

Benjamin D. Braaten, Ph.D.
Department Chair

ABSTRACT

Recent developments in engineered electromagnetic materials, also known as metamaterials paved the way for new design approaches of unique and incomprehensible electromagnetic devices and structures using electromagnetic properties which are usually not available in nature. By taking advantage of Maxwell's equation's "form-invariance" under coordinate transformations, lately, a coordinate transformation-based approach was introduced to manipulate electromagnetic waves at will, which resulted in a non-homogeneous, anisotropic transformation media dictated by the coordinate transformation. This design approach is known as "transformation electromagnetics/optics (TE/TO)" and has steered many unconventional and seemingly-impossible unique electromagnetic devices such as, the electromagnetic invisibility cloak.

The concepts of TE/TO can be extended to a region containing electromagnetic sources, which is known as source transformations. This research focused on the understanding of the theoretical and mathematical foundation of the "transformation electromagnetics/optics" and based on the understanding of the TE/TO concepts, a phased array antenna with new elements where antenna performance is a function of structural and mechanical constraints is proposed using source transformations, where each antenna element is "pinwheel" shaped antenna element transformed from a dipole element in free-space using appropriate coordinate transformations. The transformed materials are derived and through numerical simulations the radiation properties of the proposed array are demonstrated. It is anticipated that the proposed complex-geometry array will have great potential for future applications in structurally integrated and conformal arrays for wireless communications, radars, and sensing.

Additionally, the TE/TO technique is employed to design a TO-based beam-steerer which enables beam-scanning with a *single* antenna element and an *antenna array* without using phase control circuits. The proposed beam-steerer is a TE/TO-based non-homogeneous, anisotropic material shell theoretically computed using coordinate transformations. Through full-wave simulations the beam-scanning performances of the TO-based beam-rotator was demonstrated and validated. Since the practical metamaterial implementation involves losses, numerical simulations are performed incorporating losses to the derived material parameters. While currently, numerical verifications are provided, in practice, these TO-approaches will require actively tunable material parameters. Significant advancements have been made by the material scientists to design tunable materials using different approaches, which could enable the implementation of the TO-based approach practically.

ACKNOWLEDGMENTS

First, I would like to thank my advisor, Prof. Benjamin D. Braaten, for his continuous support, patience, and guidance in completing this research. He always supported me by providing intriguing fundamental thoughts for this research. Without his guidance, I would have never been able to complete this work. I also thank him for accepting me as his graduate student in a very critical phase of my graduate studies when I was looking for an advisor aligned to my research interest and also someone who can help and guide me inside and outside the lab.

I would like to extend my gratitude and thankfulness to Dr. Jeffery W. Allen from the U.S. Air Force Research Laboratory (AFRL) for introducing and guiding me through the beautiful concepts of source transformations. His constant support and guidance has been an integral part for the success of this research. I also thank him for agreeing to serve as a member of my supervisory committee.

I would like to also thank my other committee members, Prof. Jacob Glower, Prof. Ivan T. Lima, and Prof. Mijia Yang, for their continuous encouragement and support. They have taught me many things and helped me in overcoming any difficulties I had along the way in this research, specifically, their inputs during my Ph.D. preliminary defense were valuable and very helpful to further continue this research.

I also thank Prof. Indranil Sen Gupta from the Dept. of Mathematics, NDSU for guiding me through the mathematical background related to “transformation optics”, specifically, for the concepts related to tensors and covariant notations. I also would like to thank Pratyush Mishra from the same dept. for helping me through derivations related to TE/TO.

I thank my colleagues from the “Applied Electromagnetics Lab”, NDSU for their constant support and stimulating questions, which helped me to dive deeper into this research. I also want

to thank Prof. Sayan Roy from the South Dakota School of Mines and Tech. (SDSMT) for inviting me to the EE Fall Graduate Seminar Series and thus providing me a great platform to discuss and share my research.

I acknowledge the U.S. Air Force Research Laboratory (AFRL) for supporting my research financially and also the Graduate School of the North Dakota State University for providing financial support partly for this project through the 2020 Doctoral Dissertation Fellowship Award.

Finally, I would like to thank my parents, two loving elder sisters, my beautiful wife and son. I also would like to thank my friends in Fargo, who I call them my family here in USA for their constant support, help and guidance in my good times and bad times.

DEDICATION

To my mother, *Jhinu Mitra*, and my father, *Sadhan Mitra*, for their constant support and belief in me and also understanding the choices I made so far in my life!

To my beautiful and lovely wife, *Trisha*, who has been a constant support and strength during my Ph.D. journey and also for her love, care and patience to deal with me *24X7*, not an easy job, I guess!

To my son, *Shlok*, for making me realize that there is more beautiful things outside a research lab, which are equally important and need to be cherished and lived!

To my *late* mother-in-law, *Panna Chowdhury*, who was a great source of positivity and motivation!

To *Jolly Pishi*, who is a constant source of inspirations and learnings in many ways!

To *Swami Vivekananda*, I consider him my spiritual guru. He changed my life (and so many across this globe!) through his work, words and teachings. I firmly believe in his words and teachings, though barely could implement his teachings in my day-to-day life!

TABLE OF CONTENTS

LIST OF TABLES

LIST OF FIGURES

1. INTRODUCTION

Electromagnetism is a unique and profound branch of physics, which is a cause and result of electromagnetic fields due to different potential gradients or fields in different mediums. Being one of the fundamental forces, the electromagnetism has endless consequences from electrodynamics to quantum mechanics. In the year of 1873, legendary mathematical physicist Maxwell presented a set of differential equations in his book, "A Treatise on Electricity and Magnetism" [1, 2], involving oscillating electric and magnetic fields to describe propagation of electromagnetic waves in different mediums and later, those set of differential equations established the foundation of applied electromagnetics. Later, German scientist Hertz introduced the first wireless communication system by using cylindrical conductor and circular loops, which are basically a dipole antenna and loop antennas, respectively [3]. Consequently, an eminent scientist from India, J. C. Bose demonstrated the phenomenon of wireless communication within short range [4]. During the same time, Nikola Tesla developed few new techniques for wireless power transfer over long distances [5]. In 1902, for the first time, Marconi, a scientist from Italy demonstrated transatlantic wireless communication [6], which later got him the Nobel Prize in physics in 1909. Later, German physicist Braun introduced phased array antenna systems by incorporating time delays in the antenna elements to control the radiation of the antenna to a guided direction, which revolutionized the wireless communication systems in manifolds [3]. This is how the modern day wireless communication systems have evolved.

The fundamental basis of modern-day wireless communications is antennas and RF-microwave structures and the performances of the antennas and RF-microwave structures are significantly dependent on substrate material. The permittivity (ε) and permeability (μ) of the material has a huge impact on the antenna performance. If the ε and μ of the material can be

increased, it would be possible to achieve more bandwidth in a smaller volume [7]. The ε and μ can also be varied throughout its volume to focus waves or beam in desired direction [8]. Lately, a new field "metamaterials" has emerged and attained great deal of attention from the scientific community. The word "metamaterial" consists of two parts, the first part is a Greek word "meta" which means "beyond", the second part relates to "matter". A metamaterial is artificially engineered material that has properties which are not found in naturally available materials. A metamaterial can also be defined as a microstructured material that is shaped to achieve a desired either acoustic or electromagnetic wave-matter interaction [8]. Another definition from DARPA: "A metamaterial is an engineered composite that exhibits superior properties not observed in nature or in the constituent materials. The superior properties of a metamaterial are a result of their engineered constructs" [9]. Metamaterials derive their unique properties from their newly designed structures, not from their inherent or base materials.

There are natural materials available which demonstrate either a negative electric response, such as, plasma or a negative magnetic response, such as magnetically resonant crystals [8]. The effective refractive index, $\eta = \sqrt{\mu\varepsilon}$ needs to be real for the electromagnetic wave to propagate through any material. For the refractive index to be real, either ε or μ can not be negative, otherwise $\eta = \sqrt{\mu\varepsilon}$ would be imaginary. If both ε and μ are negative, the refractive index will be again real and waves can propagate, however it is essential to choose a negative index. V. G. Veselago first predicted this behavior of materials with simultaneously negative ε and μ [10]. These materials are often referred as "left-handed" materials. Smith et al [11] first reported that it is possible to produce negative index materials and it is shown that the phase-velocity is negative in these materials and simple Snell's law experiment showed that refraction occurs in opposite direction [12]. Metamaterials are naturally anisotropic and non-homogeneous.

Metamaterials and specialized complex electromagnetic materials opened the door to several new electromagnetic device techniques that were previously conceived to be very challenging. One of the very popular methods to design complex and unique electromagnetic devices and structures is transformation electromagnetics/optics (TE/TO) introduced by Pendry *et al* [13] and Leonhardt [14] in 2006, which provides a very strong and powerful tool to scientists and engineers to manipulate electromagnetic fields as never before. There is probably no other topic in recent times in the electromagnetic and optical community that has received as much attention as TE/TO. The TE/TO offers a completely new methodology of systematic design for unconventional electromagnetic devices using an appropriate coordinate transformation. It is based on a key assumption of the form-invariance of Maxwell's equations under coordinate transformations [15-17]. The underlying concept of the TE/TO technique and form-invariance of Maxwell's equations under coordinate transformations are discussed in detail in chapter 2.

The designed material properties can be derived by beginning with the familiar form of Maxwell's equations and can be adopted for arbitrary and complex geometries using the same basic approach [18]. Demonstration of two-dimensional invisibility cloaks in the microwave frequencies [19] using the state-of-the-art materials has basically stimulated overall research on designing novel devices using the TE/TO technique and has been progressing significantly. The invisibility cloak is followed by design of many electromagnetic passive devices using this approach, such as the optical cloak with reduced set of material parameters [20], all-dielectric cloak in the THz regime [21], cloaking at a distance [22], two-dimensional cloaks with arbitrary geometries [23], illusion optics [24], an anti-cloak [25], scatterers and absorbers leading to superscatterer [26], and super absorber [27] respectively, beam shifters and splitters [28], beam benders/expanders [29], refelectionless waveguide bends [30], expanding a narrow slit into a large

window [31], polarization splitter and polarization rotator [32], and flat focusing lens [33] etc. The TE/TO technique can be also be applied to the sources (e.g., current and charge distributions), where the sources will be transformed into a new current distribution, but exactly behaving the same way. This technique is known as source transformation, first explored by Luo *et al* [34]. Luo *et al* transformed a source in a way that a dipole current distribution looks like a completely different one, but exactly behaving like a dipole antenna. This process also includes proper material compensation using the same transformation.

A phased array antenna has tremendous possibilities in future wireless communication applications, such as device-to-device, vehicle ad-hoc network, and wireless body area networks (WBAN), and has achieved remarkable attention from the scientists and researchers around the globe due to its ability of altering the direction of the radiation pattern, consequently, the direction of a transmitted signal without tangibly moving the antenna elements. This technique is known as beam-steering or beam-scanning. This can be accomplished by rotating the antenna elements of the antenna array or changing the relative phases of the radio-frequency (RF) signals driving the elements. Phased array antenna scanning often poses challenges as it involves synthesis of multiple antenna elements and integration of phase control circuitry, which includes solid-state-phase shifters [35] and beam-forming networks [36], to guide or scan the radiation beam in a desired direction. Scientists and researchers from all over the globe adopted and proposed different design and synthesis approach for conformal array designs, such as orthogonal projections [37], adaptive array method [38], genetic algorithms [39], and particle swarm optimization [40]. Howbeit, all these approaches require different algorithms for different sizes and shapes of conformal arrays, makes it very difficult for an optimum design approach for a conformal design for any arbitrary and complex surfaces.

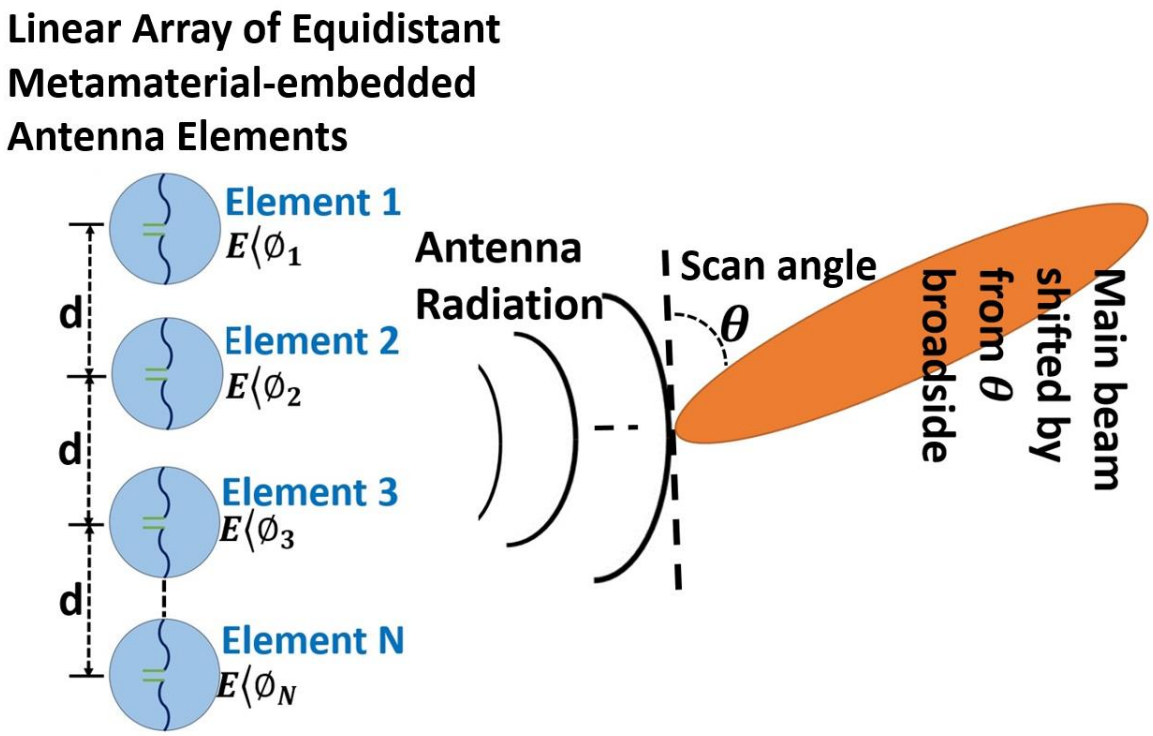

Figure 1.1. An n-element linear phased array antenna with new elements embedded in a metamaterial shell using transformation electromagnetics/optics (TE/TO) approach.

In this dissertation, the technique of source transformations, basically a transformation electromagnetics/optics approach, has been employed to design a linear array, where each individual antenna element is transformed from a single dipole element in free-space using a coordinate transformation and embedded in a complex electromagnetic media prescribed by the transformation designed using the TE/TO technique, as shown in Figure 1.1. The finite element method based full-wave simulations via COMSOL Multiphysics ® are used to numerically analyze and demonstrate the performance of the proposed TO-based antenna array for phased array scanning. The proposed array will have future applications in structurally integrated and conformal phased array antennas for wireless communications, radars, and sensing where antenna performance is a function of structural and mechanical restraints. Furthermore, transformation electromagnetics/optics (TE/TO) has been adopted to realize a non-homogeneous, anisotropic material-embedded beam-steerer using both a *single* antenna element and an antenna *array* without

phase control circuitry. Through theory and validation with numerical simulations using COMSOL Multiphysics ® it is shown that beam-scanning can be attained in a desired direction by enclosing a single antenna element with the transformation media designed using the TE/TO approach. This same technique is applied to an antenna array with fixed voltages and phases and the enclosed array is scanned and the theory is validated through full-wave simulations. The proposed methods have applications in scanning for wireless communications, radars, beam-forming, and steering.

Initially though this thesis focuses on the background and the underlying concepts of the transformation electromagnetics/optics approach with detailed derivations of Maxwell's equations in covariant notations and proof of the form-invariance of Maxwell's equation under coordinate transformations including thorough and complete derivations in order to provide the reader with the necessary background information. These are discussed in chapter 2 of the dissertation. Moreover, along with our collaborators in U.S. Air Force Research Lab (AFRL), pertinent relevant TE/TO devices examples, such as space compression, beam-shifter, and electromagnetic cloaking etc. are explored. The examples are discussed and explained in an instructive manner with detailed constitutive material parameters derivations and thorough numerical simulation methods in COMSOL Multiphysics. These TE/TO examples are detailed in chapter 3 of the dissertation.

2. TRANSFORMATION ELECTROMAGNETICS/OPTICS (TE/TO) AND FORM-INVARIANCE OF MAXWELL'S EQUATIONS

The recently introduced transformation electromagnetics/optics (TE/TO) technique [13, 14] has revolutionized the developments of metamaterials and devices based on these metamaterials. The TE/TO technique provides extraordinary flexibility of designing electromagnetic devices using an appropriate coordinate transformation method. This also provides an exceptional avenue for registering unique and novel wave-material interactions. The TE/TO design approach is based on the key assumption of the form-invariance of Maxwell's equations under coordinate transformations [15, 16]. This will be explained later in section 2.4. Another observation is the interpretation of the material parameters (ε, μ) in the transformed coordinate system as a set of material parameters in the original coordinate system [41]. Now, consider the time-domain Maxwell's curl equations:

$$\nabla \times \boldsymbol{E} = -j\omega\boldsymbol{\mu H}, \tag{2.1}$$

$$\nabla \times \boldsymbol{H} = j\omega\boldsymbol{\varepsilon E}, \tag{2.2}$$

where **E** and **H** are associated electric fields and magnetic fields in a simple coordinate system (Cartesian, cylindrical, or spherical coordinates). The divergence equations in the time-domain are:

$$\boldsymbol{B} = \boldsymbol{\mu H}, \tag{2.3}$$

$$\boldsymbol{D} = \boldsymbol{\varepsilon E}, \tag{2.4}$$

where **B** and **D** are electric and magnetic flux densities, respectively and μ and ε are permeability and permittivity, respectively.

Next let assume a Cartesian coordinate system $G(x, y, z)$ to describe the original space and $G'(x', y', z')$ describes the transformed space, as shown in Figure 2.1. The transformation from G to G' can be described by following:

$$x' = x'(x, y, z)$$
$$y' = y'(x, y, z) \tag{2.5}$$
$$z' = z'(x, y, z).$$

Under this new transformed coordinate system, the Maxwell's equations will remain form-invariant as the following [15, 16]:

$$\nabla \times \boldsymbol{E}' = -j\omega \boldsymbol{\mu}' \boldsymbol{H}', \tag{2.6}$$

$$\nabla \times \boldsymbol{H}' = j\omega \boldsymbol{\varepsilon}' \boldsymbol{E}'. \tag{2.7}$$

The material parameters in the transformed coordinate system is given by following [41]:

$$\boldsymbol{\varepsilon}' = \frac{JJT}{\det J} \boldsymbol{\varepsilon}, \tag{2.8}$$

$$\boldsymbol{\mu}' = \frac{JJT}{\det J} \boldsymbol{\mu}, \tag{2.9}$$

where, J is the Jacobian matrix of the transformation from the $G(x, y, z)$ coordinate system to the new coordinate system, $G'(x', y', z')$ and J^T is the transpose of matrix, J. J is defined as [42]:

$$J = \begin{bmatrix} \frac{\partial x'}{\partial x} & \frac{\partial x'}{\partial y} & \frac{\partial x'}{\partial z} \\ \frac{\partial y'}{\partial x} & \frac{\partial y'}{\partial y} & \frac{\partial y'}{\partial z} \\ \frac{\partial z'}{\partial x} & \frac{\partial z'}{\partial y} & \frac{\partial z'}{\partial z} \end{bmatrix}. \tag{2.10}$$

A typical TE/TO technique can be summarized as follows [42] and is illustrated in Figure 2.1:

I. Determine a known wave-material relation in the original coordinate system, i.e., a plane wave or a propagating Gaussian beam.

II. Find the volume of space in the original coordinate system and the associated volume of space in the transformed coordinate system.

III. Define the coordinate transformation you choose to map your original space to that new transformed space.

IV. Compute the material parameters in the new transformed space using equations (2.8) and (2.9).

V. Translate the computed material parameters from the transformed space and acquire the desired material in the original coordinate system.

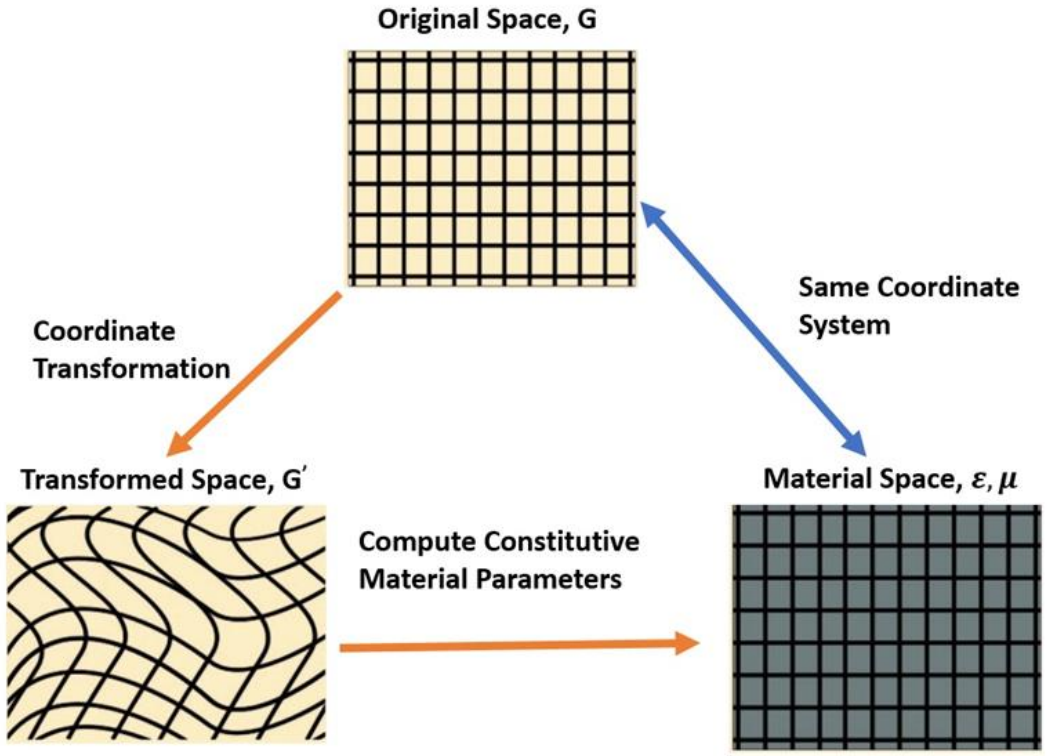

Figure 2.1. A step-by-step explanation of Transformation electromagnetics/optics (TE/TO) technique, where an original space, **G** is transformed into a new space, **G**/, with new material parameters ε, μ [43].

2.1. Jacobian Matrix

The Jacobian matrix is named after the German mathematician Carl Gustav Jacobi (1804 – 1851), who plays an important role in higher dimensional mathematics. The Jacobian matrix is one of the fundamental keys of realizing the transformation of coordinates, as under coordinate transformation it is essential to preserve the area of the original coordinate system in the new transformed coordinate system. Now, considering two set of variables $(x^1, x^2, \ldots\ldots x^n)$ and

$(x'^1, x'^2, \ldots\ldots x'^n)$ which determines the coordinates of a point in $n-$dimensional space in two different coordinate system. The relation between these two set of variables is given by following [44]:

$$x'^i = f^i(x^1, x^2, \ldots..x^n), \quad i = 1, 2, \ldots\ldots\ldots.n. \tag{2.11}$$

Differentiating (2.11) with respect to each of the coordinates x^j, we get:

$$\frac{\partial x'^i}{\partial x^j} = \begin{bmatrix} \frac{\partial x'^1}{\partial x^1} & \frac{\partial x'^1}{\partial x^2} \ldots\ldots & \frac{\partial x'^1}{\partial x^n} \\ \frac{\partial x'^2}{\partial x^1} & \frac{\partial x'^2}{\partial x^2} \ldots\ldots & \frac{\partial x'^2}{\partial x^n} \\ \vdots & \vdots & \vdots \\ \frac{\partial x'^n}{\partial x^1} & \frac{\partial x'^n}{\partial x^2} \ldots\ldots & \frac{\partial x'^n}{\partial x^n} \end{bmatrix}. \tag{2.12}$$

The determinant J of this matrix is called the Jacobian of the transformation:

$$J = \left|\frac{\partial x'^i}{\partial x^j}\right|. \tag{2.13}$$

Equation (2.11) is said to define the coordinate transformation between the two coordinate system x^i and x'^i, $i = 1, 2, 3, \ldots..n$.

Now, let's try to define the Jacobian matrix from the change of variable point of view. Given, Given, an integral of the form: $\int g'(u) f\big(g(u)\big) du$ and the change of variable is $x = g(u)$. That gives us $dx = g'(u)du$. So, we can have:

$$\int g'(u) f\big(g(u)\big) du = \int f(x) dx. \tag{2.14}$$

Since $x = g(u)$, $\frac{dx}{du} = g'(u)$, then we have the following:

$$\int f(x) dx = \int f(g(u)) \frac{dx}{du} du. \tag{2.15}$$

The Jacobian is what generalizes $\frac{dx}{du}$ in the above formula.

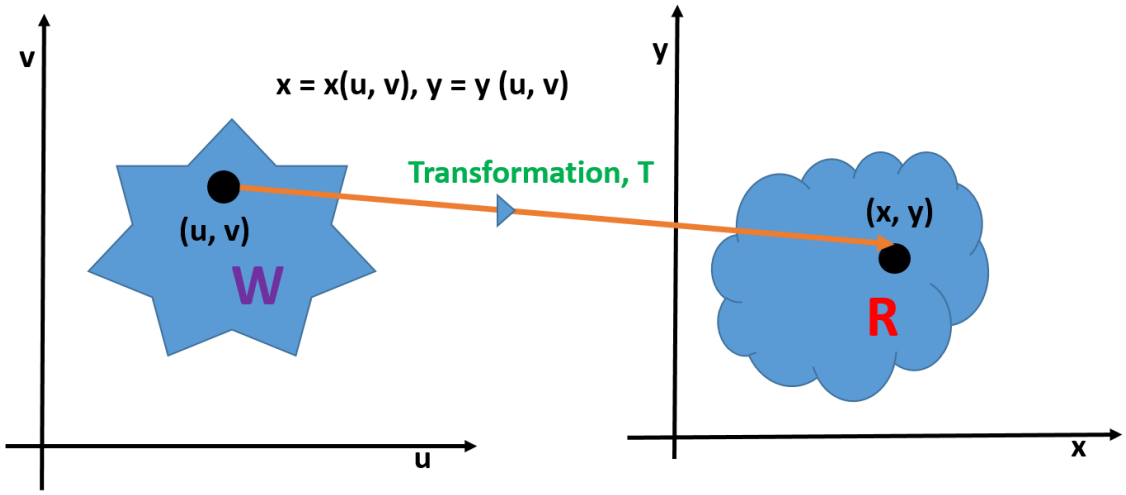

Figure 2.2. A coordinate transformation between region R in the xy-plane and the region V in the uv-plane, where transformation, T (u, v) = (x, y) [45].

Let R denote a region in the xy-plane and W a region in the uv-plane, as shown in Figure 2.2. The change of variable in this case is defined as the transformation from the uv-plane to the xy-plane, given by $T(u,v) = (x,y)$, where, $x = x(u,v)$, $y = y(u,v)$. It is assumed that first order partials of $x = x(u,v)$ and $y = y(u,v)$ are continuous. The transformation, T will map a region W in the uv-plane into another region R into the xy-plane. The region of integration will be divided into small regions, once we apply the double integral. This is done by placing a grid over the region of integration. The region of integration is approximated by little rectangles of area $dA = dudv$, as shown in Figure 2.3a. After the transformation, T is applied, the uv-plane and the grid are also transformed in the region of integration. In the transformed region R, the grids are no longer rectangles, as illustrated in Figure 2.3b. The small rectangle grids transformed into parallelograms and the area dA is not $dxdy$ anymore. We need to find out the new area of the R region in the xy-plane.

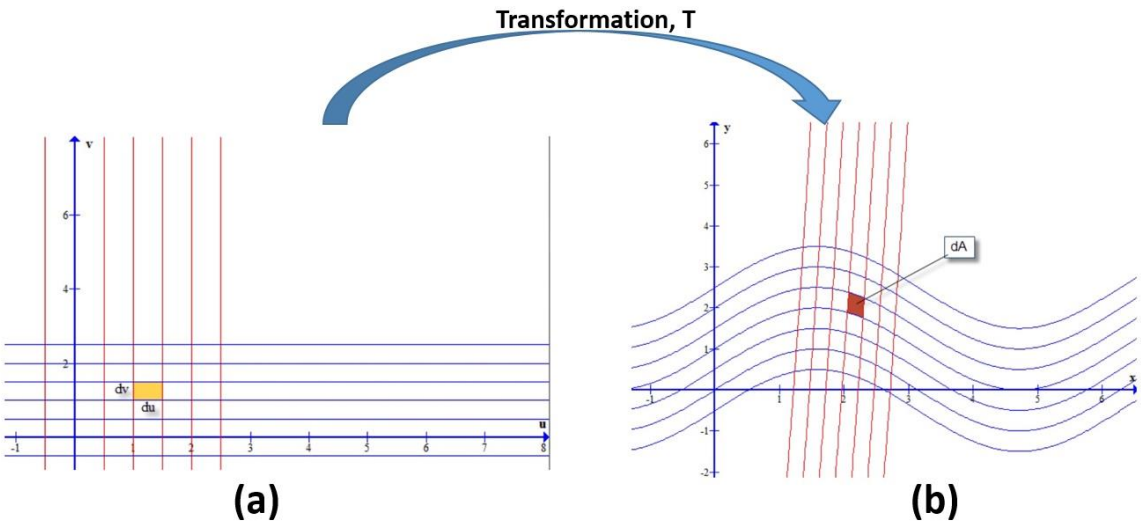

Figure 2.3. The area of the regions before and after transformation (a) Grid in the uv-plane (b) Grid in the xy-plane after the transformation, T is applied [45].

According the differential formula, if $x = x(u, v)$ then, we can write:

$$dx = \frac{\partial x}{\partial u}\, du + \frac{\partial x}{\partial v}\, dv. \tag{2.16}$$

Similarly, if $y = y(u, v)$ then

$$dy = \frac{\partial y}{\partial u}\, du + \frac{\partial y}{\partial v}\, dv. \tag{2.17}$$

We can write this in a matrix form:

$$\begin{bmatrix} dx \\ dy \end{bmatrix} = \begin{bmatrix} \frac{\partial x}{\partial u} & \frac{\partial x}{\partial v} \\ \frac{\partial y}{\partial u} & \frac{\partial y}{\partial v} \end{bmatrix} \begin{bmatrix} du \\ dv \end{bmatrix}. \tag{2.18}$$

The matrix $\begin{bmatrix} \frac{\partial x}{\partial u} & \frac{\partial x}{\partial v} \\ \frac{\partial y}{\partial u} & \frac{\partial y}{\partial v} \end{bmatrix}$ is called the Jacobian matrix of the transformation T which maps (u, v) to (x, y), where $x = x(u, v)$, $y = y(u, v)$. In the case of functions of three variables where transformation T maps (u, v, w) to (x, y, z), then the Jacobian matrix is

$$\begin{bmatrix} \frac{\partial x}{\partial u} & \frac{\partial x}{\partial v} & \frac{\partial x}{\partial w} \\ \frac{\partial y}{\partial u} & \frac{\partial y}{\partial v} & \frac{\partial y}{\partial w} \\ \frac{\partial z}{\partial u} & \frac{\partial z}{\partial v} & \frac{\partial z}{\partial w} \end{bmatrix}. \tag{2.19}$$

Now, we can compute the area dA in the xy-plane. The area of the parallelogram grid in the xy-plane can be computed by the cross product of $\overline{dx}$ and $\overline{dy}$ vectors [45]. Then, we have $dA = \left|\overline{dx} \times \overline{dy}\right|$, where $\overline{dx} = \left\{\frac{\partial x}{\partial u}\, du, \frac{\partial y}{\partial u} du, 0\right\}$ and $\overline{dy} = \left\{\frac{\partial x}{\partial v}\, dv, \frac{\partial y}{\partial v} dv, 0\right\}$. So, the area dA in the transformed space, R in the xy-plane can be written as follows:

$$dA = \begin{bmatrix} \hat{\imath} & \hat{\jmath} & \hat{k} \\ \frac{\partial x}{\partial u}\, du & \frac{\partial y}{\partial u} du & 0 \\ \frac{\partial x}{\partial v}\, dv & \frac{\partial y}{\partial v} dv & 0 \end{bmatrix} = \left|\frac{\partial x}{\partial u}\frac{\partial y}{\partial v} - \frac{\partial x}{\partial v}\frac{\partial y}{\partial u}\right| dudv. \tag{2.20}$$

So, the transformation of region W in the uv-plane into the region R in the xy-plane can be rewritten in the change of variable formula as follows [45]:

$$\iint f(x,y)dx\, dy = \iint f\big(x(u,v), y(u,v)\big) \underbrace{\left|\frac{\partial(x,y)}{\partial(u,v)}\right|}_{\text{Jacobian determinant}} dudv. \tag{2.21}$$

2.2. Tensors

The primary aim of tensor analysis is to study the relations which remain valid when we transform from one coordinate system to a different one. It came to attention of Albert Einstein (1879-1955), when he wanted explain the validity of his theory of relativity for any coordinate system. One of the main thoughts behind this was that laws of physics should not be dependent on frame of reference the physicist chooses. Based on this hypothesis, Einstein found the tensor analysis as an extraordinary tool to represent his theory of relativity. The concept of tensor has been originated from the works of differential geometry by Gauss, Riemann, and Christoffel [44]. To explain physical quantities, sometimes the concept of vectors is not enough. One example could

be measurement of electric field strength. The charge density can be measured by the four velocities of the observer, and hence can be represented by a vector, but for the electric field strength, in some direction will not only be dependent on direction, also on the four velocities of the observer. In that case, the vector is not enough to represent the measurement. This kind of example forced the physicists and mathematicians to come up with a generalization of vector quantity to a quantity known tensor.

Let try to explain tensor analysis through a simple straight line equation in Cartesian coordinates, where the straight line equation is given as following:

$$y = ax + b, \tag{2.22}$$

where, a and b are coefficients. The solution of this equation is $(x_1(t),\ x_2(t), \ldots \ldots x_n(t))$. Now, writing the Geodesic equation [44] for (2.22), we get:

$$\frac{d^2x_i}{dt^2} + \lceil ij \frac{dx_i}{dt}\frac{dx_j}{dt} = 0. \tag{2.23}$$

where, $\lceil ij$ is Christofell symbol [44] and for Cartesian coordinate system, $\lceil ij \equiv 0$. This gives from equation (2.23), $\frac{d^2x_i}{dt^2} = 0$.

$$=> x_i(t) = at + b. \tag{2.24}$$

Equation (2.24) is said to be the covariant tensor of (2.22), it simply means it will carry the same form under any coordinate system, i.e. both (2.22) and (2.24) represent a straight line in two different coordinate system.

2.3. Maxwell's Equations in Covariant Notation

It is well-known in the Applied Electromagnetics community that Maxwell's equations are set of partial differential equations that form the foundation of classical electromagnetism. The equations describe how electric and magnetic fields are generated by charges, currents, and how they change. The equations are named after the physicist and mathematician James C. Maxwell,

who used these equations to explain and propose light as an electromagnetic phenomenon. These equations can be expressed and written in many forms as the Maxwell's equations are form-invariance [15, 16]. Maxwell's equations in differential form are:

$$\nabla \times \bar{H} = \frac{\partial \bar{D}}{\partial t} + \bar{J}, \tag{2.25a}$$

$$\nabla \times \bar{E} = -\frac{\partial \bar{B}}{\partial t}, \tag{2.25b}$$

$$\nabla . \bar{D} = \rho, \tag{2.25c}$$

$$\nabla . \bar{B} = 0. \tag{2.25d}$$

Rewriting these equations in Cartesian components in covariant notation, we get:

$$\sum_j \sum_k \in^{ijk} \frac{\partial H_k}{\partial x^j} = \frac{\partial D^i}{\partial t} + J^i, \tag{2.26a}$$

$$\sum_j \sum_k \in^{ijk} \frac{\partial E_k}{\partial x^j} = -\frac{\partial B^i}{\partial t}, \tag{2.26b}$$

$$\sum_i \frac{\partial D^i}{\partial x^i} = \rho, \tag{2.26c}$$

$$\sum_i \frac{\partial B^i}{\partial x^i} = 0, \tag{2.26d}$$

where, $\in^{ijk}$ is a completely anti-symmetric Levi-Cevita tensor [44]. In Cartesian components, the Levi-Cevita tensor is defined by following:

$$\in^{ijk} = \begin{cases} +1, if\ (i,j,k) is\ (1,2,3),(2,3,1), or (3,1,2) \\ -1, if\ (i,j,k) is\ (3,2,1),(1,3,2), or (2,1,3) \\ 0, if\ i = j, or\ j = k, or\ k = i \end{cases} \tag{2.27}$$

That is $\in^{ijk}$ is 1 if (i, j, k) is an even permutation of (1, 2, 3), -1 if it is an odd permutation, and 0 if any index is repeated.

Now, it is imperative to prove that Maxwell's equations are same in both differential form and covariant notation. Let's start with the left hand side of (2.25a):

$$\nabla \times \bar{H} = \begin{bmatrix} \hat{\imath} & \hat{\jmath} & \hat{k} \\ \dfrac{\partial}{\partial x^1} & \dfrac{\partial}{\partial x^2} & \dfrac{\partial}{\partial x^3} \\ H_1 & H_2 & H_3 \end{bmatrix}$$

or,

$$\nabla \times \bar{H} = \hat{\imath}\left(\frac{\partial H_3}{\partial x^2} - \frac{\partial H_2}{\partial x^3}\right) + \hat{\jmath}\left(\frac{\partial H_1}{\partial x^3} - \frac{\partial H_3}{\partial x^1}\right) + \hat{k}\left(\frac{\partial H_2}{\partial x^1} - \frac{\partial H_1}{\partial x^2}\right). \tag{2.28}$$

From the left hand side of (2.26a), we get:

$$\sum_{j=1}^{3}\sum_{k=1}^{3} \in^{ijk} \frac{\partial H_k}{\partial x^j} = \in^{i11} \frac{\partial H_1}{\partial x^1} + \in^{i12} \frac{\partial H_2}{\partial x^1} + \in^{i22} \frac{\partial H_2}{\partial x^2} + \in^{i21} \frac{\partial H_1}{\partial x^2} + \in^{i13} \frac{\partial H_1}{\partial x^3} + \in^{i31} \frac{\partial H_3}{\partial x^1} +$$

$$\in^{i23} \frac{\partial H_3}{\partial x^2} + \in^{i32} \frac{\partial H_2}{\partial x^3} + \in^{i33} \frac{\partial H_3}{\partial x^3}. \tag{2.29}$$

As j = k, i.e., it makes $\in^{ijk}$= 0, which makes $\in^{i11} \frac{\partial H_1}{\partial x^1}$, $\in^{i22} \frac{\partial H_2}{\partial x^2}$, and $\in^{i33} \frac{\partial H_3}{\partial x^3}$ terms zero. So, rewriting (2.29), we get:

$$\sum_{j=1}^{3}\sum_{k=1}^{3} \in^{ijk} \frac{\partial H_k}{\partial x^j} = \in^{i12} \frac{\partial H_2}{\partial x^1} + \in^{i21} \frac{\partial H_1}{\partial x^2} + \in^{i13} \frac{\partial H_1}{\partial x^3} + \in^{i31} \frac{\partial H_3}{\partial x^1} + \in^{i23} \frac{\partial H_3}{\partial x^2} + \in^{i32} \frac{\partial H_2}{\partial x^3}. \tag{2.30}$$

Now, for i = 1, $\in^{i12} \frac{\partial H_2}{\partial x^1}$, $\in^{i21} \frac{\partial H_1}{\partial x^2}$, $\in^{i13} \frac{\partial H_1}{\partial x^3}$, and $\in^{i31} \frac{\partial H_3}{\partial x^1}$ all becomes zero. So, (2.30) can be rewritten as:

$$\sum_{j=1}^{3}\sum_{k=1}^{3} \in^{ijk} \frac{\partial H_k}{\partial x^j} = \in^{i23} \frac{\partial H_3}{\partial x^2} + \in^{i32} \frac{\partial H_2}{\partial x^3} = \frac{\partial H_3}{\partial x^2} - \frac{\partial H_2}{\partial x^3}. \tag{2.31}$$

Similarly,

$$\sum_{k=1}^{3}\sum_{i=1}^{3} \in^{ijk} \frac{\partial H_k}{\partial x^j} = \frac{\partial H_1}{\partial x^3} - \frac{\partial H_3}{\partial x^1}, \tag{2.32}$$

$$\sum_{i=1}^{3}\sum_{j=1}^{3} \in^{ijk} \frac{\partial H_k}{\partial x^j} = \frac{\partial H_2}{\partial x^1} - \frac{\partial H_1}{\partial x^2}. \tag{2.33}$$

So, equation (2.28) can be rewritten in covariant notation:

$$\nabla \times \bar{H} = \sum_j \sum_k \in^{ijk} \frac{\partial H_k}{\partial x^j}. \tag{2.34}$$

According to Einstein's summation convention, if any index term is repeated, then a summation with respect to the index over the range 1, 2, 3….n is implied. According to this, the

expression $\sum_i^n a_i x^i$ can be written as $a_i x^i$. So, we can rewrite the equation (2.34) as follows:

$$\nabla \times \bar{H} = \in^{ijk} \partial_j H_k, \text{ where } \partial_j = \frac{\partial}{\partial x^j}. \tag{2.35}$$

Similarly, we can also write the right hand side of equation (2.25a)

$$\frac{\partial \bar{D}}{\partial t} + \bar{J} = \frac{\partial D^i}{\partial t} + J^i \tag{2.36}$$

Now, starting with the left hand side of equation (2.25b)

$$\nabla \times \bar{E} = \begin{bmatrix} \hat{\imath} & \hat{\jmath} & \hat{k} \\ \dfrac{\partial}{\partial x^1} & \dfrac{\partial}{\partial x^2} & \dfrac{\partial}{\partial x^3} \\ E_1 & E_2 & E_3 \end{bmatrix}$$

or,

$$\nabla \times \bar{E} = \hat{\imath} \left(\frac{\partial E_3}{\partial x^2} - \frac{\partial E_2}{\partial x^3}\right) + \hat{\jmath} \left(\frac{\partial E_1}{\partial x^3} - \frac{\partial E_3}{\partial x^1}\right) + \hat{k} \left(\frac{\partial E_2}{\partial x^1} - \frac{\partial E_1}{\partial x^2}\right). \tag{2.37}$$

From the left hand side of (2.26b), we get:

$$\sum_{j=1}^3 \sum_{k=1}^3 \in^{ijk} \frac{\partial E_k}{\partial x^j} = \in^{i11} \frac{\partial E_1}{\partial x^1} + \in^{i12} \frac{\partial E_2}{\partial x^1} + \in^{i22} \frac{\partial E_2}{\partial x^2} + \in^{i21} \frac{\partial E_1}{\partial x^2} + \in^{i13} \frac{\partial E_1}{\partial x^3} +$$

$$\in^{i31} \frac{\partial E_3}{\partial x^1} + \in^{i23} \frac{\partial E_3}{\partial x^2} + \in^{i32} \frac{\partial E_2}{\partial x^3} + \in^{i33} \frac{\partial E_3}{\partial x^3}. \tag{2.38}$$

As j = k, i.e., it makes $\in^{ijk} = 0$, which makes $\in^{i11} \frac{\partial E_1}{\partial x^1}$, $\in^{i22} \frac{\partial E_2}{\partial x^2}$, and $\in^{i33} \frac{\partial E_3}{\partial x^3}$ terms zero. So, rewriting (2.38), we get:

$$\sum_{j=1}^3 \sum_{k=1}^3 \in^{ijk} \frac{\partial E_k}{\partial x^j} = \in^{i12} \frac{\partial E_2}{\partial x^1} + \in^{i21} \frac{\partial E_1}{\partial x^2} + \in^{i13} \frac{\partial E_1}{\partial x^3} + \in^{i31} \frac{\partial E_3}{\partial x^1} + \in^{i23} \frac{\partial E_3}{\partial x^2} + \in^{i32} \frac{\partial E_2}{\partial x^3}. \tag{2.39}$$

Now, for i = 1, $\in^{i12} \frac{\partial E_2}{\partial x^1}$, $\in^{i21} \frac{\partial E_1}{\partial x^2}$, $\in^{i13} \frac{\partial E_1}{\partial x^3}$, and $\in^{i31} \frac{\partial E_3}{\partial x^1}$ all becomes zero. So, (2.39) can be rewritten as:

$$\sum_{j=1}^3 \sum_{k=1}^3 \in^{ijk} \frac{\partial E_k}{\partial x^j} = \in^{i23} \frac{\partial E_3}{\partial x^2} + \in^{i32} \frac{\partial E_2}{\partial x^3} = \frac{\partial E_3}{\partial x^2} - \frac{\partial E_2}{\partial x^3}. \tag{2.40}$$

Similarly,

$$\sum_{k=1}^3 \sum_{i=1}^3 \in^{ijk} \frac{\partial E_k}{\partial x^j} = \frac{\partial E_1}{\partial x^3} - \frac{\partial E_3}{\partial x^1}, \tag{2.41}$$

$$\sum_{i=1}^{3}\sum_{j=1}^{3} \in^{ijk} \frac{\partial E_k}{\partial x^j} = \frac{\partial E_2}{\partial x^1} - \frac{\partial E_1}{\partial x^2}. \tag{2.42}$$

So, (2.35) can be rewritten in covariant notation:

$$\nabla \times \bar{E} = \sum_j \sum_k \in^{ijk} \frac{\partial E_k}{\partial x^j}. \tag{2.43}$$

Using Einstein's summation convention and taking the shorthand $\partial_j = \frac{\partial}{\partial x^j}$, (2.43) can be written as the following:

$$\nabla \times \bar{H} = \sum_j \sum_k \in^{ijk} \frac{\partial E_k}{\partial x^j} = \in^{ijk} \partial_j E_k. \tag{2.44}$$

Similarly, we can also write the right hand side of (2.25b) as

$$\frac{\partial \bar{B}}{\partial t} = -\frac{\partial B^i}{\partial t}. \tag{2.45}$$

Now, taking the left hand side of (2.25c) gives

$$\nabla . \bar{D} = \left(\frac{\partial}{\partial x^1}, \frac{\partial}{\partial x^2}, \frac{\partial}{\partial x^3}\right) . (D^1, D^2, D^3),$$

$$\nabla . \bar{D} = \left(\frac{\partial D^1}{\partial x^1} + \frac{\partial D^2}{\partial x^2} + \frac{\partial D^3}{\partial x^3}\right),$$

$$\nabla . \bar{D} = \sum_j \frac{\partial D^j}{\partial x^j}. \tag{2.46}$$

Using Einstein's summation convention and taking the shorthand $\partial_j = \frac{\partial}{\partial x^j}$, (2.46) can be written as the following:

$$\nabla . \bar{D} = \partial_j D^j. \tag{2.47}$$

Therefore, (2.25c) can be written in Cartesian coordinates in covariant notation as the following:

$$\nabla . \bar{D} = \partial_j D^j = \partial_j \varepsilon_{ij} E_j = \rho. \tag{2.48}$$

Similarly, taking the left hand side of (2.25d) gives

$$\nabla . \bar{B} = \left(\frac{\partial}{\partial x^1}, \frac{\partial}{\partial x^2}, \frac{\partial}{\partial x^3}\right) . (B^1, B^2, B^3),$$

$$\nabla.\bar{B} = \left(\frac{\partial B^1}{\partial x^1} + \frac{\partial B^2}{\partial x^2} + \frac{\partial B^3}{\partial x^3}\right),$$

$$\nabla.\bar{B} = \sum_j \frac{\partial B^j}{\partial x^j}. \tag{2.49}$$

Using Einstein's summation convention and taking the shorthand $\partial_j = \frac{\partial}{\partial x^j}$, (2.49) can be written as the following:

$$\nabla.\bar{B} = \partial_j B^j.$$

Similarly, (2.25d) can be written in Cartesian component in covariant notation as the following:

$$\nabla.\bar{B} = \partial_j B^j = \partial_j \mu_{ij} H_j = 0. \tag{2.50}$$

2.4. Form Invariance of Maxwell's Equations under Coordinate Transformation

One of the key assumptions of transformation electromagnetics/optics (TE/TO) is that the differential form of Maxwell's equations is form invariant under any coordinate transformation and this property of Maxwell's equations has been long known [16]. In this process, the associated fields will not be affected, rather the material parameters will contain any change in terms of new coordinate system or transformed coordinate system. This property makes TE/TO technique a unique tool to design electromagnetic and optical media of any arbitrary shape and material that adapt wave propagation properties. Maxwell's equations can be written in covariant notation in Cartesian components as the following:

$$\in^{ijk} \partial_j H_k = \varepsilon^{ij} \frac{\partial \boldsymbol{E_j}}{\partial \boldsymbol{t}} + J^i, \tag{2.51a}$$

$$\in^{ijk} \partial_j E_k = -\mu^{ij} \frac{\partial H_j}{\partial t}, \tag{2.51b}$$

$$\partial_j \varepsilon^{ij} E_j = \rho, \tag{2.51c}$$

$$\partial_j \mu^{ij} H_j = 0. \tag{2.51d}$$

Here, the indices (i, j, k) each run from 1 to 3 and x^i identifies a particular coordinate (i.e., x, y, and z), which means x^1=> x, x^2=>y, and x^3=>z.

Now, the properties of equation (2.51) will be considered under a coordinate transformation, $x' \to x$, where x is the original coordinate system and x' is the transformed coordinate system. Our objective is to prove that Maxwell's equations will remain the same or will be form-invariant under this new or transformed coordinate system. The electric field ($\bar{E}$) and the magnetic field ($\bar{H}$) can be transformed as follows:

$$E_{i'} = A^{i}_{i'} E_i$$

$$E_i = A^{i'}_{i} E_{i'}$$

and $H_i = A^{i'}_{i} H_{i'}$, where the Jacobian matrix is given by

$$A^{i'}_{i} = \frac{\partial x^{i'}}{\partial x^i},$$

The variable x^i is the original coordinates and $x^{i'}$ is the transformed coordinate system. Now, according to the chain rule the partial derivatives must transform in the similar way. So,

$$\partial_{i'} = \frac{\partial}{\partial x^{i'}} = \left(\frac{\partial x^i}{\partial x^{i'}}\right)\frac{\partial}{\partial x^i},$$

and

$$\partial_{i'} = A^{i'}_{i}\, \partial_i. \tag{2.52}$$

Now, substituting (2.52) into (2.51b) we get the following:

$$\in^{ijk} \partial_j\left(A^{k'}_{k} E_{k'}\right) = -\mu^{ij}\, \partial\left(\frac{A^{j'}_{j} H_{j'}}{\partial t}\right). \tag{2.53}$$

The left hand side of (2.53) can be written as following:

$$\in^{ijk} \partial_j\left(A^{k'}_{k} E_{k'}\right) = \in^{ijk} A^{k'}_{k} \partial_j E_{k'} + \in^{ijk} E_{k'} \partial_j A^{k'}_{k},$$

as $\frac{\partial}{\partial x}(u.v) = u\,\frac{\partial v}{\partial x} + v\frac{\partial u}{\partial x}$.

Note that, $\in^{ijk}\ \partial_j A_k^{k'} = \in^{ijk}\ \partial_j \partial_k x^{k'}$ as $A_i^{i'} = \frac{\partial x^{i'}}{\partial x^i}$.

Now rewriting the left hand side of (2.53)

$$\in^{ijk}\ A_k^{k'} \partial_j E_{k'} + \in^{ijk}\ E_{k'} \partial_j \partial_k x^{k'}$$

$$= \in^{ijk}\ [A_k^{k'} \partial_j E_{k'} + E_{k'}\ \partial_j\ \partial_k x^{k'}]$$

$$= \in^{ijk}\ [A_k^{k'} \partial_j E_{k'} + E_{k'} \partial_k\ \partial_j\ x^{k'}]$$

$$= \in^{ijk}\ A_k^{k'} \partial_j E_{k'}\ \ [\partial_j\ x^{k'} = \frac{\partial}{\partial x^j}\ (x^{k'}) = 0]$$

$$= \in^{ijk}\ A_k^{k'} \frac{\partial x^{j'}}{\partial x^j} \frac{\partial}{\partial x^{j'}}\ E_{k'}\ \ [\partial_j = \frac{\partial}{\partial x^j} = \left(\frac{\partial x^{j'}}{\partial x^j}\right) . \frac{\partial}{\partial x^{j'}}]$$

$$= \in^{ijk}\ A_k^{k'} A_j^{j'} \partial_{j'} E_{k'}.$$

Therefore, (2.53) can be written as the following:

$$\in^{ijk}\ A_k^{k'} A_j^{j'} \partial_{j'} E_{k'} = -\mu^{ij}\ \partial \left(\frac{A_j^{j'} H_{j'}}{\partial t}\right). \tag{2.54}$$

Now, using the definition of the determinant, we get the following:

$$\in^{i'j'k'} |A_n^{n'}| = A_i^{i'} A_k^{k'} A_j^{j'}\ \in^{ijk}. \tag{2.55}$$

Inserting (2.55) into (2.54), we get the following:

$$\frac{\in^{i'j'k'} |A| \partial_{j'}}{A_i^{i'}} E_{k'} = -\mu^{ij} A_j^{j'}\ \left(\frac{\partial H_{j'}}{\partial t}\right),$$

and

$$\in^{i'j'k'}\ \partial_{j'} E_{k'} = -\frac{A_i^{i'} A_j^{j'}}{|A|}\ \mu^{ij} \left(\frac{\partial H_{j'}}{\partial t}\right). \tag{2.56}$$

Again, substituting (2.52) into (2.51a) we get the following:

$$\in^{ijk}\ \partial_j \left(A_k^{k'} H_{k'}\right) = \varepsilon^{ij}\ \partial \left(\frac{A_j^{j'} E_{j'}}{\partial t}\right) + J^i. \tag{2.57}$$

The left hand side of (2.57) can be written as following:

$$\in^{ijk} \partial_j\left(A_k^{k'} H_{k'}\right) = \in^{ijk} A_k^{k'} \partial_j H_{k'} + \in^{ijk} H_{k'} \partial_j A_k^{k'}$$

as $\frac{\partial}{\partial x}\ (u.v) = u\ \frac{\partial v}{\partial x} + v\frac{\partial u}{\partial x}$.

Note that, $\in^{ijk} \partial_j A_k^{k'} = \in^{ijk} \partial_j \partial_k x^{k\prime}$ as $A_i^{i\prime} = \frac{\partial x^{i\prime}}{\partial x^i}$.

Now rewriting the left hand side of (2.57)

$$\in^{ijk} A_k^{k'} \partial_j H_{k'} + \in^{ijk} H_{k'} \partial_j \partial_k x^{k\prime}$$

$$= \in^{ijk} [A_k^{k'} \partial_j H_{k'} + E_{k'} \partial_j \partial_k x^{k'}]$$

$$= \in^{ijk} [A_k^{k'} \partial_j E_{k'} + H_{k'} \partial_k \partial_j x^{k'}]$$

$$= \in^{ijk} A_k^{k'} \partial_j H_{k'} \ [\partial_j x^{k'} = \frac{\partial}{\partial x^j}\ (x^{k\prime}) = 0]$$

$$= \in^{ijk} A_k^{k'} \frac{\partial x^{j\prime}}{\partial x^j} \frac{\partial}{\partial x^{j\prime}} H_{k'} \ [\partial_j = \frac{\partial}{\partial x^j} = \left(\frac{\partial x^{j\prime}}{\partial x^j}\right).\frac{\partial}{\partial x^{j\prime}}]$$

$$= \in^{ijk} A_k^{k'} A_j^{j'} \partial_{j\prime} H_{k'}.$$

Therefore, (2.57) can be written as the following:

$$\in^{ijk} A_k^{k'} A_j^{j'} \partial_{j\prime} H_{k'} = \varepsilon^{ij} \partial\left(\frac{A_j^{j'} E_{j'}}{\partial t}\right) + J^i. \tag{2.58}$$

Now, using the definition of the determinant, we get the following:

$$\in^{i\prime j\prime k\prime} |A_n^{n\prime}| = A_i^{i'} A_k^{k'} A_j^{j'} \in^{ijk}. \tag{2.59}$$

Inserting (2.59) into (2.58), we get the following:

$$\frac{\in^{i\prime j\prime k\prime} |A| \partial_{j\prime}}{A_i^{i'}} H_{k'} = \varepsilon^{ij} \partial\left(\frac{A_j^{j'} E_{j'}}{\partial t}\right) + J^i,$$

$$\in^{i\prime j\prime k\prime} \partial_{j\prime} H_{k'} = \frac{A_i^{i'} A_j^{j'}}{|A|} \varepsilon^{ij} \left(\frac{\partial E_{j'}}{\partial t}\right) + \frac{A_i^{i'}}{|A|} J^i. \tag{2.60}$$

Now, Gauss's law from (2.51c) can be transformed and rewritten as follows:

$$\partial_i \varepsilon^{ij} E_j = \rho,$$

$$A_i^{i'}\partial_{i'}\varepsilon^{ij}\,A_j^{j'}E_{j'} = \rho,$$

$$\frac{A_i^{i'}\partial_{i'}\varepsilon^{ij}\,A_j^{j'}E_{j'}}{|A|} = \frac{\rho}{|A|}. \tag{2.61}$$

The left hand side of (2.61) can be written as follows:

$$\partial_{i'}\frac{A_i^{i'}\varepsilon^{ij}\,A_j^{j'}E_{j'}}{|A|} = A_i^{i'}\varepsilon^{ij}E_{j'}\partial_{i'}\frac{A_i^{i'}}{|A|} + \frac{A_j^{j'}\partial_{i'}(A_i^{i'}\varepsilon^{ij}E_{j'})}{|A|}.$$

Hence (2.61) can be rewritten as following:

$$\partial_{i'}\frac{A_i^{i'}\varepsilon^{ij}\,A_j^{j'}E_{j'}}{|A|} - A_i^{i'}\varepsilon^{ij}E_{j'}\partial_{i'}\frac{A_i^{i'}}{|A|} = \frac{\rho}{|A|}. \tag{2.62}$$

The second term on the left hand side is zero and the inverse of the matrix inverse can be calculated using the co-factor formula:

$$\frac{A_i^{i'}}{|A_k^{k'}|} = \frac{\epsilon^{i'u'v'}\in_{iuv}A_u^{u'}A_v^{v'}}{2}. \tag{2.63}$$

and taking the partial derivative:

$$\frac{\partial_{i'}A_u^{u'}\epsilon^{i'u'v'}\in_{iuv}A_u^{u'}A_v^{v'}}{2}. \tag{2.64}$$

This term is also zero and as the partial derivatives are commutative, i.e. $\frac{\partial}{\partial x^i}.\frac{\partial}{\partial x^u} = \frac{\partial}{\partial x^u}.\frac{\partial}{\partial x^i}$, while the exchange of i' and u' is anti-symmetric. The contraction of a symmetric tensor with an anti-symmetric one is zero. Rewriting equation (2.62) results in as following:

$$\partial_{i'}\frac{A_i^{i'}\varepsilon^{ij}\,A_j^{j'}E_{j'}}{|A|} = \frac{\rho}{|A|}. \tag{2.65}$$

Similarly, equation (2.51d) can be transformed and written as follows:

$$\partial_i\mu^{ij}\,H_j = 0,$$

$$A_i^{i'}\partial_{i'}\mu^{ij}\,A_j^{j'}H_{j'} = 0,$$

and

$$\frac{A_i^{i'}\partial_{i'}\mu^{ij}A_j^{j'}H_{j'}}{|A|}=0\ . \tag{2.66}$$

The left hand side of (2.66) can be written as follows:

$$\partial_{i'}\frac{A_i^{i'}\mu^{ij}A_j^{j'}H_{j'}}{|A|}=\ A_i^{i'}\mu^{ij}H_{j'}\partial_{i'}\ \frac{A_i^{i'}}{|A|}+\ \frac{A_j^{j'}\partial_{i'}(A_i^{i'}\mu^{ij}H_{j'})}{|A|}. \tag{2.67}$$

The left hand side of (2.67) can be written as follows:

$$\partial_{i'}\frac{A_i^{i'}\mu^{ij}\ A_j^{j'}H_{j'}}{|A|}=\ A_i^{i'}\mu^{ij}H_{j'}\partial_{i'}\ \frac{A_i^{i'}}{|A|}+\ \frac{A_j^{j'}\partial_{i'}(A_i^{i'}\mu^{ij}H_{j'})}{|A|}.$$

Hence equation (2.66) can be rewritten as following:

$$\partial_{i'}\frac{A_i^{i'}\mu^{ij}\ A_j^{j'}H_{j'}}{|A|}-A_i^{i'}\mu^{ij}H_{j'}\partial_{i'}\ \frac{A_i^{i'}}{|A|}=0. \tag{2.68}$$

The second term on the left hand side is zero and the inverse of the matrix inverse can be calculated using the co-factor formula:

$$\frac{A_i^{i'}}{|A_k^{k'}|}=\ \frac{\epsilon^{i'u'v'}\in_{iuv}A_u^{u'}A_v^{v'}}{2}, \tag{2.69}$$

and taking the partial derivative:

$$\frac{\partial_{i'}A_u^{u'}\epsilon^{i'u'v'}\in_{iuv}A_u^{u'}A_v^{v'}}{2}. \tag{2.70}$$

This term is also zero and as the partial derivatives are commutative, i.e., $\frac{\partial}{\partial x^i}.\frac{\partial}{\partial x^u}=\frac{\partial}{\partial x^u}.\frac{\partial}{\partial x^i}$, while the exchange of i' and u' is anti-symmetric. The contraction of a symmetric tensor with an anti-symmetric one is zero. Rewriting equation (2.68) results in the following:

$$\partial_{i'}\frac{A_i^{i'}\mu^{ij}\ A_j^{j'}H_{j'}}{|A|}=0\ . \tag{2.71}$$

In all the above transformed equations, the material parameters, current sources and charges can be realized in the transformed space using the appropriate coordinate transformation

rules and this process keeps the Maxwell's equations form-invariant in the new coordinate system or transformed coordinate system. This unique property gives leverage to the scientists and engineers to come up with unconventional electromagnetic devices. The above derivations of transformation electromagnetics/optics (TE/TO) form invariance of Maxwell's equations under coordinate system closely follows the work reported in [8] and [46, 47].

Table 2.1. Form-invariance of Maxwell's equations under a coordinate transformation and material parameters, charge, and current distribution in the new coordinates using transformation rules [8, 47].

Original Equations	Transformed Equations	Transformation Rules	Transformed Equations using the Rules
$\in^{ijk} \partial_j H_k = \varepsilon^{ij} \frac{\partial E_j}{\partial t} + J^i$	$\in^{i'j'k'} \partial_{j'} H_{k'} = \frac{A_i^{i'} A_j^{j'}}{\lvert A\rvert} \varepsilon^{ij} \left(\frac{\partial E_{j'}}{\partial t}\right) + \frac{A_i^{i'}}{\lvert A\rvert} J^i$	$\varepsilon^{i'j'} = \frac{A_i^{i'} A_j^{j'}}{\lvert A\rvert} \varepsilon^{ij}$	$\in^{i'j'k'} \partial_{j'} H_{k'} = \varepsilon^{i'j'} \left(\frac{\partial E_{j'}}{\partial t}\right) + J^{i'}$
$\in^{ijk} \partial_j E_k = -\mu^{ij} \frac{\partial H_j}{\partial t}$	$\in^{i'j'k'} \partial_{j'} E_{k'} = -\frac{A_i^{i'} A_j^{j'}}{\lvert A\rvert} \mu^{ij} \left(\frac{\partial H_{j'}}{\partial t}\right)$	$\mu^{i'j'} = \frac{A_i^{i'} A_j^{j'}}{\lvert A\rvert} \mu^{ij}$	$\in^{i'j'k'} \partial_{j'} E_{k'} = -\mu^{i'j'} \left(\frac{\partial H_{j'}}{\partial t}\right)$
$\partial_i \varepsilon^{ij} E_j = \rho$	$\partial_{i'} \frac{A_i^{i'} \varepsilon^{ij} A_j^{j'} E_{j'}}{\lvert A\rvert} = \frac{\rho}{\lvert A\rvert}$	$\rho' = \frac{\rho}{\lvert A\rvert}$	$\partial_{i'} \varepsilon^{i'j'} E_{j'} = \rho'$
$\partial_i \mu^{ij} H_j = 0$	$\partial_{i'} \frac{A_i^{i'} \mu^{ij} A_j^{j'} H_{j'}}{\lvert A\rvert} = 0$	$J^{i'} = \frac{A_i^{i'}}{\lvert A\rvert} J^i$	$\partial_{i'} \mu^{i'j'} H_{j'} = 0$

3. TRANSFORMATION ELECTROMAGNETICS/OPTICS (TE/TO) EXAMPLES

In this chapter the use of the form invariance of Maxwell's equations as a design tool is explored through several transformation electromagnetics/optics (TE/TO) examples. To establish a better understanding and foundation of this theory, the instructive examples of devices shown here have been explored by our group at NDSU and collaborators at AFRL using the TE/TO method. This background work will be presented and discussed in this chapter.

3.1. Simple Coordinate Transformation

To understand the TE/TO approach let's start with a simple coordinate transformation. It is important to understand and visualize the effect of the coordinate transformation as a design step of transformation electromagnetics structures and devices. Understanding the coordinate transformation means understanding the function of the device that will be designed by the TE/TO method. Figure 3.1a shows a 2D grid illustrating Cartesian space, in which constant x and constant y are plotted for discretely spaced x and y values, respectively.

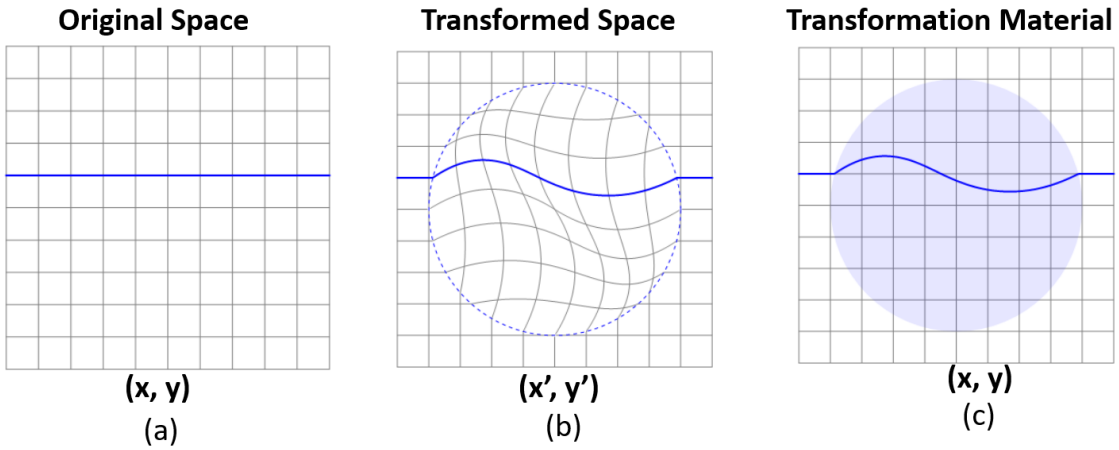

Figure 3.1. Visualizing a coordinate transformation with grids are formed by equally spaced constant x and constant y lines [48], (a) a 2D grid illustrating Cartesian Space, (b) distorted grid in (x', y') space by transformation given from equation 3.1, (c) transformed space with transformed material.

Consider the following 2D coordinate transformation defined by

$$x' = x + ay\,(r - b), r < b$$

and

$$y' = y + ax\,(r - b), r < b, \tag{3.1}$$

which conducts a distortion on the region of space within the circle $r = b$. The distortion is illustrated by the distorted lines in Figure 3.1b, which represents the transformed space (x', y'). The transformation becomes identical to free-space for $r \geq b$, so that the transformation region remains local.

Now, considering: $r = \sqrt{x^2 + y^2}$, (3.1) becomes

$$x' = x + ay\left(\sqrt{x^2 + y^2} - b\right), r < b,$$

and

$$y' = y + ax\left(\sqrt{x^2 + y^2} - b\right), r < b. \tag{3.2}$$

The material parameters due to coordinate transformations can be written from (2.8) and (2.9) as the following:

$$\varepsilon' = \mu' = \frac{J\varepsilon J^T}{|J|}. \tag{3.3}$$

The Jacobian matrix for a 2D coordinate transformation is given by

$$J = \begin{vmatrix} \frac{\partial x'}{\partial x} & \frac{\partial x'}{\partial y} \\ \frac{\partial y'}{\partial x} & \frac{\partial y'}{\partial y} \end{vmatrix}. \tag{3.4}$$

Now, taking the partial derivatives of the transformation from (3.2) for the Jacobian

$$\frac{\partial x'}{\partial x} = \frac{\partial}{\partial x}\left\{x + ay\left(\sqrt{x^2 + y^2} - b\right)\right\} = \frac{\sqrt{x^2+y^2}+axy}{\sqrt{x^2+y^2}}, \tag{3.5}$$

$$\frac{\partial x'}{\partial y} = \frac{\partial}{\partial y}\left\{x + ay\left(\sqrt{x^2 + y^2} - b\right)\right\} = \frac{a(2y^2+x^2)-ab\sqrt{x^2+y^2}}{\sqrt{x^2+y^2}}, \tag{3.6}$$

$$\frac{\partial y'}{\partial x} = \frac{\partial}{\partial x}\{y + ax\left(\sqrt{x^2+y^2} - b\right)\} = \frac{a(2x^2+y^2) - ab\sqrt{x^2+y^2}}{\sqrt{x^2+y^2}} \tag{3.7}$$

and

$$\frac{\partial y'}{\partial y} = \frac{\partial}{\partial y}\{y + ax\left(\sqrt{x^2+y^2} - b\right)\} = \frac{\sqrt{x^2+y^2} + axy}{\sqrt{x^2+y^2}}. \tag{3.8}$$

So, re-writing the Jacobian matrix from (3.4) gives

$$J = \begin{vmatrix} a_{11} & a_{12} \\ a_{21} & a_{22} \end{vmatrix}. \tag{3.9}$$

where $a_{11} = a_{22} = \frac{\sqrt{x^2+y^2}+axy}{\sqrt{x^2+y^2}}$, $a_{12} = \frac{a(2y^2+x^2)-ab\sqrt{x^2+y^2}}{\sqrt{x^2+y^2}}$, and $a_{21} = \frac{a(2x^2+y^2)-ab\sqrt{x^2+y^2}}{\sqrt{x^2+y^2}}$.

Putting $r = \sqrt{x^2+y^2}$ back to the above matrix parameters gives

$$a_{11} = a_{22} = \frac{r+axy}{r}, a_{12} = \frac{a(r^2+y^2)-abr}{r}, \text{and } a_{21} = \frac{a(r^2+x^2)-abr}{r}.$$

Equation (3.9) can be re-written as the following:

$$J = \begin{bmatrix} \frac{f}{r} & \frac{ag}{r} \\ \frac{ah}{r} & \frac{f}{r} \end{bmatrix}, \tag{3.10}$$

where, $g = c - br$, $h = d - br$, $f = r + axy$, $c = r^2 + y^2$, and $d = r^2 + x^2$. Now, (3.3) results in the material parameters due to transformation as the following:

$$\varepsilon' = \mu' = \frac{J\varepsilon J^T}{|J|} = \frac{r^2}{f^2-a^2gh}\begin{vmatrix} \frac{f^2+a^2g^2}{r^2} & \frac{af(g+h)}{r^2} \\ \frac{af(g+h)}{r^2} & \frac{f^2+a^2h^2}{r^2} \end{vmatrix} = \begin{vmatrix} \frac{f^2+a^2g^2}{f^2-a^2gh} & \frac{af(g+h)}{f^2-a^2gh} \\ \frac{af(g+h)}{f^2-a^2gh} & \frac{f^2+a^2h^2}{f^2-a^2gh} \end{vmatrix} = \begin{vmatrix} \frac{k}{m} & \frac{k}{m} \\ \frac{n}{m} & \frac{l}{m} \end{vmatrix} \tag{3.11}$$

where, $f^2 - a^2gh = m, af(g+h) = n, f^2 + a^2g^2 = k,$ and $f^2 + a^2h^2 = l.$ Equation (3.11) represents the transformed material parameters for the simple coordinate transformation in (3.1).

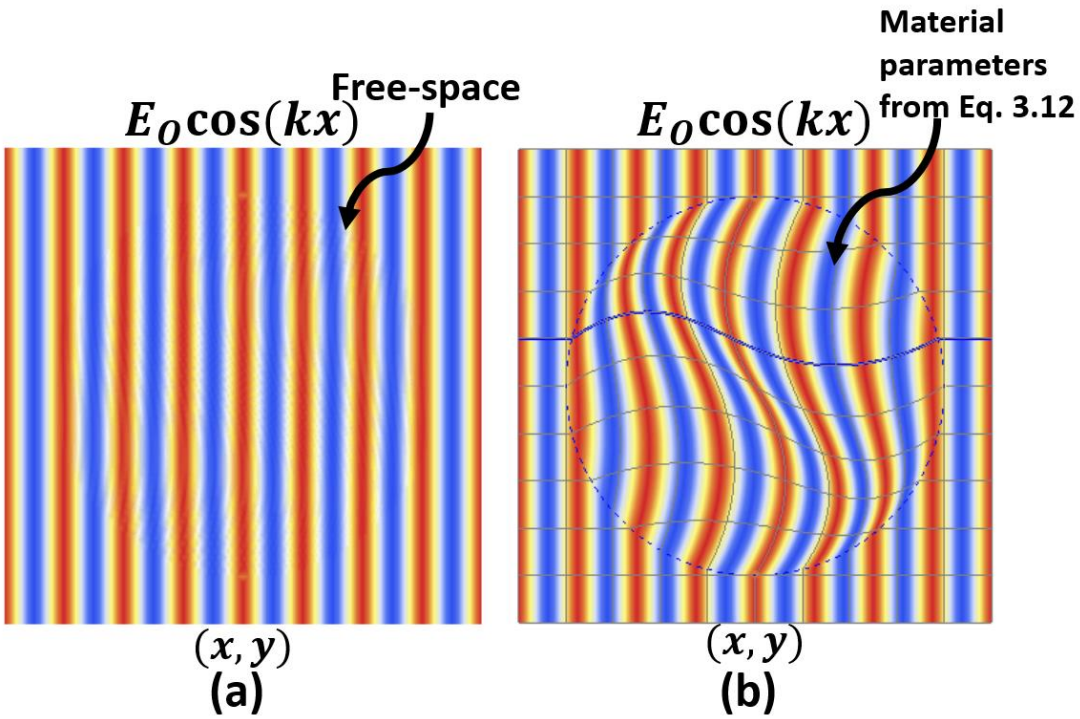

Figure 3.2. Visualizing the simple coordinate transformation from equation (3.1) [48], (a) a plane wave in (x, y) coordinate system, (b) the distorted plane wave due to coordinate transformation in the transformation region.

The deformation of the grid lines gives a direct understanding and visualization of the impact of the coordinate transformation. This can be further demonstrated using a plane wave simulation. Figure 3.2a shows that a plane wave of $E(x, y) = E_O \cos(kx)$ in the (x, y) coordinate system in free-space. The effect of coordinate transformation is shown in Figure 3.2b, where the wave-fronts are now distorted, conforming the distorted grid lines from Figure 3.1b. The fields associated with the plane wave solutions are fixed to the original coordinate system, which necessarily pushes the gridlines around according to coordinate transformation to distort the wave in a predictable manner using the material parameters calculated in (3.12) as shown in Figure 3.2b.

3.2. 2D Space Compression

Another simple use of the TE/TO technique is to compress space along any direction. If we compress the space in Figure 3.3a by a factor k along the x-direction, we require that in the

compressed region

$$\frac{dx'}{dx} = \begin{cases} k, & l_1 < x < l_2 \\ 1, & x \le l_1 \\ 1, & x \ge l_2 \end{cases} \tag{3.12}$$

where the space to be compressed in the region $l_1 < x < l_2$. This compression transformation can be applied to a region including an optical device, such as lens [49]. The result of the transformation will be to reduce the profile of the optical devices along the optical axis. Then, l_1 and l_2 are the bounds of the transformation in the unprimed or in the real space. Integration of (3.13) gives us the map in the transformed coordinates as the following:

$$x'(x) = \begin{cases} kx + c\,, & l_1 < x < l_2 \\ l_1{}' + (x - l_1), & x \le l_1\,. \\ l_2{}' + (x - l_2), & x \ge l_2 \end{cases} \tag{3.13}$$

The integration constant is determined by setting a boundary condition $x' = x$. The bounds of the optical device in the transformed space are given by $l_1{}' = x'(\,l_1) = kl_1 + c$ and $l_2{}' = x'(\,l_2) = kl_2 + c$.

Now, from Table 2.1, the general prescription of transformation optical media using TE/TO technique is as the following:

$$\varepsilon^{i'j'} = \frac{A_i^{i'}}{|A|} A_j^{j'} \varepsilon^{ij}, \tag{3.14}$$

and

$$\mu^{i'j'} = \frac{A_i^{i'}}{|A|} A_j^{j'} \mu^{ij}. \tag{3.15}$$

where, $A_i^{i'} = \frac{\partial x^{i'}}{\partial x^i}$ is Jacobian Matrix.

Using the above equation, the material parameters of the transformed or compressed space due to the transformation can be calculated as the following:

$$\varepsilon^{i'j'} = \begin{vmatrix} k & 0 & 0 \\ 0 & 1/k & 0 \\ 0 & 0 & 1/k \end{vmatrix} \tag{3.16}$$

and

$$\mu^{i'j'} = \begin{vmatrix} k & 0 & 0 \\ 0 & 1/k & 0 \\ 0 & 0 & 1/k \end{vmatrix}. \tag{3.17}$$

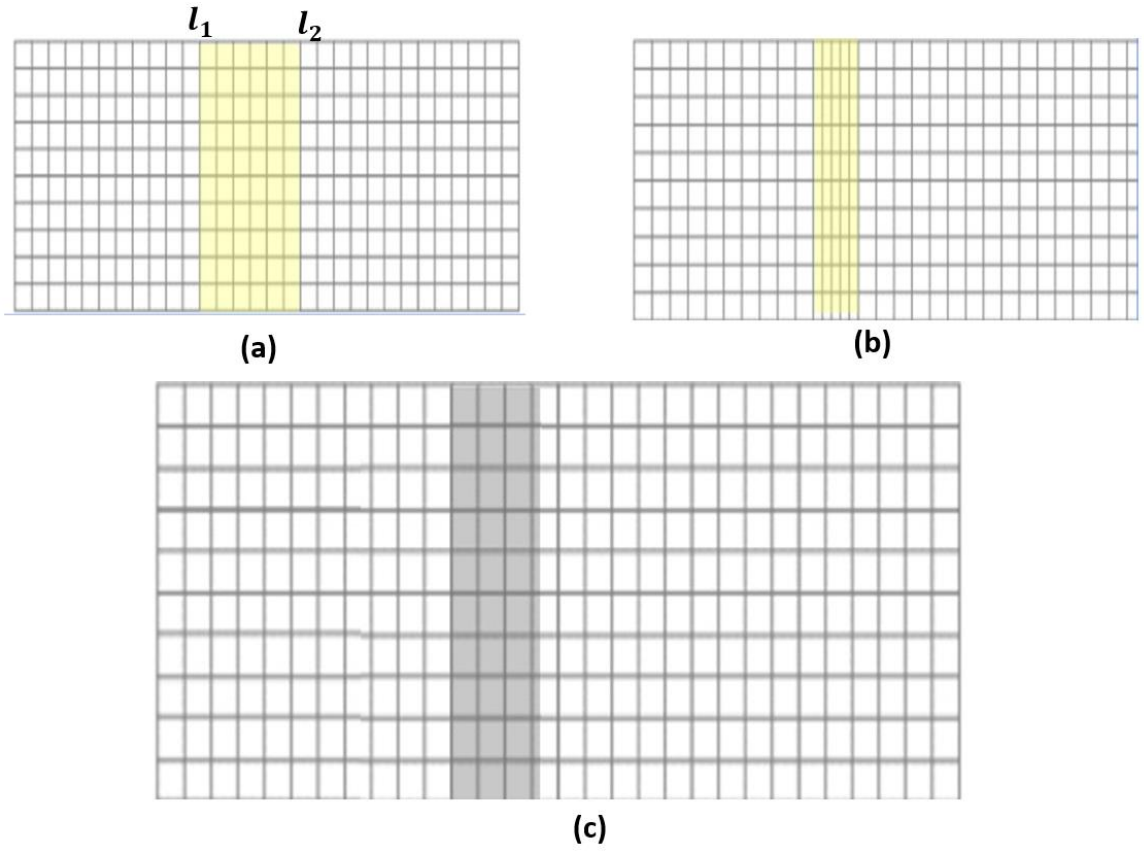

Figure 3.3. Plot of the space compression transformation expressed by equation (3.14) [49]. Here, the integration constant is chosen so that $x = 0$ maps to $x' = 0$, (a) uncompressed flat space (original space), (b) compressed space where the shaded region in (a) is compressed by a factor 2, (c) transformation media by the compression that occurs.

In other words, the space compression can be achieved as long as the region of compression is replaced with the anisotropic material parameters described by (3.16) and (3.17). All aspects of wave scattering must remain unaltered within the region of compression, for instance, in case of a vacuum, the resultant compressed space must be reflectionless and lossless. Furthermore, any

wave that passes through the space must remain unchanged/undisturbed; that is, an external observer would not be able to distinguish that the wave had passed through the region with the material specified by (3.16) and (3.17) or free-space [48].

To demonstrate the success of the transformation a commercially available finite element simulation software COMSOL Multiphysics is used [50]. A two dimensional rectangular slab was used as shown in Figure 3.4, where L is chosen as, $L = C_{const}/1\ GHz = 0.3$ m, and the compression space, W = 0.02 m. A TE plane wave was infringed from the Floquet port 1, which is basically the left side of the rectangular slab at an angle of 45^0. The constitutive parameters are defined in equation (3.15) and (3.16) in terms of transformed or compressed space, where k is the compression factor and here k was chosen to be 0.5.

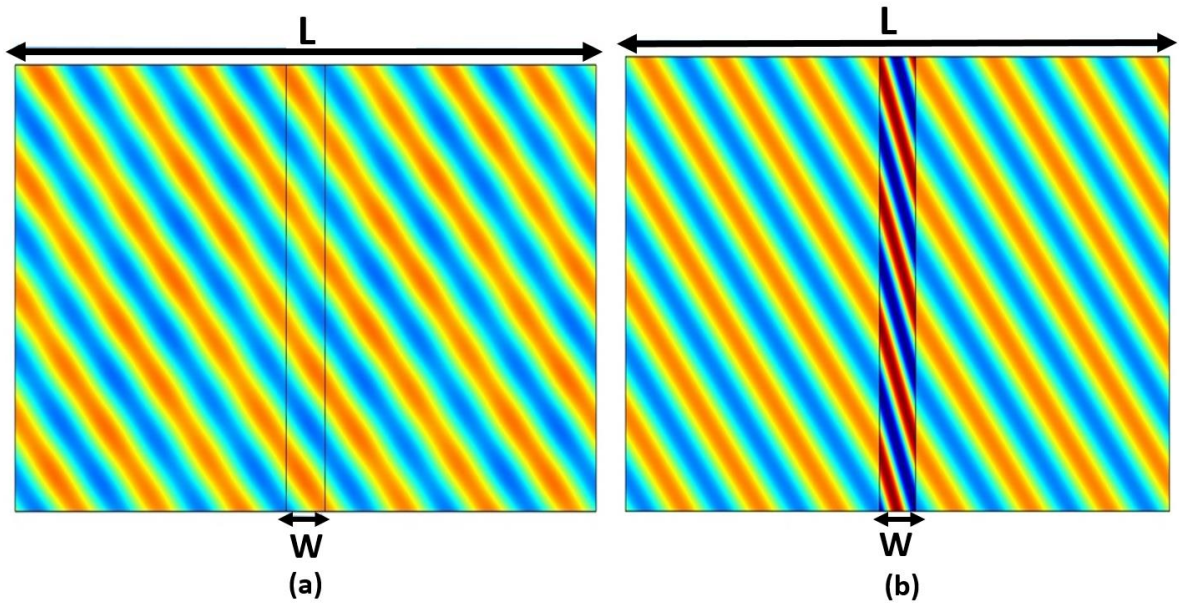

Figure 3.4. A simple example of space compression (a) a 2D rectangular slab, where the region W is "uncompressed", the whole space is air, (b) the 2D rectangular slab with the region W is "compressed" by a factor 2, either side of the region "W" is air.

The compression transformation from (3.13) was also validated using a Gaussian beam in COMSOL Multiphysics as shown in Figure 3.5. Figure 3.5a shows a 2 GHz Gaussian beam in free-space. The beam propagates along x–direction from left to right. A compression region of

"W" was chosen to show the compression of the beam in Figure 3.5b. The beam was compressed two times. Similar transformation can also be used to expand the beam in the same region, as shown in Figure 3.5c. Here, the beam was expanded by two times.

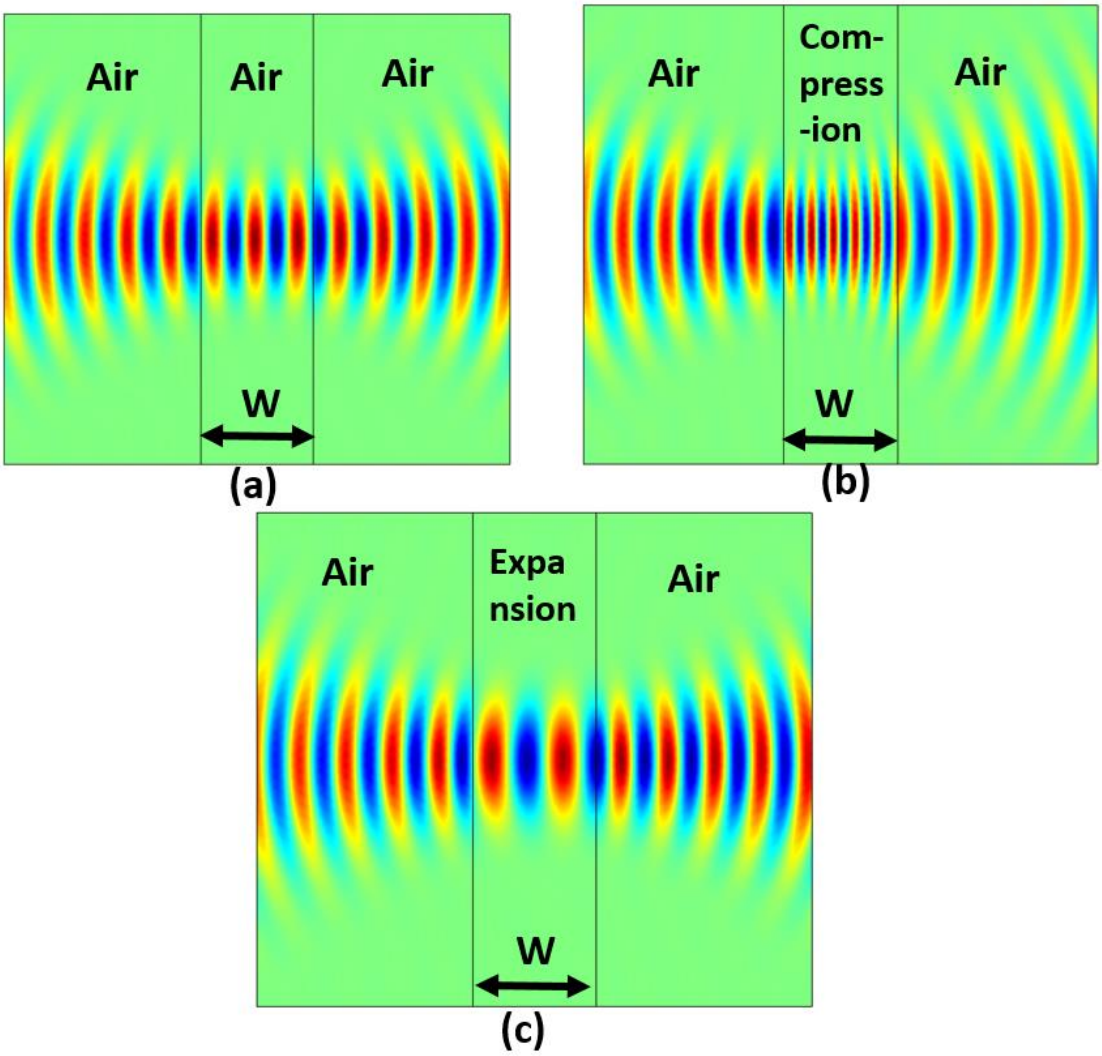

Figure 3.5. Numerical simulations of compression transformation in COMSOL Multiphysics using a Gaussian beam, (a) a 2 GHz Gaussian beam in free-space, (b) the beam is compressed by two times in a chosen region of compression, (c) the beam is expanded by two times is the similar region of transformation.

The compression transformation has relevance and applications in antenna design. Overall the antenna system profile can be reduced without any change in system metrics, except inclusion of a complex material defined by the transformation [48]. A compression transformation can be

used to move two antennas closer together while not affecting their radiation properties [48]. Such transformations could be useful to reduce the interference between two antenna systems, specifically since the transformation handles the near-fields of the antennas.

3.3. Beam-Shifter

The beam-shifter [29, 51] is probably one of the finest and simplest example of how the TE/TO technique can be employed to freely control the behavior of electromagnetic beam to a desired direction. In this device the beam is translated in a desired direction as it propagates through a medium. The first step is to find a set of coordinates in which the beam appears to shift its direction in a desired way. Such coordinate system is shown in Figure 3.6. Consider a beam shifter with thickness t starting from x_o, a coordinate transformation for shifting the beam is as the following:

$$\begin{cases} x'(x,y,z) = x \\ y'(x,y,z) = f(x,y) \\ z'(x,y,z) = z \end{cases} \qquad x_0 < x < x_0 + t. \tag{3.18}$$

As a two-dimensional (2D) condition is considered here, the new component $y'(x,y,z)$ is independent of z. There will be no materials introduced in the regions (regions 1, 3, and 5 in Figure 3.6b) where there is no beam-shifting required. In those regions the Jacobian will be just an identity matrix. The materials will be introduced into the regions of up-shifting (region 2) and down-shifting (region 4) as shown in Figure 3.6b. The Jacobian matrix of the transformation and its determinant are

$$J = \begin{bmatrix} 1 & 0 & 0 \\ b_{21} & b_{22} & 0 \\ 0 & 0 & 1 \end{bmatrix} \tag{3.19}$$

and

$$|J| = b_{22}, \tag{3.20}$$

where, $b_{21} = {\partial f(x,y)}/{\partial x}$ and $b_{22} = {\partial f(x,y)}/{\partial y}$.

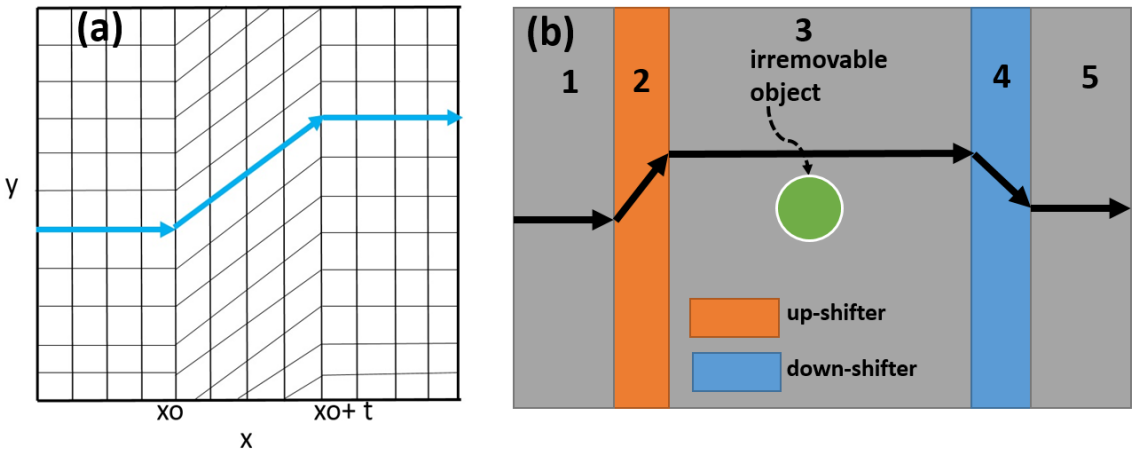

Figure 3.6. A linear coordinate transformation of a beam shifter and its application (a) appropriate coordinate transformation for up-shifting (b) a set of beam shifters for both up-shifting and down-shifting.

As depicted in Figure 3.6, the linear coordinate transformation for up-shifting is given by [51]

$$\begin{cases} x'(x,y,z) = x \\ y'(x,y,z) = Q(x - x_0) + y \\ z'(x,y,z) = z \end{cases} \qquad x_0 < x < x_0 + t \tag{3.21}$$

where Q is the beam-shifter controlling factor. We can control the amount of beam-shifting by adjusting Q. The transformation in (3.21) can shift the beam upwards, so we call it an up-shifter, which is depicted in Figure 3.6b. Equations (2.8) and (2.9) result in the following constitutive material parameters for up-shifting:

$$\varepsilon_u{}^{i'j'} = \mu_u{}^{i'j'} = \begin{vmatrix} 1 & Q & 0 \\ Q & Q^2 + 1 & 0 \\ 0 & 0 & 1 \end{vmatrix}. \tag{3.22}$$

To restore the beam to its original path, a device opposite to the up-shifter is needed; namely the down-shifter shown in Figure 3.6b. The coordinate transformation and the material parameters for the down-shifter are given by [51]

$$\begin{cases} x'(x,y,z) = x \\ y'(x,y,z) = -Q(x-x_0)+y \qquad x_0 < x < x_0 + t \\ z'(x,y,z) = z \end{cases} \tag{3.23}$$

and

$$\varepsilon_d{}^{i'j'} = \mu_d{}^{i'j'} = \begin{vmatrix} 1 & -Q & 0 \\ -Q & Q^2+1 & 0 \\ 0 & 0 & 1 \end{vmatrix}. \tag{3.24}$$

In Figure 3.6b, there is an irremovable object in its way of the beam, so a set of beam-shifters is needed to guide the beam around the object, which is set to be a perfect electric conductor (PEC). As depicted in Figure 3.6b, the region 2 was defined as an up-shifter and the region 4 was defined as a down-shifter. Regions 1, 3, and 5 were set as free-space. Both the beam-shifters were set of same thickness Q. A two-dimensional full-wave simulation was performed in COMSOL Multiphysics to validate the performances of the beam-shifters. To avoid any kind of reflections, the regions were bounded by perfectly matched layers (PML) and the polarization of the wave was set to be perpendicular to the $x-y$ plane. The source was a Gaussian beam [52, 53] of 2 GHz. A PEC object was set in the center as shown in Figure 3.6b. The numerical simulations in COMSOL are shown in Figure 3.7. Figure 3.7a shows a 2 GHz Gaussian beam in free-space. Next, an irremovable object was introduced in its way and the presence of the PEC object perturbed the beam and it scattered significantly, which is shown in Figure 3.7b. To guide the beam around the PEC scatterer, the up- and down- shifters from Figure 3.6b were introduced in COMSOL, as shown in Figure 3.7c. In Figure 3.7c, the up-shifter sets the beam up in region 2 and the down-shifter sets the beam down in region 4 to avoid the PEC object successfully. As compared to Figure 3.7a, the beam in Figure 3.7c remained unperturbed and the beam-shifters were able to force the beam to steer around the irremovable PEC object.

The performances of the beam-shifters were also tested with different parameters by varying the "beam-controlling" factor Q. In Figure 3.8a and 3.8b, the Q- value changed to 1.2 and 1.5, respectively, but the geometry was kept the same as Figure 3.7. It is observed that with the increase of Q- value, the beam bending was also increased. It can be explained from (3.21) and (3.23) that the beam shifts more when the Q- value increases. However, it is not necessarily appropriate to increase the value of Q. According to (3.22) and (3.24), the permittivity and permeability have components lower than -1, which is not practical to implement, as the difficulty in the fabrication of the materials will increase.

A similar approach can be adopted as proposed in [29, 51] to propose a new application of multiple up- and down-beam-shifters (as shown in Figure 3.9) where the magnetic radiation pattern of a dipole antenna was steered around an irremovable perfect electric conductor (PEC) object before propagating on its original route.

In Figure 3.9, the radiation pattern of a dipole antenna is hindered by an irremovable PEC object. The use of two beam-shifters is also shown as a method to deviate the dipole radiation pattern around the PEC object before it propagates on its original path. More specifically, the material properties of the up-shifter and down-shifter are computed using (3.22) and (3.24), respectively. A 2D full wave simulation was performed using COMSOL [50] to demonstrate the performance of the beam-shifters. First, a half-wavelength dipole in free space was considered and a frequency of 20 GHz was chosen.

The magnetic field radiation of the dipole in free-space was computed first in COMSOL and is shown in Figure 3.10a. Next, two irremovable PEC objects were introduced on each side of the dipole in Figure 3.10b and it is shown how the magnetic field perturbs in the presence of the objects. To move the beam around these objects, the beam-shifters in Figure 3.9 were introduced

in COMSOL, as shown in Figure 3.10c. The space in Figure 3.10c was divided in to 9 regions, where regions 1, 3, 5, 7 and 9 are free space. Regions 2 and 6 are up-shifters, and regions 4 and 8 are down-shifters. The numerical simulation results in Figure 3.10c demonstrates that the normalized magnetic field from the half-wave dipole can be shifted around the objects and restore the magnetic field pattern to its original route. In both cases, a beam-shifter controlling factor of Q = 1.5 was chosen. It is the same for both cases, as both the up- and down- shifters have similar thicknesses and need a similar amount of beam-shifting.

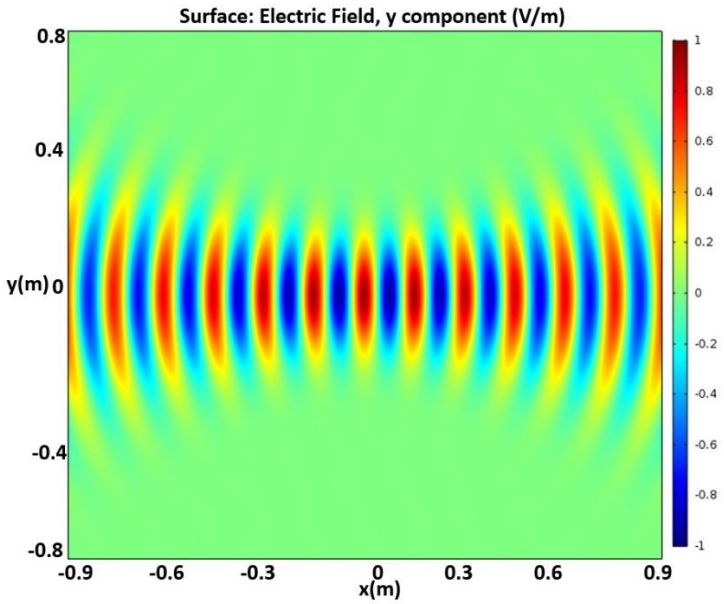

(a)

Figure 3.7. COMSOL Simulations demonstrating the performances of beam-shifters. (a) a 2 GHz Gaussian beam in free-space, (b) the beam experiences significance scattering due to presence of an irremovable object, (c) a set of beam shifters with Q =1. Regions 1, 3, and 5 are free-space. Region 2 is an up-shifter and region 4 is a down shifter.

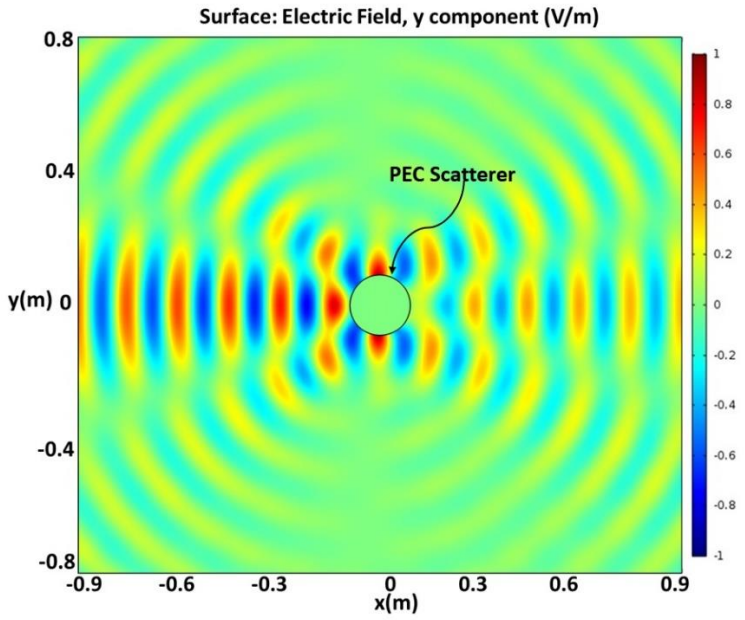

(b)

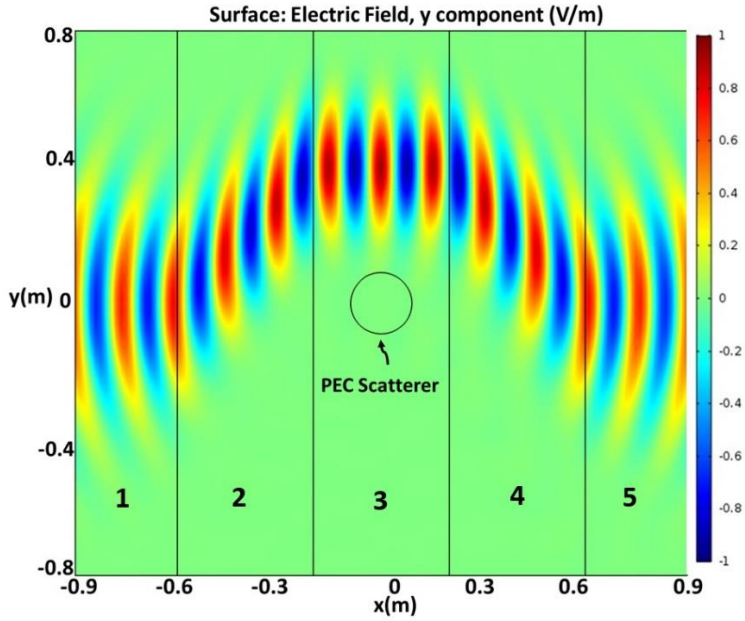

(c)

Figure 3.7. COMSOL Simulations demonstrating the performances of beam-shifters. (a) a 2 GHz Gaussian beam in free-space, (b) the beam experiences significance scattering due to presence of an irremovable object, (c) a set of beam shifters with Q =1. Regions 1, 3, and 5 are free-space. Region 2 is an up-shifter and region 4 is a down shifter (continued).

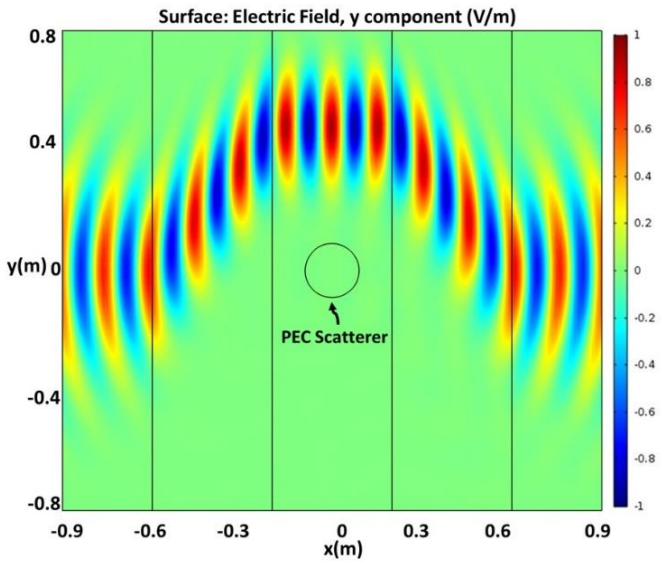

(a)

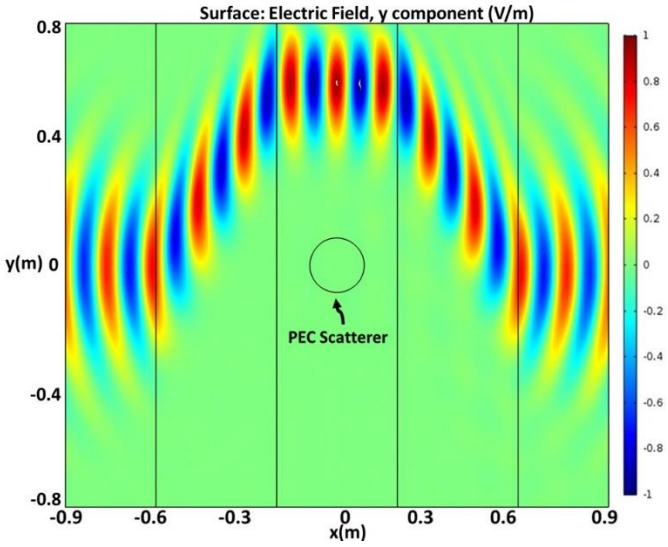

(b)

Figure 3.8. COMSOL Simulations demonstrating the performances of beam-shifters with different Q values. (a) Q = 1.2, (b) Q = 1.5.

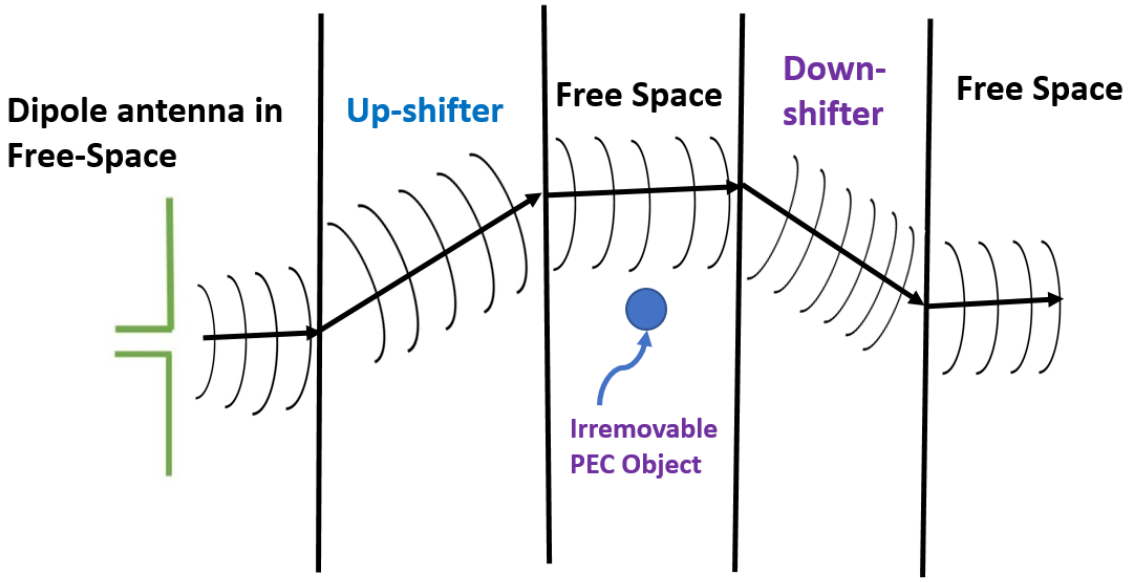

Figure 3.9. Novel application of beam-shifters using linear coordinate transformation. A dipole antenna in free-space. An up-shifter is used to avoid the irremovable PEC object and a down-shifter is used to restore the beam to its original path.

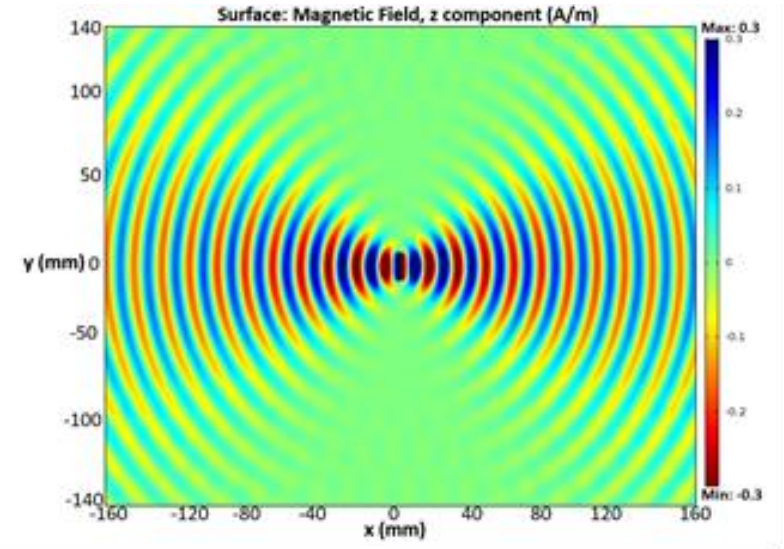

(a)

Figure 3.10. Full wave COMSOL simulations demonstrating the performances of the beam-shifters, (a) the magnetic field distribution of a half-wave dipole in free-space, (b) the magnetic field is perturbed by a set of irremovable PEC objects, (c) set of beam shifters used to steer-away the beam around the PEC objects. Regions 1, 3, 5, 7 and 9 are free-space. Regions 2 and 6 are up-shifters and regions 4 and 8 are down-shifters.

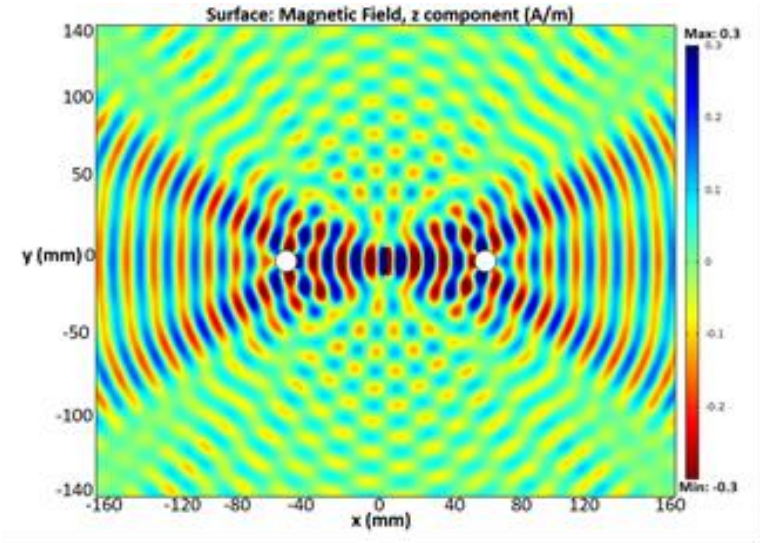

(b)

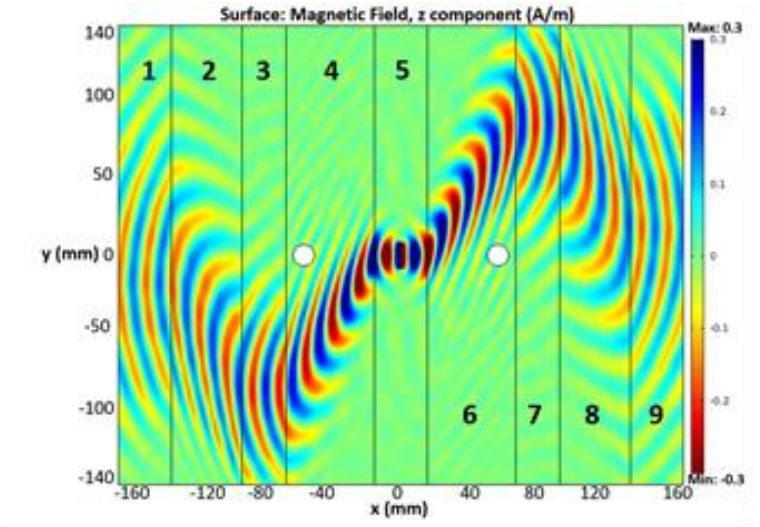

(c)

Figure 3.10. Full wave COMSOL simulations demonstrating the performances of the beam-shifters, (a) the magnetic field distribution of a half-wave dipole in free-space, (b) the magnetic field is perturbed by a set of irremovable PEC objects, (c) set of beam shifters used to steer-away the beam around the PEC objects. Regions 1, 3, 5, 7 and 9 are free-space. Regions 2 and 6 are up-shifters and regions 4 and 8 are down-shifters (continued).

3.4. Electromagnetic Cloaking

The electromagnetic cloak has drawn a lot of attention from the scientific community, because it has been shown that it is possible to make someone or some object invisible. The concept was first introduced by Pendry *et al* [13], and later was demonstrated by Schurig *et al* [19]. Cummer *et al* [54] introduced a nice platform to perform the full-wave simulation of the electromagnetic cloaking. The TE/TO technique has been employed to transform a space in the electromagnetic cloak. The idea of cloaking is that a given volume of space is hidden such a way that the observer from the outside will not be able to see the object hidden in that concealed space. This is achieved by surrounding the object that will be cloaked by a metamaterial shell designed using the TE/TO technique, which guides the electromagnetic wave around the concealed object in the metamaterial shell and goes back to its original orientation. In the metamaterial shell, the wave travels more than the speed of light to catch its original trajectory. Thus for an external observer, it looks like the wave remains unperturbed through the hidden object and the object simply does not exist to the observer, as illustrated in Figure 3.11.

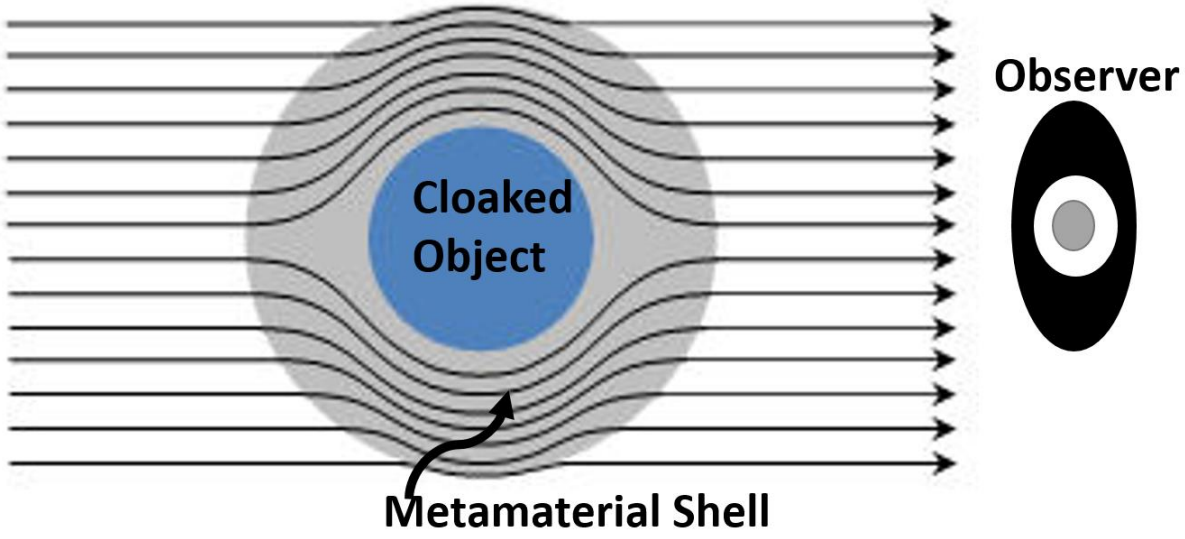

Figure 3.11. An electromagnetic cloak using a metamaterial shell.

The concept behind the cloak is to find a coordinate transformation which will take all space smaller than a given radius and shrink it to a point. To facilitate this kind of transformation, it is important to find an intermediate transformation between Cartesian and cloaking coordinates. Also, this process allows a coordinate transformation between two non-Cartesian coordinate systems which was very helpful and instrumental in taking forward other TE/TO works involving source transformations [55, 56]. One of the natural choices for this intermediate coordinate system is cylindrical coordinates, if one chooses to cloak a cylindrical object. Instead of a cylindrical object, one also can choose an elliptical cylindrical [57] and two-dimensional eccentric elliptical objects [58] to conceal. Here, we choose a cylindrical object to cloak for demonstration. The full derivation of the cloaking material parameters are included to explain and outline the conceptual design of a transformation electromagnetics/optics device involving intermediate coordinate transformations. The derivations here closely follow the works from [8].

Figure 3.12 explains the electromagnetic cloaking process steps-by-step. Firstly, the Cartesian coordinates are transformed to the cylindrical coordinate system. The cylindrical coordinates work as an intermediate coordinate system for this case. Then, cylindrical coordinates are transformed into cloaking coordinates defined by the cloaking transformation. This transformation shrinks all the area inside a cylindrical shell of some specific radius into a point. It is well accepted that one can retain material parameters using cylindrical coordinates, which introduces materials into the system. This makes the light waves bend around the concealed object. Finally, to complete the transformation process the material is retrieved in the Cartesian coordinate system, to maintain the form invariance of Maxwell's equations.

The coordinate transformation from Cartesian coordinates to cylindrical coordinates is given by:

$$r = \sqrt{x^2 + y^2}\,,$$

$$\theta = tan^{-1}(\frac{y}{x}), \tag{3.25}$$

$$z = z\,.$$

The Jacobian for this transformation is

$$A_1 = \begin{bmatrix} \frac{\partial r}{\partial x} & \frac{\partial r}{\partial y} & \frac{\partial r}{\partial z} \\ \frac{\partial \theta}{\partial x} & \frac{\partial \theta}{\partial y} & \frac{\partial \theta}{\partial z} \\ \frac{\partial z}{\partial x} & \frac{\partial z}{\partial y} & \frac{\partial z}{\partial z} \end{bmatrix}. \tag{3.26}$$

Now,

$$\frac{\partial r}{\partial x} = \frac{\partial}{\partial x}\left(\sqrt{x^2 + y^2}\right) = \frac{x}{\sqrt{x^2+y^2}} = \frac{x}{r} = cos\theta,$$

$$\frac{\partial r}{\partial y} = \frac{\partial}{\partial y}\left(\sqrt{x^2 + y^2}\right) = \frac{y}{\sqrt{x^2+y^2}} = \frac{y}{r} = sin\theta,$$

$$\frac{\partial r}{\partial z} = \frac{\partial}{\partial z}\left(\sqrt{x^2 + y^2}\right) = 0,$$

and

$$\frac{\partial \theta}{\partial x} = \frac{\partial}{\partial x}\left(tan^{-1}\left(\frac{y}{x}\right)\right) = -\frac{y}{x^2+y^2} = -\frac{\frac{y}{\sqrt{x^2+y^2}}}{\sqrt{x^2+y^2}} = -\frac{sin\theta}{r}.$$

Similarly, $\frac{\partial \theta}{\partial y} = \frac{cos\theta}{r}$, $\frac{\partial z}{\partial x} = 0$, $\frac{\partial z}{\partial y} = 0$, and $\frac{\partial z}{\partial z} = 1$.

Equation (3.26) can be re-written as the following:

$$A_1 = \begin{bmatrix} cos\theta & sin\theta & 0 \\ -\frac{sin\theta}{r} & \frac{cos\theta}{r} & 0 \\ 0 & 0 & 1 \end{bmatrix}, \tag{3.27}$$

where $|A_1| = 1$. The equations in table 2.1 result in the following material parameters:

$$\varepsilon' = \mu' = \frac{A\varepsilon A^T}{|A|} = \begin{bmatrix} r & 0 & 0 \\ 0 & \frac{1}{r} & 0 \\ 0 & 0 & r \end{bmatrix}. \tag{3.28}$$

The concealed object was chosen to be a spherical region of radius R_1 and the cloaking shell is considered to be compressed in a spherical shell of radius r' and the relationship is given as $R_1 < r < R_2$. The fields in the region $r < R_2$ are compressed into the region $R_1 < r < R_2$ using the following transformation:

$$R_1 < r < R_2 \begin{cases} r' = R_1 + \frac{r(R_2 - R_1)}{R_2} \\ \theta' = \theta \\ z' = z \end{cases} . \tag{3.29}$$

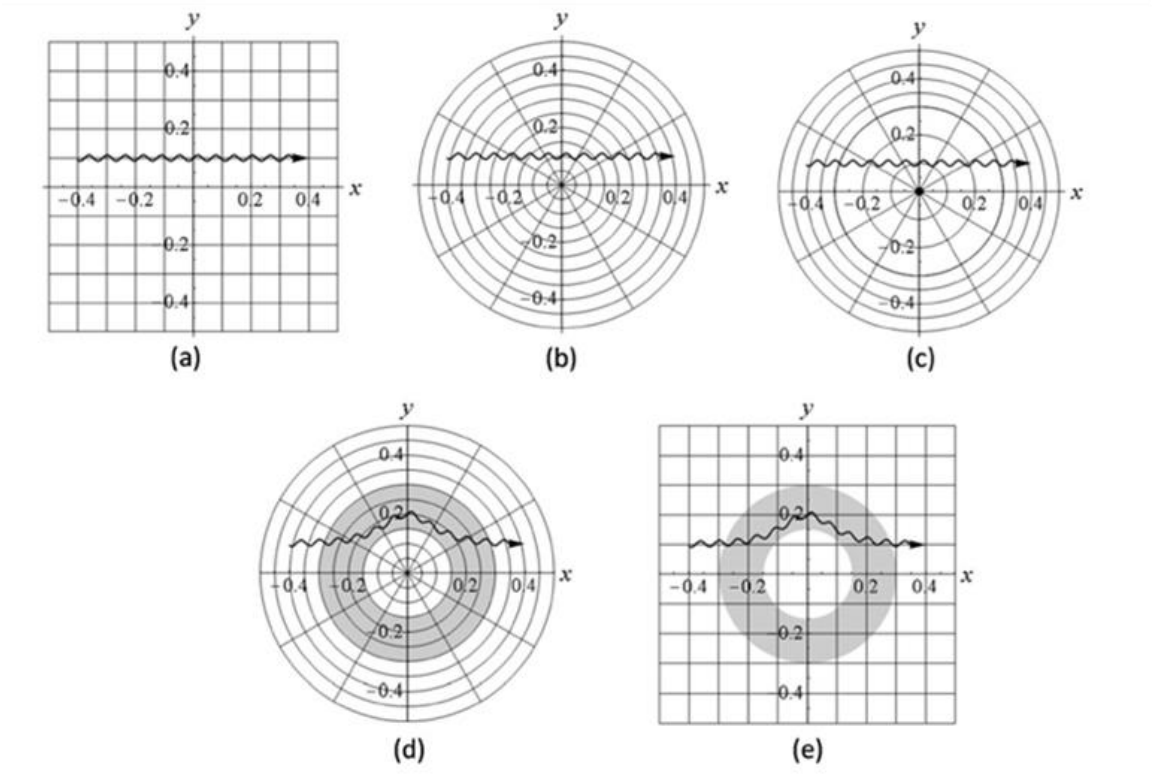

Figure 3.12. The step-by-step explanation of electromagnetic cloaking process [8], (a) a light beam in Cartesian coordinates (b) The Cartesian coordinates transformed into a cylindrical coordinates (c) intermediate coordinate transformation from cylindrical to cloaking space, until this point, the material parameters are not introduced and the light beam remains unchanged in its direction (d) the cloaking material is introduced and the light beam changes its direction and bent around the concealed region (e) to complete the transformation process the material was retrieved in the Cartesian coordinate system, to maintain the form invariance of Maxwell's equations.

Now the material parameters can be defined as (a) for region $r < R_1$, ε' and μ'can be any value. Actually, this region is the object, which will be concealed in the metamaterial shell; (b) for region $R_1 < r < R_2$, the material parameters need to be derived.

The Jacobian for the above transformation is

$$A_2 = \begin{bmatrix} \frac{\partial r'}{\partial r} & \frac{\partial r'}{\partial \theta} & \frac{\partial r'}{\partial z} \\ \frac{\partial \theta'}{\partial r} & \frac{\partial \theta'}{\partial \theta} & \frac{\partial \theta'}{\partial z} \\ \frac{\partial z'}{\partial r} & \frac{\partial z'}{\partial \theta} & \frac{\partial z'}{\partial z} \end{bmatrix}. \tag{3.30}$$

Here, $\frac{\partial r'}{\partial r} = \frac{\partial}{\partial r}\left\{R_1 + \frac{r(R_2 - R_1)}{R_2}\right\} = \frac{(R_2 - R_1)}{R_2}$, $\frac{\partial \theta'}{\partial \theta} = 1$, and $\frac{\partial z'}{\partial z} = 1$.

Equation (3.30) can be written as the following:

$$A_2 = \begin{bmatrix} \frac{(R_2 - R_1)}{R_2} & 0 & 0 \\ 0 & 1 & 0 \\ 0 & 0 & 1 \end{bmatrix}, |A_2| = \frac{(R_2 - R_1)}{R_2}. \tag{3.31}$$

This results in the material parameters

$$\varepsilon'' = \mu'' = \frac{A_2 \varepsilon' {A_2}^T}{|A_2|}$$

$$= \frac{1}{a} * \begin{bmatrix} a & 0 & 0 \\ 0 & 1 & 0 \\ 0 & 0 & 1 \end{bmatrix} * \begin{bmatrix} r & 0 & 0 \\ 0 & \frac{1}{r} & 0 \\ 0 & 0 & r \end{bmatrix} * \begin{bmatrix} a & 0 & 0 \\ 0 & 1 & 0 \\ 0 & 0 & 1 \end{bmatrix}$$

$$= \frac{1}{a} * \begin{bmatrix} ar & 0 & 0 \\ 0 & \frac{1}{r} & 0 \\ 0 & 0 & r \end{bmatrix} * \begin{bmatrix} a & 0 & 0 \\ 0 & 1 & 0 \\ 0 & 0 & 1 \end{bmatrix}$$

$$= \frac{1}{a} * \begin{bmatrix} a^2 r & 0 & 0 \\ 0 & \frac{1}{r} & 0 \\ 0 & 0 & r \end{bmatrix} \tag{3.32}$$

where $a = \frac{(R_2 - R_1)}{R_2}$.

Substituting $a = \frac{(R_2 - R_1)}{R_2}$ in (3.32) gives:

$$\varepsilon'' = \mu'' = \begin{bmatrix} \frac{r(R_2-R_1)}{R_2} & 0 & 0 \\ 0 & \frac{R_2}{r(R_2-R_1)} & 0 \\ 0 & 0 & \frac{rR_2}{(R_2-R_1)} \end{bmatrix}. \tag{3.33}$$

Substituting in with $r = \frac{R_2(r'-R_1)}{(R_2-R_1)}$, we get

$$\varepsilon'' = \mu'' = \begin{bmatrix} (r'-R_1) & 0 & 0 \\ 0 & \frac{1}{(r'-R_1)} & 0 \\ 0 & 0 & \frac{{R_2}^2(r'-R_1)}{(R_2-R_1)^2} \end{bmatrix}. \tag{3.34}$$

Until this point there were only coordinate transformations performed. Nothing has changed in the physics of the problem, i.e., if the inverse transformations were performed one would arrive at Cartesian coordinates with empty space. Another interpretation of this statement is that Maxwell's equations are form invariant in both the cylindrical and cloaking coordinates as long as the material parameters from (3.34) are maintained. Now, to introduce material into the system, the inverse of the cylindrical transformation is needed to be performed. Inverting the relations from cylindrical to Cartesian gives,

$$\begin{aligned} x &= rcos\theta, \\ y &= rsin\theta, \\ z &= z. \end{aligned} \tag{3.35}$$

The Jacobian for the inverse transformation is

$$A_3 = \begin{bmatrix} cos\theta & -rsin\theta & 0 \\ sin\theta & rcos\theta & 0 \\ 0 & 0 & 1 \end{bmatrix}, \tag{3.36}$$

where $|A_3| = r$.

The material parameters result in the following:

$$\varepsilon''' = \mu''' = \frac{A_3 \varepsilon'' {A_3}^T}{|A_3|}. \tag{3.37}$$

For inverse transformation, (3.34) can be written as the following:

$$\varepsilon'' = \mu'' = \begin{bmatrix} r - R_1) & 0 & 0 \\ 0 & \frac{1}{(r-R_1)} & 0 \\ 0 & 0 & \frac{{R_2}^2(r-R_1)}{(R_2-R_1)^2} \end{bmatrix}. \tag{3.38}$$

Substituting (3.38) into (3.37) gives

$$\varepsilon''' = \mu''' = \frac{1}{r} * \begin{bmatrix} cos\theta & -rsin\theta & 0 \\ sin\theta & rcos\theta & 0 \\ 0 & 0 & 1 \end{bmatrix} * \begin{bmatrix} r - R_1) & 0 & 0 \\ 0 & \frac{1}{(r-R_1)} & 0 \\ 0 & 0 & \frac{{R_2}^2(r-R_1)}{(R_2-R_1)^2} \end{bmatrix} * {A_3}^T$$

$$= \frac{1}{r} * \begin{bmatrix} (r-R_1)cos\theta & -\frac{rsin\theta}{(r-R_1)} & 0 \\ (r-R_1)sin\theta & \frac{rcos\theta}{(r-R_1)} & 0 \\ 0 & 0 & \frac{{R_2}^2(r-R_1)}{(R_2-R_1)^2} \end{bmatrix} * \begin{bmatrix} cos\theta & sin\theta & 0 \\ -rsin\theta & rcos\theta & 0 \\ 0 & 0 & 1 \end{bmatrix}$$

$$= \frac{1}{r} * \begin{bmatrix} (r-R_1)cos^2\theta + \frac{r^2sin^2\theta}{r-R_1} & (r-R_1)sin\theta cos\theta - \frac{r^2sin\theta cos\theta}{(r-R_1)} & 0 \\ (r-R_1)sin\theta cos\theta - \frac{r^2sin\theta cos\theta}{(r-R_1)} & (r-R_1)sin^2\theta + \frac{r^2cos^2\theta}{r-R_1} & 0 \\ 0 & 0 & \frac{{R_2}^2(r-R_1)}{(R_2-R_1)^2} \end{bmatrix}.$$

Then

$$\varepsilon''' = \mu''' = \begin{bmatrix} \frac{(r-R_1)}{r}cos^2\theta + \frac{rsin^2\theta}{(r-R_1)} & \frac{(r-R_1)}{r}sin\theta cos\theta - \frac{rsin\theta cos\theta}{(r-R_1)} & 0 \\ \frac{(r-R_1)}{r}sin\theta cos\theta - \frac{rsin\theta cos\theta}{(r-R_1)} & \frac{(r-R_1)}{r}sin^2\theta + \frac{rcos^2\theta}{(r-R_1)} & 0 \\ 0 & 0 & \frac{{R_2}^2(r-R_1)}{r(R_2-R_1)^2} \end{bmatrix}. \tag{3.39}$$

Then the final material parameters for cloaking an object are

$$\varepsilon''' = \mu''' = \begin{bmatrix} \varepsilon_r cos^2\theta + \varepsilon_\emptyset sin^2\theta & (\varepsilon_r - \varepsilon_\emptyset)cos\theta sin\theta & 0 \\ (\varepsilon_r - \varepsilon_\emptyset)cos\theta sin\theta & \varepsilon_\emptyset cos^2\theta + \varepsilon_r sin^2\theta & 0 \\ 0 & 0 & \frac{{R_2}^2(r-R_1)}{r(R_2-R_1)^2} \end{bmatrix}, \tag{3.40}$$

where, $\varepsilon_r = \mu_r = \frac{(r-R_1)}{r}$, $\varepsilon_\emptyset = \mu_\emptyset = \frac{r}{(r-R_1)}$, and $\varepsilon_r - \varepsilon_\emptyset = \frac{(r-R_1)}{r} - \frac{r}{(r-R_1)} = \frac{R_1(R_1-2r)}{r(r-R_1)}$. For region $r > R_2$, $\varepsilon' = \mu' = 1$. On the outer surface of the annulus ($r = R_2$), the material parameters can be described as a perfectly matched layer (PML), which makes the region reflectionless.

Figure 3.13 shows the full-wave simulations of electromagnetic cloaking using COMSOL Multiphysics. Figure 3.13a shows an unperturbed TE wave in free-space. A perfect electric conductor (PEC) was introduced in Figure 3.13b and significant scattering properties were observed. The metamaterial shell was introduced in Figure 3.13c and it was observed that the TE wave was guided around the inner cylinder and the scattering properties were significantly reduced. It is observed carefully there might be some scattering observed in Figure 3.13c. This is due to small numerical errors in simulations and can be reduced with very fine meshing.

Multiple-antenna technologies have gained much of attention in the recent past because of the huge gain they can introduce and the channel capacity levels in the modern day communication systems [59]. However, it poses some real challenges, such as, near-field mutual coupling effects that can drastically degrade the electrical parameters of the individual radiating antenna in multiple-antenna environments [60]. Various antenna design technologies [61, 62] have been proposed to reduce the severely adverse effects of scattering in multiple-antenna environment. Recent developments in transformation optics (TO)-based electromagnetic cloaking [13] yield a new direction towards solving antenna design problems in a multiple-antenna environment. Researchers also experimentally demonstrated the principles of cloaking in microwave frequencies for the first time using the new advancements in metamaterial technology [19]. In [63], researchers demonstrated a shielding technology using an eccentric elliptical cloak to restore the antenna parameters in a multi-element antenna environment. Based on similar motivation, an application of electromagnetic cloaking is presented here to reduce the adverse scattering effects of an

individual dipole antenna in a multiple-antenna environment in which the antenna operates, as shown in Figure 3.14.

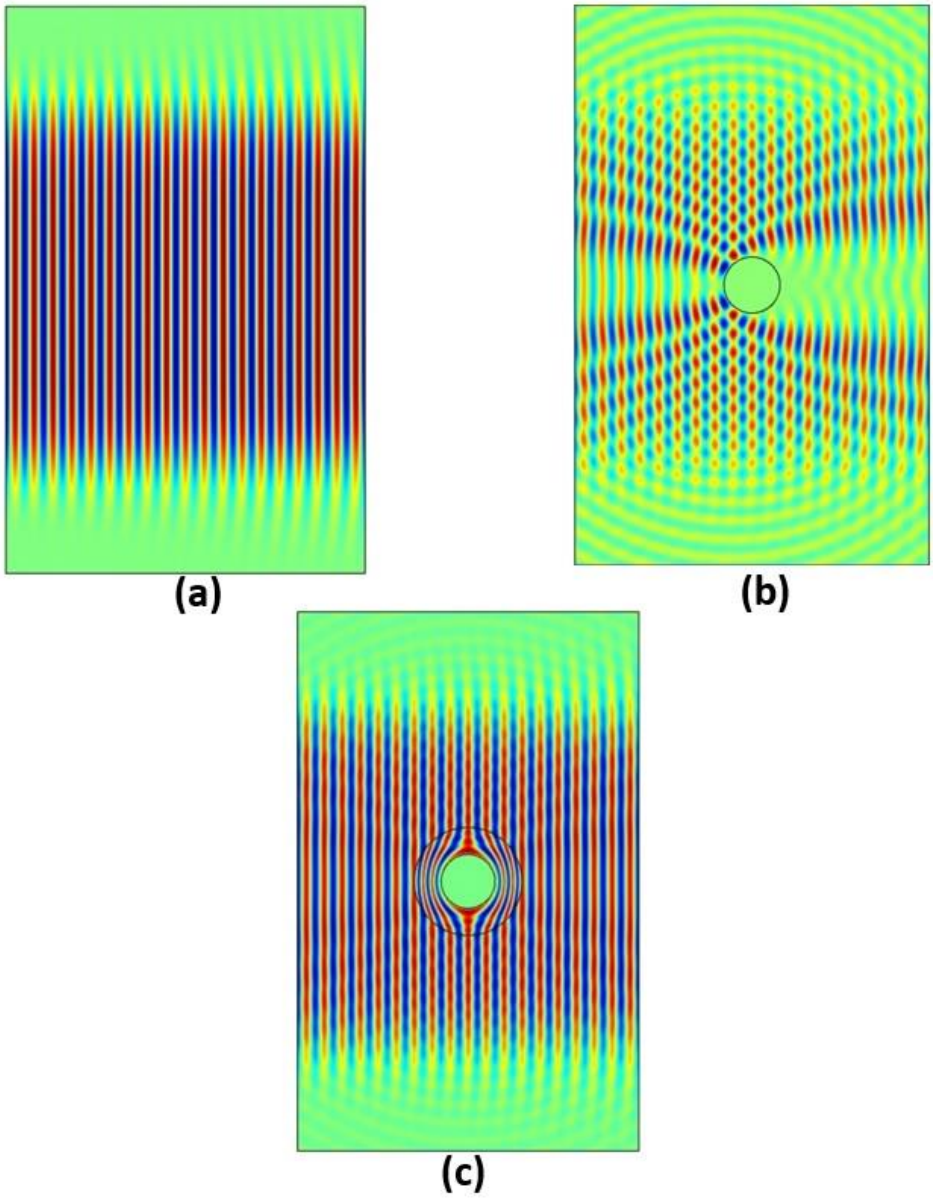

Figure 3.13. Full wave COMSOL simulations demonstrating electromagnetic cloaking of a concealed object. (a) an unperturbed TE wave in the free space, (b) a perfect electric conductor (PEC) is introduced and significant scattering properties observed, (c) a metamaterial shell is introduced around the cloaked object, and the wave bend around the object, thus mitigates the scattering significantly.

Specifically, it is shown that the distortion in a dipole antenna's radiation parameters due to the presence of other antennas in close proximity can be entirely restored by using a properly

designed cloaking region (shown as dotted grey circle in Figure 3.14). Full-wave electromagnetic simulations in COMSOL Multiphysics are used to demonstrate the performance of the antennas and cloaks in a multiple-antenna environment.

Next, consider N dipole antennas operating at N different frequencies concurrently located in close vicinity to each other. The dipole antennas are denoted as D_i and their corresponding frequencies are denoted as f_i ($i = 1, 2, 3 \ldots N$). Then, let the cloak C_i be designed with dispersive material parameters such that it works as a perfect cloak at different frequencies other than f_i and assumes free-space material parameters at f_i. That means if dipole antenna D_i is enclosed by the cloak C_i for all i, then each antenna will not see the presence of all other antennas and will behave as if there were no other antennas.

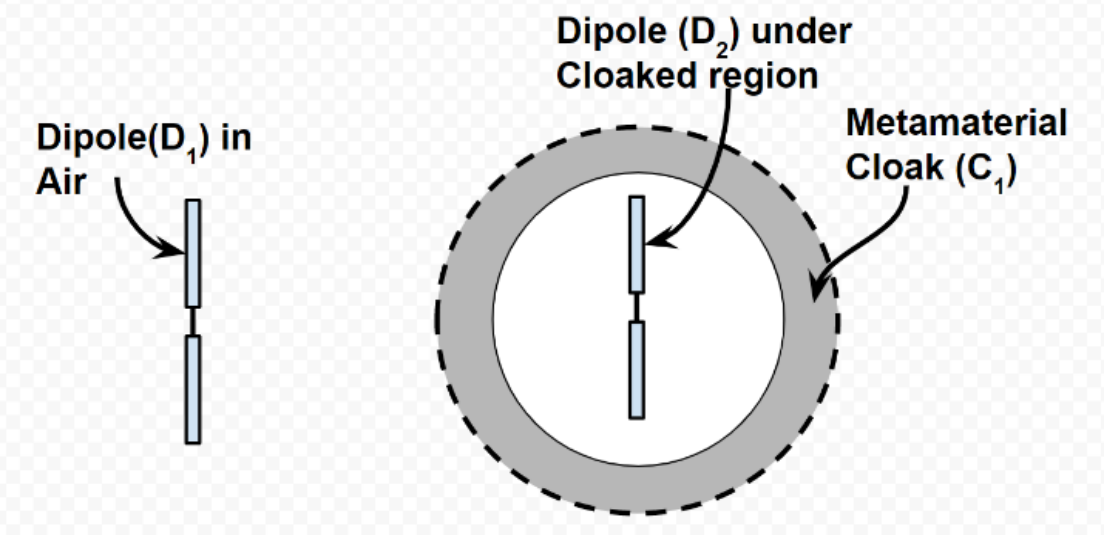

Figure 3.14. A multiple-antenna environment involving dipole antennas D_1 and D_2. D_1 radiates at frequency f_1 and D_2 radiates at frequency f_2.

This phenomenon is illustrated in Figure 3.14 with an example of two dipole antennas (D_1 and D_2) and a cylindrical metamaterial cloak C_1. The dipole element D_1 operating at frequency f_1 transmits and receives through air. An adjacent dipole antenna D_2 operating at frequency f_2 is enclosed by a cloak C_1, which is designed to cloak electromagnetic waves at frequency f_1. This

process can be reversed by enclosing antenna D_1 with the cloak C_1 and designing C_1 to cloak at frequency f_2. In our study, 2D line-dipole elements and 2D cylindrical cloak are utilized and finite-element analysis based COMSOL Multiphysics electromagnetic simulator was used to demonstrate the dispersion effects of multiple antennas and to investigate the effects of electromagnetic cloaking on the reduction of electromagnetic waves scattering. The current distribution of each dipole is approximated as the current distribution of a thin wire along $x = 0$ and is defined by taking the limit of a volume current to arrive at a sheet current density [55, 56].

The performance of the proposed dispersion reduction technique in multiple-antenna environments using electromagnetic cloaking was demonstrated through numerical solutions in the commercially available finite-element simulation software COMSOL Multi-physics ®, as shown in Figure 3.14. Figure 3.15 presents the three radiation scenarios involving two line dipole antennas D_1 and D_2 designed for operating at f_1 = 10 GHz and f_2 = 12 GHz, respectively. The lengths of D_1 and D_2 are 30 mm and 25 mm, respectively. The dipole D_1 is positioned in the origin and the dipole element D_2 was positioned at (75 mm, 0). The appropriate dimensions and the material parameters of the cylindrical electromagnetic cloak C_1 were adopted from [54] for a frequency of 10 GHz. The inner boundary radius of the cloak C_1 was 16 mm and the outer boundary radius was 30 mm. Figure 3.15a presents the y-component of electric field distribution when D_1 radiates in free-space and no other antennas were present. When D_1 radiates in the presence of unexcited antenna D_2, the near-filed radiation of D_1 was significantly perturbed and scattered by D_2, as shown as in Figure 3.15b. In Figure 3.15c, the dipole element D_2 was enclosed by the cloak C_2 and the antenna D_1 radiates in such a way as if there was no other antenna, which confirms the fact that cloaking of antenna D_2 significantly reduces the scattering effects. This is more evident from Figure 3.15d, which shows almost no field distribution outside the metamaterial

cloak when the difference between the fields in Figure 3.15a and Figure 3.15c was taken, validating the results further.

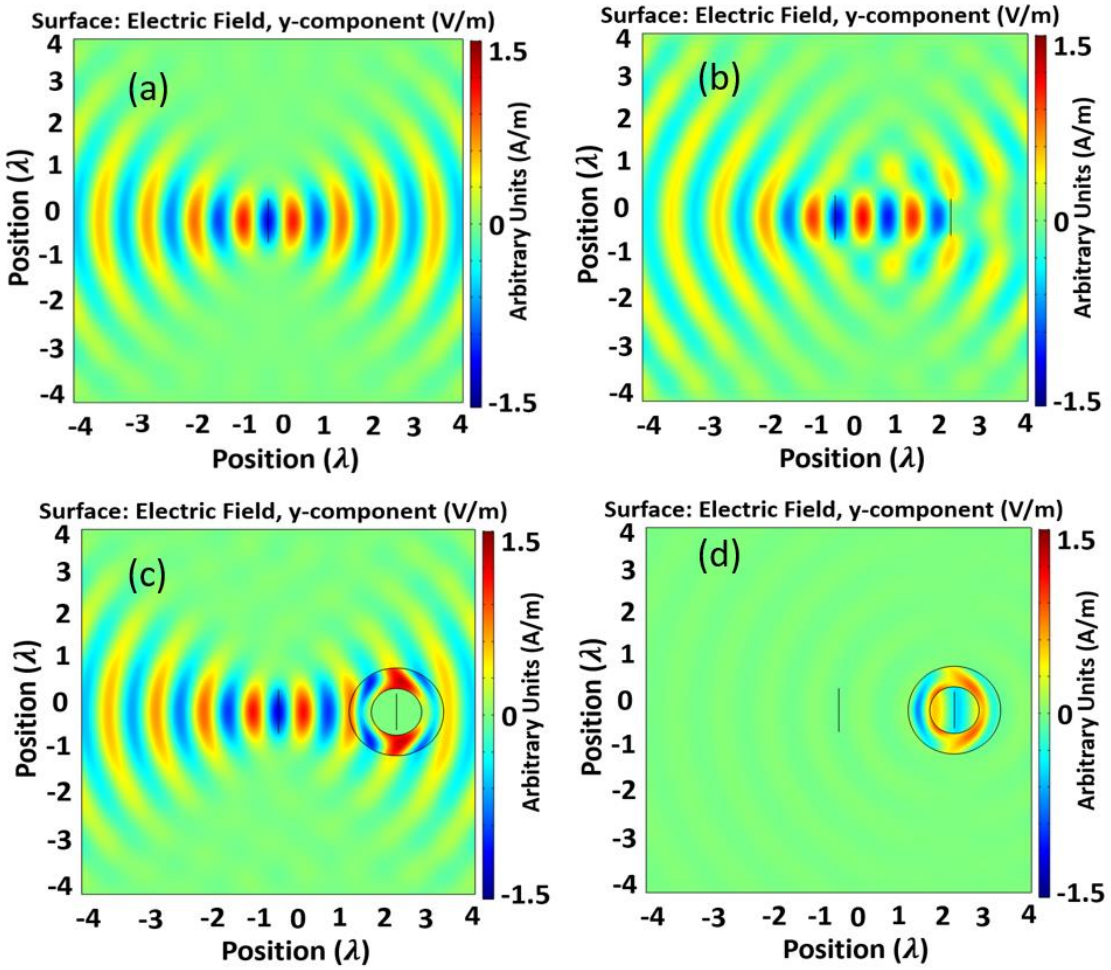

Figure 3.15. The y-component of the electric field of the dipole antenna element from: (a) dipole antenna (D_1) of length L = λ in free-space, (b) the electric field of dipole, D_1 got scattered significantly in the presence of another dipole, D_2, (c) the scattering of dipole, D_1 was significantly reduced when the dipole, D_2 is enclosed by cloak C_1, and (d) the difference between the fields (a) and (c).

Moreover, the far-field patterns of the three radiation scenarios are illustrated in Figure 3.16. The normalized pattern shows that the field patterns of the dipole D_1 in free-space and the field patterns of D_1 in the presence of unexcited dipole D_2 is significantly different, as the dispersion happens. It only gets restored when the dipole D_2 was enclosed by the cylindrical cloak C_1 to reduce the scattering effects.

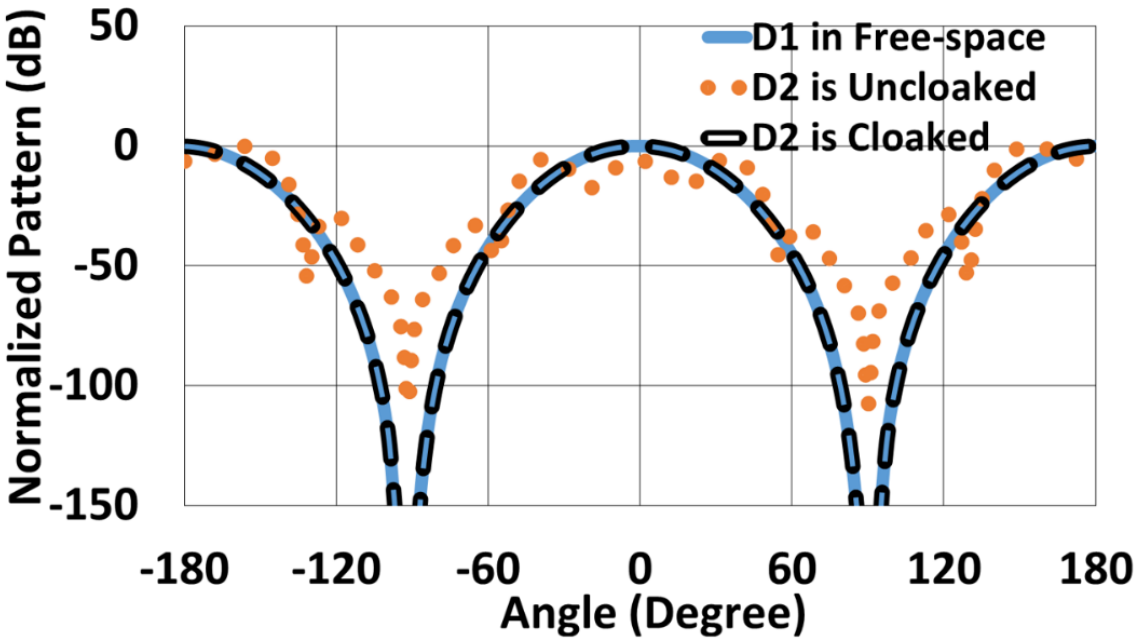

Figure 3.16. Normalized far-field radiation patterns of the dipole antennas in multiple-antenna environment.

4. A PHASED ARRAY ANTENNA WITH NEW ELEMENTS DESIGNED USING SOURCE TRANSFORMATIONS

In this chapter, transformation electromagnetics/optics (TE/TO) has been shown to be a useful technique in designing electromagnetic devices with very unique properties. Here, the concepts of transformation optics for single elements is extended to an array of "pinwheel" shaped elements for the first time. Through full-wave finite element analysis (FEA), it is shown that a transformed "pinwheel" linear array can be designed to operate identically to a uniformly spaced linear dipole array. Thus, the "pinwheel" antenna array will maintain all the advantages of array processing of a simple dipole antenna array. The proposed method has applications in structurally integrated and conformal phased arrays for wireless communications, radars, and sensing where structural and mechanical constrains do not align with antenna performance.

The same coordinate transformation technique can also be applied to a region with sources (e.g., current and charge distributions), where the sources will be transformed along with the material and behave exactly the same way as the original untransformed source [34, 55, 56]. The use of source transformations yields fascinating opportunities for the design of complex radiation structures by enabling the fabrication of unique structures with engineered material properties, allowing the transformed geometries to mimic the performance of original ones, which is especially useful when physical constraints require spatial changes to be made to the source. One of the first applications of this technique was suggested by Luo *et al.* [34], who transformed a dipole current source into a completely new distribution while preserving its properties as a dipole antenna. Kundtz *et al.* [55] took this concept further and introduced an optical source transformation using a "pinwheel" transformation, where they approximated the sheet current of a simple dipole as a volume current and transformed it to a new current distribution using a

"pinwheel" coordinate transformation. Based on these pioneering works, several conformal arrays have been proposed [64 - 66]. Popa *et al.* [64] proposed a conformal array design, where a nonuniform circular array radiates as a uniformly spaced linear array. Kwon [65] proposed a TO-based circular array design, which performs as a series of line sources embedded in a rectangular metamaterial media. However, these designs used "point" charges or electric line sources as the radiating sources in their numerical solution to validate their proposed concept. A more practical antenna source was not considered in these TO-based phased array designs.

Here, the source transformation approach is used to design a new linear array, where each individual antenna element is transformed from a single dipole element in free-space (as shown in Figure 4.1a). The result is an antenna array that radiates the same field as the linear dipole array depicted in Figure 4.1b. As shown in Figure 4.1a, the individual antenna element of the transformed linear array is a relatively extreme demonstration of a "pinwheel" shaped antenna which is transformed from a dipole antenna element similar to the transformation introduced in [55]. Furthermore, the transformed antenna element in the array is surrounded by a complex electromagnetic media as prescribed by the transformation (shown as dotted grey circle in Figure 4.1). Specifically, through numerical simulations, it is shown that a linear array of complex "pinwheel" antenna elements can perform as an array of linear dipole antennas in free-space for potential applications in structurally integrated and conformal phased arrays, where the antenna performance is a function of structural and mechanical restraints. The finite element analysis (FEA)-based full-wave simulations via COMSOL Multiphysics ® are used to numerically analyze and demonstrate the performance of the proposed TO-based antenna array for phased array scanning. The proposed "pinwheel" antenna array has potential applications in structurally

integrated and conformal phased array antennas where the antenna performance is a function of structural and mechanical restraints.

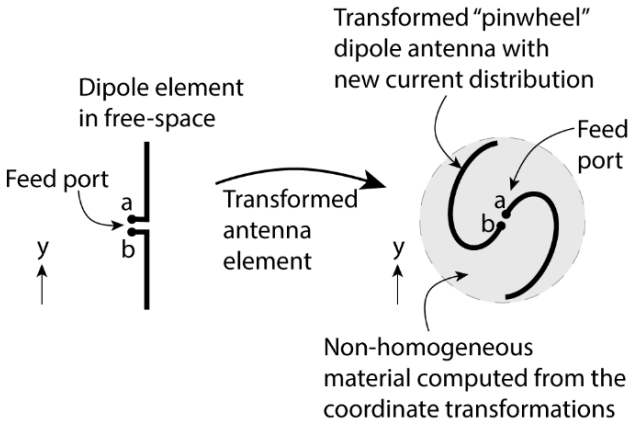

(a)

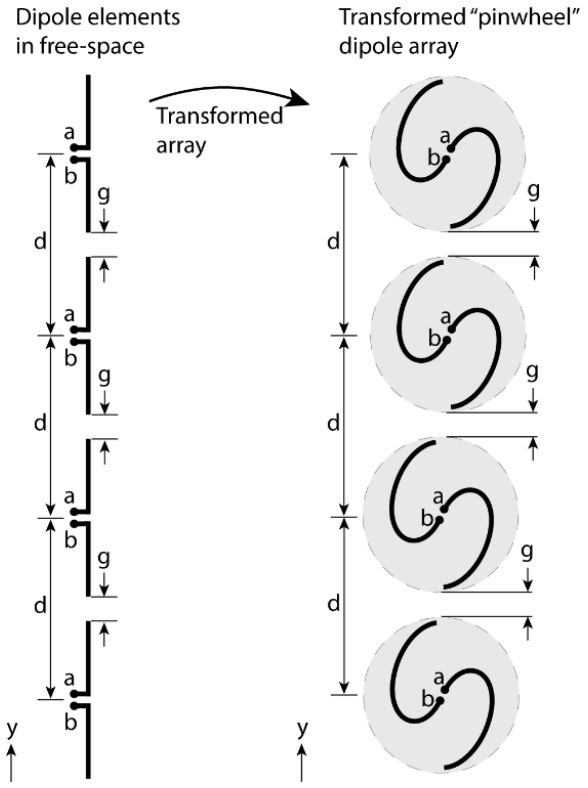

(b)

Figure 4.1. Proposed material-embedded antenna array using TO technique: (a) "pinwheel" transformation of a single dipole antenna element with TO-embedded media; (b) transformation of linear dipole array (reference array) (left) into a linear array of "pinwheel" antenna elements (right).

The “pinwheel” transformation shows that with the approach of the transformation electromagnetics/optics, it is possible to design electromagnetic structures and devices of many different complex and arbitrary geometries. Antennas designed in this way have many advantages compared to standard dipole antennas. A “pinwheel”-shaped antenna can be embedded into transformed regions to avoid interference, such as the cloak. The “pinwheel”-shaped antenna may also make use of the inherent properties of metamaterials to meet unique design parameters. For instance, a transformation designed antenna such as a “pinwheel”-shaped antenna may have less overall metal than a standard dipole antenna. The natural dispersion of metamaterials may then result in an antenna that interferes only very weakly at frequencies away from its frequency of operation. Under certain circumstances, the overall weight of the antenna may also be reduced compared to standard dipole antennas.

Next, consider the N-element dipole phased array along the y-axis represented in Figure 4.1b (left) and positioned in free-space, denoted as the “reference array”. Each of the elements in the “reference array” are equally spaced with the edge-to-edge distance between the elements of $g = \lambda/15$, where λ is the free-space wavelength at which the phased array is designed to operate. A two dimensional (2D) space is considered to illustrate the proposed “pinwheel” array.

The current distribution of each of the elements from the “reference array” is defined by $\boldsymbol{I_n} = \boldsymbol{J}.e^{i(n-1)\emptyset}$, where $\boldsymbol{J}$ is used to approximate the current distribution on a thin wire at $x = 0$ and $\mathrm{n} = 1,2 \ldots \mathrm{N}$, and $\emptyset$ is the phase between the adjacent antenna elements. In this case, an array of four elements is chosen to validate the proposed method. Each of the dipoles in the “reference array” is of $\lambda/2$ length spanning over a distance of 2.2λ. We intend to transform the reference array into a linear array of equidistant complex geometry antennas, where each antenna element of the “reference array” will be transformed into a “pinwheel”-shaped antenna, as shown in Figure

1b. The first task is to transform the individual dipole elements of the "reference array" into a "pinwheel"-shaped antenna element. The method of including sources using "pinwheel' transformation into transformation electromagnetics is described in the Figure 4.2 step-by-step.

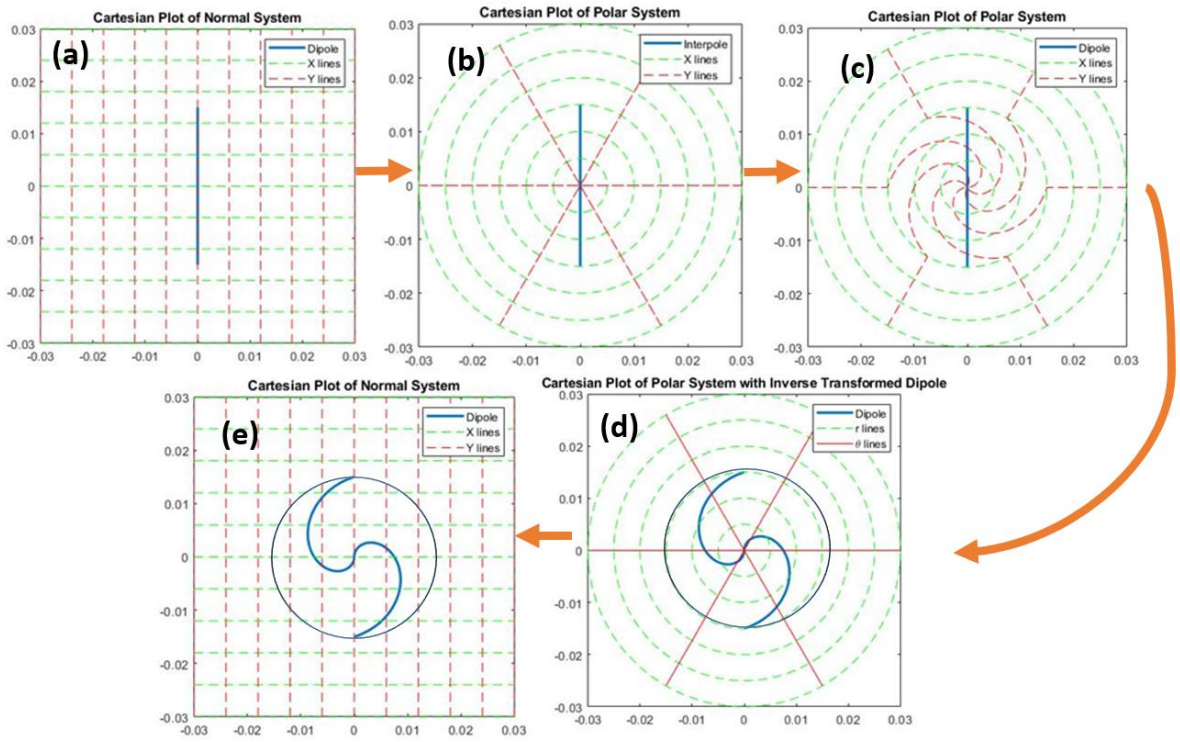

Figure 4.2. The source transformation technique using the line current of a dipole antenna [8, 55]: (a) the current is defined in a Cartesian coordinate system, (b) the current is transformed into a cylindrical coordinate system, (c) the current is transformed into the "pinwheel" coordinates, (d) the transformation is applied on the dipole line current, i.e., still the same current expression from (c) is used, but the "prime are dropped" ($\theta' \to \theta$ and $r' \to r$), (e) the current distribution is expressed in the original coordinates, i.e., in Cartesian coordinates. In (d) and (e), the circle refers to the material shell.

The material parameters for the space under transformation is given by Table 2.1 where

$$\boldsymbol{\varepsilon}' = \boldsymbol{\mu}' = \frac{A\varepsilon A^T}{det\, A}, \tag{4.1}$$

$A = \partial(x', y', z')/\partial(x, y, z)$ is the Jacobian matrix and A^T is transpose of the Jacobian matrix. The coordinate transform from Cartesian to cylindrical coordinates is defined by:

$$\rho = \sqrt{x^2 + y^2},$$

$$\theta = \arctan(\frac{y}{x}), \tag{4.2}$$

$$z = z.$$

The Jacobian of this transformation is

$$A1 = \begin{bmatrix} \cos(\theta) & \sin(\theta) & 0 \\ -\frac{\sin(\theta)}{\rho} & \frac{\cos(\theta)}{\rho} & 0 \\ 0 & 0 & 1 \end{bmatrix}, \tag{4.3}$$

where $|A1| = \frac{1}{\rho}$.

The material parameters can be derived as the following:

$$\varepsilon' = \mu' = \frac{A1*\varepsilon*A1^T}{|A1|} = \begin{bmatrix} \rho & 0 & 0 \\ 0 & \frac{1}{\rho} & 0 \\ 0 & 0 & \rho \end{bmatrix}. \tag{4.4}$$

The cylindrical to "Pinwheel" coordinates transformation is defined by following:

$$\rho' = \rho,$$

$$\theta' = \begin{cases} \theta & , \ \rho > R_1 \\ \theta + \Delta\theta \left(1 - \frac{\rho}{R_1}\right), & \rho < R_{1,} \end{cases} \tag{4.5}$$

and

$$z' = z.$$

The Jacobian for this transformation is

$$A2 = \begin{bmatrix} \frac{\partial\rho'}{\partial\rho} & \frac{\partial\rho'}{\partial\theta} & \frac{\partial\rho'}{\partial z} \\ \frac{\partial\theta'}{\partial\rho} & \frac{\partial\theta'}{\partial\theta} & \frac{\partial\theta'}{\partial z} \\ \frac{\partial z'}{\partial\rho} & \frac{\partial z'}{\partial\theta} & \frac{\partial z'}{\partial z} \end{bmatrix}. \tag{4.6}$$

Now,

$$\frac{\partial\rho'}{\partial\rho} = 1, \frac{\partial\rho'}{\partial\theta} = 0, \frac{\partial\rho'}{\partial z} = 0,$$

$$\frac{\partial\theta'}{\partial\rho} = \frac{\partial}{\partial\rho}\left\{\theta + \Delta\theta \left(1 - \frac{\rho}{R_1}\right)\right\} = \frac{\partial}{\partial\rho}\left(\theta + \Delta\theta - \frac{\Delta\theta\rho}{R_1}\right) = -\frac{\Delta\theta}{R_1}\left(\frac{\partial\rho}{\partial\rho}\right) = -\frac{\Delta\theta}{R_1},$$

$$\frac{\partial\theta'}{\partial\theta} = \frac{\partial}{\partial\theta}\left\{\theta + \Delta\theta\ \left(1 - \frac{\rho}{R_1}\right)\right\} = \frac{\partial\theta}{\partial\theta} = 1,$$

$$\frac{\partial\theta'}{\partial z} = 0,\ \frac{\partial z'}{\partial\rho} = 0, \frac{\partial z'}{\partial\theta} = 0, \text{and } \frac{\partial z'}{\partial z} = 1.$$

The (4.6) can be re-written as the following:

$$A2 = \begin{bmatrix} 1 & 0 & 0 \\ -\frac{\Delta\theta}{R_1} & 1 & 0 \\ 0 & 0 & 1 \end{bmatrix}, \tag{4.7}$$

where $|A2| = 1$.

The material parameters in the pinwheel coordinates can be derived as the following:

$$\varepsilon'' = \mu'' = \frac{A2 * \varepsilon' * A2^T}{|A2|}$$

$$= \begin{bmatrix} 1 & 0 & 0 \\ -\frac{\Delta\theta}{R_1} & 1 & 0 \\ 0 & 0 & 1 \end{bmatrix} * \begin{bmatrix} \rho & 0 & 0 \\ 0 & \frac{1}{\rho} & 0 \\ 0 & 0 & \rho \end{bmatrix} * \begin{bmatrix} 1 & -\frac{\Delta\theta}{R_1} & 0 \\ 0 & 1 & 0 \\ 0 & 0 & 0 \end{bmatrix}$$

$$= \begin{bmatrix} \rho & 0 & 0 \\ -\frac{\rho\Delta\theta}{R_1} & \frac{1}{\rho} & 0 \\ 0 & 0 & 1 \end{bmatrix} * \begin{bmatrix} 1 & -\frac{\Delta\theta}{R_1} & 0 \\ 0 & 1 & 0 \\ 0 & 0 & 0 \end{bmatrix}$$

$$= \begin{bmatrix} \rho & -\frac{\rho\Delta\theta}{R_1} & 0 \\ -\frac{\rho\Delta\theta}{R_1} & \frac{1}{\rho} + \frac{\rho\Delta\theta^2}{{R_1}^2} & 0 \\ 0 & 0 & 1 \end{bmatrix}. \tag{4.8}$$

In the "pinwheel" coordinates the material parameters from (4.8) can be written as:

$$\varepsilon'' = \mu'' = \begin{bmatrix} \rho' & -\frac{\rho'\Delta\theta}{R_1} & 0 \\ -\frac{\rho'\Delta\theta}{R_1} & \frac{1}{\rho'} + \frac{\rho'\Delta\theta^2}{{R_1}^2} & 0 \\ 0 & 0 & 1 \end{bmatrix}. \tag{4.9}$$

Now, to retrieve the material parameters in the Cartesian coordinate system, the inverse of the cylindrical transformation is used. Which allows us to realize the inverse relationship between the cylindrical and Cartesian coordinates.

The inverting relations are: $x = \rho cos\theta, y = \rho sin\theta$, and $z = z$. The Jacobian for this inverse transformation:

$$A3 = \begin{bmatrix} cos\theta & -\rho sin\theta & 0 \\ sin\theta & \rho cos\theta & 0 \\ 0 & 0 & 1 \end{bmatrix}, \tag{4.10}$$

where $|A3| = \rho$.

"Dropping the primes", (4.9) can be written as the following:

$$\varepsilon'' = \mu'' = \begin{bmatrix} \rho & -\frac{\rho\Delta\theta}{R_1} & 0 \\ -\frac{\rho\Delta\theta}{R_1} & \frac{1}{\rho} + \frac{\rho\Delta\theta^2}{{R_1}^2} & 0 \\ 0 & 0 & 1 \end{bmatrix}. \tag{4.11}$$

The material parameters can be derived as the following:

$$\varepsilon''' = \mu''' = \frac{A3 * \varepsilon'' * A3^T}{|A3|}$$

$$= \frac{1}{\rho} * \begin{bmatrix} cos\theta & -\rho sin\theta & 0 \\ sin\theta & \rho cos\theta & 0 \\ 0 & 0 & 1 \end{bmatrix} * \begin{bmatrix} \rho & -\frac{\rho\Delta\theta}{R_1} & 0 \\ -\frac{\rho\Delta\theta}{R_1} & \frac{1}{\rho} + \frac{\rho\Delta\theta^2}{{R_1}^2} & 0 \\ 0 & 0 & 1 \end{bmatrix} * \begin{bmatrix} cos\theta & sin\theta & 0 \\ -\rho sin\theta & \rho cos\theta & 0 \\ 0 & 0 & 1 \end{bmatrix}$$

$$= \frac{1}{\rho} * \begin{bmatrix} \rho cos\theta + \frac{\rho^2\Delta\theta sin\theta}{R_1} & -\frac{\rho\Delta\theta cos\theta}{R_1} + (-\rho sin\theta)(\frac{1}{\rho} + \frac{\rho\Delta\theta^2}{{R_1}^2}) & 0 \\ \rho sin\theta - \frac{\rho^2\Delta\theta cos\theta}{R_1} & -\frac{\rho\Delta\theta sin\theta}{R_1} + (\rho cos\theta)(\frac{1}{\rho} + \frac{\rho\Delta\theta^2}{{R_1}^2}) & 0 \\ 0 & 0 & 1 \end{bmatrix} * \begin{bmatrix} cos\theta & sin\theta & 0 \\ -\rho sin\theta & \rho cos\theta & 0 \\ 0 & 0 & 1 \end{bmatrix}$$

$$= \frac{1}{\rho} * \begin{bmatrix} \left(x + \frac{\rho\Delta\theta y}{R_1}\right) & -\left\{\frac{\Delta\theta x}{R_1} + y\left(\frac{1}{\rho} + \frac{\rho\Delta\theta^2}{{R_1}^2}\right)\right\} & 0 \\ \left(y - \frac{\rho\Delta\theta x}{R_1}\right) & -\left\{\frac{\Delta\theta y}{R_1} - x\left(\frac{1}{\rho} + \frac{\rho\Delta\theta^2}{{R_1}^2}\right)\right\} & 0 \\ 0 & 0 & 1 \end{bmatrix} * \begin{bmatrix} cos\theta & sin\theta & 0 \\ -\rho sin\theta & \rho cos\theta & 0 \\ 0 & 0 & 1 \end{bmatrix}$$

$$= \frac{1}{\rho} * \begin{bmatrix} A & B & 0 \\ C & D & 0 \\ 0 & 0 & 1 \end{bmatrix} * \begin{bmatrix} cos\theta & sin\theta & 0 \\ -\rho sin\theta & \rho cos\theta & 0 \\ 0 & 0 & 1 \end{bmatrix}, \tag{4.12}$$

where, inverting relations were used, and $A = \left(x + \frac{\rho\Delta\theta y}{R_1}\right)$, $B = -\left\{\frac{\Delta\theta x}{R_1} + y\left(\frac{1}{\rho} + \frac{\rho\Delta\theta^2}{{R_1}^2}\right)\right\}$, $C = \left(y - \frac{\rho\Delta\theta x}{R_1}\right)$, and $D = -\left\{\frac{\Delta\theta y}{R_1} - x\left(\frac{1}{\rho} + \frac{\rho\Delta\theta^2}{{R_1}^2}\right)\right\}$.

Equation (4.12) can be written as the following:

$$\varepsilon''' = \mu''' = \frac{1}{\rho} * \begin{bmatrix} A\cos\theta - B\rho\sin\theta & A\sin\theta + B\rho\cos\theta & 0 \\ C\cos\theta - D\rho\sin\theta & C\sin\theta + D\rho\cos\theta & 0 \\ 0 & 0 & 1 \end{bmatrix}$$

$$\varepsilon''' = \mu''' = \begin{bmatrix} (\frac{A\cos\theta}{\rho} - B\sin\theta) & (\frac{A\sin\theta}{\rho} + B\cos\theta) & 0 \\ (\frac{C\cos\theta}{\rho} - D\sin\theta) & (\frac{C\sin\theta}{\rho} + D\cos\theta) & 0 \\ 0 & 0 & 1/\rho \end{bmatrix}. \quad (4.13)$$

Now,

$$\frac{A\cos\theta}{\rho} - B\sin\theta = \frac{\left(x + \frac{\rho\Delta\theta y}{R_1}\right)\cos\theta}{\rho} + \left\{\frac{\Delta\theta x}{R_1} + y\left(\frac{1}{\rho} + \frac{\rho\Delta\theta^2}{{R_1}^2}\right)\right\}\sin\theta$$

$$= \left(x + \frac{\rho\Delta\theta y}{R_1}\right)\frac{\cos\theta}{\rho} + \left\{\frac{\Delta\theta x}{R_1} + \left(\frac{y}{\rho} + \frac{\rho y\Delta\theta^2}{{R_1}^2}\right)\right\}\sin\theta$$

$$= \frac{x\cos\theta}{\rho} + \frac{\rho\cos\theta\Delta\theta y}{R_1\rho} + \frac{x\sin\theta\Delta\theta}{R_1} + \frac{y\sin\theta}{\rho} + \frac{\rho\sin\theta y\Delta\theta^2}{{R_1}^2}$$

$$= \frac{x^2}{\rho^2} + \frac{xy\Delta\theta}{R_1\rho} + \frac{xy\Delta\theta}{R_1\rho} + \frac{y^2}{\rho^2} + \frac{y^2\Delta\theta^2}{{R_1}^2}$$

$$= \frac{{R_1}^2x^2 + 2R_1\rho xy\Delta\theta + {R_1}^2y^2 + \rho^2y^2\Delta\theta^2}{{R_1}^2\rho^2}$$

$$= \frac{{R_1}^2(x^2+y^2) + 2R_1\rho xy\Delta\theta + \rho^2y^2\Delta\theta^2}{{R_1}^2\rho^2}$$

$$= \frac{{R_1}^2\rho^2 + 2R_1\rho xy\Delta\theta + \rho^2y^2\Delta\theta^2}{{R_1}^2\rho^2}$$

$$= \frac{{R_1}^2\rho + 2R_1xy\Delta\theta + \rho y^2\Delta\theta^2}{{R_1}^2\rho}.$$

$$\therefore \frac{A\cos\theta}{\rho} - B\sin\theta = 1 + \frac{y*\Delta\theta(\frac{2R_1x}{\rho} + y*\Delta\theta)}{R_1^2}.$$

Then,

$$\frac{C\sin\theta}{\rho} + D\cos\theta = \left(y - \frac{\rho\Delta\theta x}{R_1}\right)\frac{\sin\theta}{\rho} - \left(\frac{y\Delta\theta}{R_1} - \frac{x}{\rho} - \frac{x\rho\Delta\theta^2}{{R_1}^2}\right)\cos\theta$$

$$= \frac{y\sin\theta}{\rho} - \frac{\rho\sin\theta\Delta\theta x}{R_1\rho} - \frac{y\Delta\theta\cos\theta}{R_1} + \frac{x\cos\theta}{\rho} + \frac{x\rho\cos\theta\Delta\theta^2}{{R_1}^2}$$

$$= \frac{y^2}{\rho^2} - \frac{xy\Delta\theta}{R_1\rho} - \frac{xy\Delta\theta}{R_1\rho} + \frac{x^2}{\rho^2} + \frac{x^2\Delta\theta^2}{{R_1}^2}$$

$$= \frac{{R_1}^2y^2 - 2R_1\rho xy\Delta\theta + {R_1}^2x^2 + \rho^2x^2\Delta\theta^2}{{R_1}^2\rho^2}$$

$$= \frac{{R_1}^2(x^2+y^2) - 2R_1\rho xy\Delta\theta + \rho^2x^2\Delta\theta^2}{{R_1}^2\rho^2}$$

$$= \frac{{R_1}^2\rho^2 - 2R_1\rho xy\Delta\theta + \rho^2x^2\Delta\theta^2}{{R_1}^2\rho^2}$$

$$= \frac{{R_1}^2\rho - 2R_1xy\Delta\theta + \rho x^2\Delta\theta^2}{{R_1}^2\rho}.$$

$$\therefore \frac{Csin\theta}{\rho} + Dcos\theta = 1 + \frac{x*\Delta\theta(-\frac{2R_1y}{\rho} + x*\Delta\theta)}{R_1^2}.$$

Then,

$$\frac{Asin\theta}{\rho} + Bcos\theta = \left(x + \frac{\rho\Delta\theta y}{R_1}\right)\frac{sin\theta}{\rho} - (\frac{\Delta\theta x}{R_1} + \left(\frac{y}{\rho} + \frac{\rho y\Delta\theta^2}{{R_1}^2}\right))cos\theta$$

$$= \frac{xsin\theta}{\rho} + \frac{\rho sin\theta\Delta\theta y}{R_1y} - \frac{xcos\theta\Delta\theta}{R_1} - \frac{ycos\theta}{\rho} - \frac{\rho cos\theta y\Delta\theta^2}{{R_1}^2}$$

$$= \frac{xy}{\rho^2} + \frac{y^2\Delta\theta}{R_1\rho} - \frac{x^2\Delta\theta}{R_1\rho} - \frac{xy}{\rho^2} - \frac{xy\Delta\theta^2}{{R_1}^2}$$

$$= \frac{{R_1}^2xy + R_1\rho y^2\Delta\theta - R_1\rho x^2\Delta\theta - {R_1}^2xy - \rho^2xy\Delta\theta^2}{{R_1}^2\rho^2}$$

$$= \frac{-\rho^2xy\Delta\theta^2 + R_1\rho\Delta\theta(y^2 - x^2)}{{R_1}^2\rho^2}$$

$$= \frac{-\rho^2xy\Delta\theta^2 + R_1\rho\Delta\theta(\rho^2sin^2\theta - \rho^2cos^2\theta)}{{R_1}^2\rho^2}$$

$$= \frac{-\rho^2xy\Delta\theta^2 - \rho^2(cos^2\theta - sin^2\theta)R_1\rho\Delta\theta}{{R_1}^2\rho^2}$$

$$= \frac{-\rho^2xy\Delta\theta^2 - \rho^2\cos(2\theta)R_1\rho\Delta\theta}{{R_1}^2\rho^2}$$

$$= \frac{-\rho^2(xy\Delta\theta^2 + R_1\rho\Delta\theta\cos(2\theta))}{{R_1}^2\rho^2}$$

$$= \frac{-(xy\Delta\theta^2 + R_1\rho\Delta\theta\cos(2\theta))}{{R_1}^2}.$$

$$\therefore \frac{Asin\theta}{\rho} + Bcos\theta = -\frac{\Delta\theta(xy\Delta\theta + R_1\rho\cos(2\theta))}{{R_1}^2}.$$

Then,

$$\frac{Ccos\theta}{\rho} - Dsin\theta = \left(y - \frac{\rho\Delta\theta x}{R_1}\right)\frac{cos\theta}{\rho} + \left(\frac{y\Delta\theta}{R_1} - \frac{x}{\rho} - \frac{x\rho\Delta\theta^2}{{R_1}^2}\right)sin\theta$$

$$= \frac{ycos\theta}{\rho} - \frac{\rho cos\theta\Delta\theta x}{R_1\rho} + \frac{ysin\theta\Delta\theta}{R_1} - \frac{xsin\theta}{\rho} - \frac{x\rho sin\theta\Delta\theta^2}{{R_1}^2}$$

$$= \frac{xy}{\rho^2} - \frac{x^2\Delta\theta}{R_1\rho} + \frac{y^2\Delta\theta}{R_1\rho} - \frac{xy}{\rho^2} - \frac{xy\Delta\theta^2}{{R_1}^2}$$

$$= -\frac{x^2\Delta\theta}{R_1\rho} + \frac{y^2\Delta\theta}{R_1\rho} - \frac{xy\Delta\theta^2}{{R_1}^2}$$

$$= \frac{-R_1x^2\Delta\theta + R_1y^2\Delta\theta - \rho xy\Delta\theta^2}{{R_1}^2\rho}$$

$$= \frac{-R_1\Delta\theta(x^2 - y^2) - \rho xy\Delta\theta^2}{{R_1}^2\rho}$$

$$= \frac{-R_1\Delta\theta(\rho^2cos^2\theta - \rho^2sin^2\theta) - \rho xy\Delta\theta^2}{{R_1}^2\rho}$$

$$= \frac{-\rho xy\Delta\theta^2 - \rho^2R_1\Delta\theta\cos(2\theta)}{{R_1}^2\rho}$$

$$= \frac{-\rho\Delta\theta(xy\Delta\theta + \rho R_1\cos(2\theta))}{{R_1}^2\rho}.$$

$$\therefore \frac{Ccos\theta}{\rho} - Dsin\theta = -\frac{\Delta\theta(xy\Delta\theta + R_1\rho\cos(2\theta))}{{R_1}^2}.$$

So, (4.13) can be written as the following, which represents the material parameters in Cartesian coordinates:

$$\varepsilon''' = \mu''' = \begin{pmatrix} 1 + \frac{y*\Delta\theta(\frac{2R_1x}{\rho} + y*\Delta\theta)}{R_1^2} & -\frac{\Delta\theta(xy\Delta\theta + R_1\rho cos(2\theta))}{R_1^2} & 0 \\ -\frac{\Delta\theta(xy\Delta\theta + R_1\rho cos(2\theta))}{R_1^2} & 1 + \frac{x*\Delta\theta(-\frac{2R_1y}{\rho} + x*\Delta\theta)}{R_1^2} & 0 \\ 0 & 0 & 1 \end{pmatrix}. \quad (4.14)$$

The material parameters from (4.14) was validated through numerical simulations in COMSOL Multiphysics. It is also worth noting that the results lead to a perfect impedance matching with no reflection at the boundaries of the material region and free space.

A transverse electromagnetic (TEM) wave of 10 GHz was used to validate the material parameters, as shown in Figure 4.3. Equation (4.14) also results in anisotropic and inhomogeneous permittivity and permeability tensors. Both electromagnetic parameters ε and μ have the same behavior, as shown in Figure 4.4. Such an anisotropic and inhomogeneous transformation medium can be realized by discrete metamaterials and structures such as periodic split ring resonators (SRRs) [67].

The current distribution of a dipole in Figure 4.1a along $x = 0$ was chosen to be [55]:

$$\bar{\boldsymbol{J}} = \begin{pmatrix} 0 \\ \frac{1}{\sqrt{\delta * \pi}} e^{-\frac{x^2}{\delta}} \\ 0 \end{pmatrix} = \begin{pmatrix} J_x \\ J_y \\ J_z \end{pmatrix}, \tag{4.15}$$

where the limit $\delta \to 0$ can be taken to approximate the above equation to the sheet current density and is set to be infinitesimally small relative to the length of the dipole. The half-wave dipole is initially defined by its current distribution in Cartesian coordinates and is converted into cylindrical coordinates to facilitate the transformation.

The transformed current density, $\boldsymbol{J}'$, under coordinate transformation is given by [16]:

$$\boldsymbol{J}' = \frac{A}{|A|}\boldsymbol{J}. \tag{4.16}$$

The coordinate transform from Cartesian to cylindrical coordinates is defined by:

$$\rho = \sqrt{x^2 + y^2},$$

$$\theta = \arctan(\frac{y}{x}), \tag{4.17}$$

and

$$z = z.$$

The Jacobian of this transformation is

$$A1 = \begin{bmatrix} \cos(\theta) & \sin(\theta) & 0 \\ -\frac{\sin(\theta)}{\rho} & \frac{\cos(\theta)}{\rho} & 0 \\ 0 & 0 & 1 \end{bmatrix}, \tag{4.18}$$

where $|A1| = \frac{1}{\rho}$.

The current in the cylindrical coordinates is then:

$$\bar{\boldsymbol{J_1}} = \frac{A_1}{|A_1|}\bar{\boldsymbol{J}}. \tag{4.19}$$

Now,

$$\frac{A_1}{|A_1|} = \rho \begin{bmatrix} \cos(\theta) & \sin(\theta) & 0 \\ -\frac{\sin(\theta)}{\rho} & \frac{\cos(\theta)}{\rho} & 0 \\ 0 & 0 & 1 \end{bmatrix}$$

$$= \begin{bmatrix} \rho\cos(\theta) & \rho\sin(\theta) & 0 \\ -sin\theta & cos\theta & 0 \\ 0 & 0 & \rho \end{bmatrix}.$$

So, we can write (4.19) as the following:

$$\bar{\boldsymbol{J_1}} = \begin{bmatrix} \rho\cos(\theta) & \rho\sin(\theta) & 0 \\ -sin\theta & cos\theta & 0 \\ 0 & 0 & \rho \end{bmatrix} * \begin{pmatrix} 0 \\ J_y \\ 0 \end{pmatrix},$$

$$= \begin{bmatrix} 0 + j_y\rho sin\theta + 0 \\ 0 + j_y cos\theta + 0 \\ 0 + 0 + 0 \end{bmatrix},$$

$$= J_y * \begin{bmatrix} \rho sin\theta \\ cos\theta \\ 0 \end{bmatrix}.$$

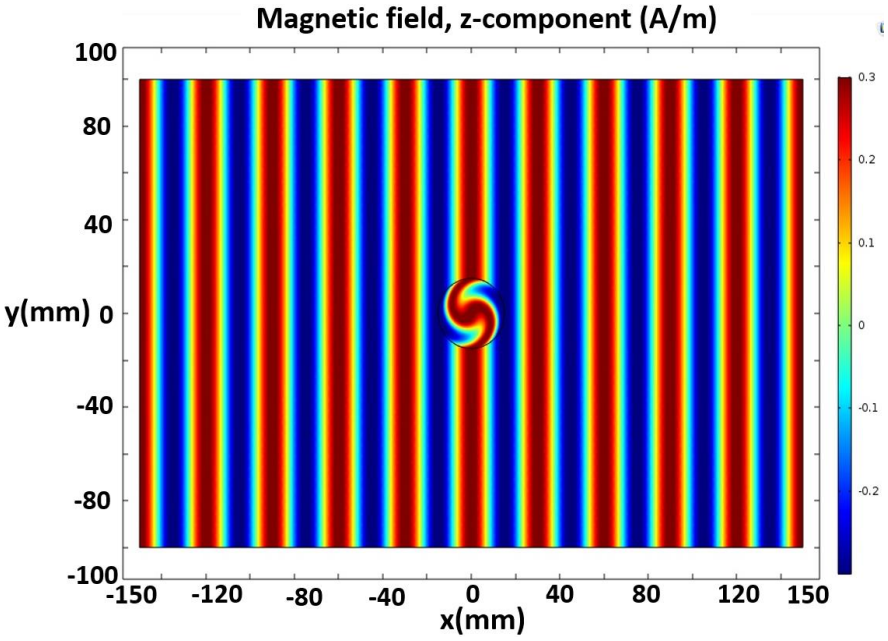

(a)

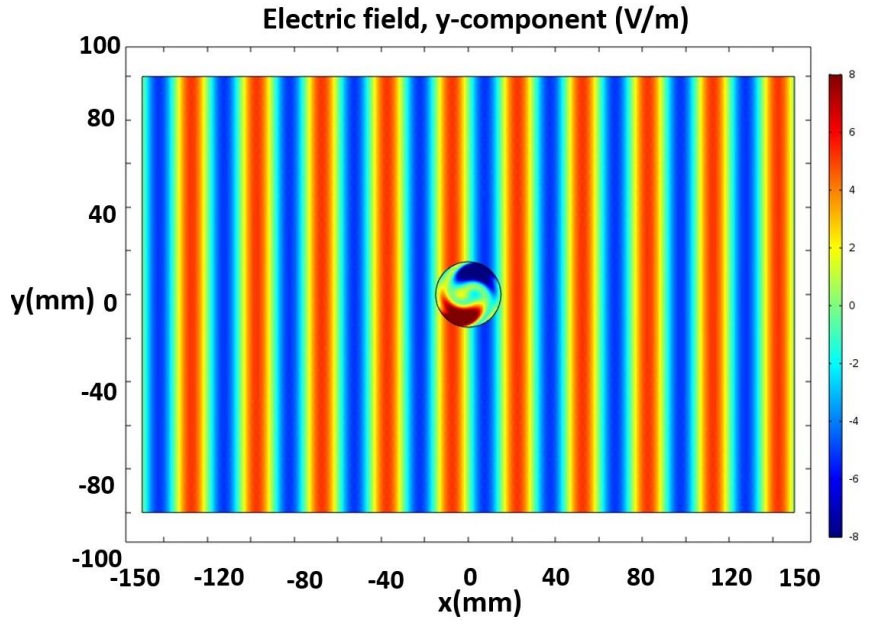

(b)

Figure 4.3. Perfect TEM wave with no scattering, verifying the material parameters are correct (a) z-component of magnetic field (b) y-component of electric field.

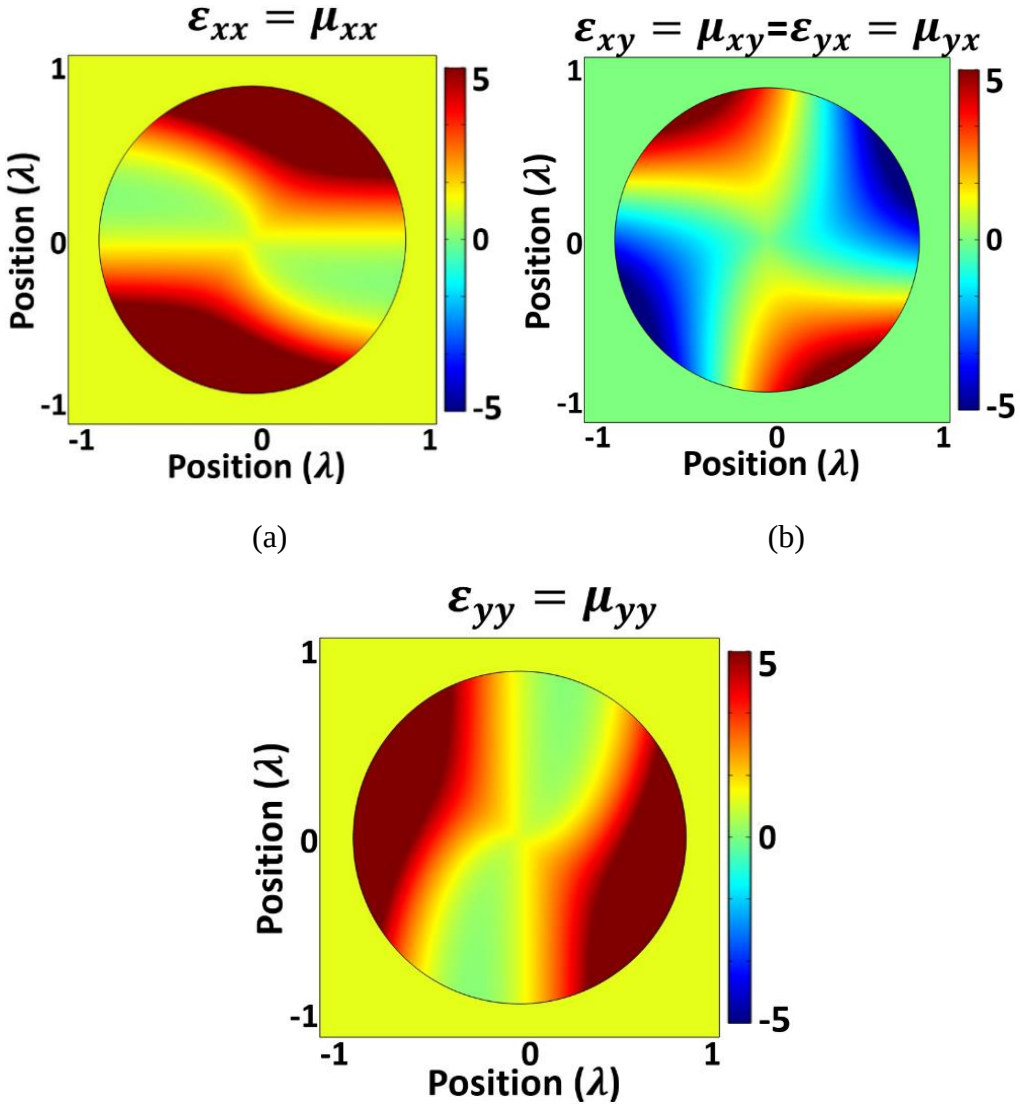

(a) (b)

(c)

Figure 4.4. Spatial variation of material parameters inside the shell (a) $\varepsilon_{xx} = \mu_{xx}$, (b) $\varepsilon_{xy} = \mu_{xy} = \varepsilon_{yx} = \mu_{yx}$, (c) $\varepsilon_{yy} = \mu_{yy}$. The material parameters ε_{xy}, μ_{xy}, ε_{yx}, and μ_{yx} are equal.

Also,

$$\frac{1}{\sqrt{\delta * \pi}} exp\left(-\frac{(\rho cos\theta)^2}{\delta}\right) * \begin{bmatrix} \rho sin\theta \\ cos\theta \\ 0 \end{bmatrix} = \mathbf{K} * \begin{bmatrix} \rho sin\theta \\ cos\theta \\ 0 \end{bmatrix}, \tag{4.20}$$

where, $\mathbf{K} = \frac{1}{\sqrt{\delta * \pi}} exp\left(-\frac{(\rho cos\theta)^2}{\delta}\right)$.

The Jacobian for the cylindrical to "pinwheel" coordinate transformations are given by (4.7) as:

$$A2 = \begin{bmatrix} 1 & 0 & 0 \\ -\frac{\Delta\theta}{R_1} & 1 & 0 \\ 0 & 0 & 1 \end{bmatrix}, \quad |A2| = 1.$$

Then the current in the "pinwheel" coordinates is:

$$\bar{J_2} = \frac{A_2}{|A_2|}\bar{J_1},$$

$$= \begin{bmatrix} 1 & 0 & 0 \\ -\frac{\Delta\theta}{R_1} & 1 & 0 \\ 0 & 0 & 1 \end{bmatrix} * \begin{bmatrix} \mathbf{K}\rho sin\theta \\ \mathbf{K}cos\theta \\ 0 \end{bmatrix}$$

$$= \begin{bmatrix} \mathbf{K}\rho sin\theta + 0 + 0 \\ -\frac{\Delta\theta}{R_1}\mathbf{K}\rho sin\theta + \mathbf{K}cos\theta + 0 \\ 0 \end{bmatrix}$$

$$= \begin{bmatrix} \mathbf{K}\rho sin\theta \\ \mathbf{K}cos\theta - \frac{\rho\Delta\theta}{R_1}\mathbf{K}sin\theta \\ 0 \end{bmatrix}$$

$$= \mathbf{K}\begin{bmatrix} \rho sin\theta \\ cos\theta - \frac{\rho\Delta\theta}{R_1}sin\theta \\ 0 \end{bmatrix}$$

$$= \mathbf{K}\begin{bmatrix} \rho sin\theta \\ \frac{R_1 cos\theta - \rho\Delta\theta sin\theta}{R_1} \\ 0 \end{bmatrix}$$

$$= \frac{\mathbf{K}}{R_1}\begin{bmatrix} R_1\rho sin\theta \\ R_1 cos\theta - \rho\Delta\theta sin\theta \\ 0 \end{bmatrix}.$$

Then

$$\bar{J_2} = \frac{1}{R_1\sqrt{\delta * \pi}} exp\left(-\frac{(\rho cos\theta)^2}{\delta}\right) * \begin{bmatrix} R_1\rho sin\theta \\ R_1 cos\theta - \rho\Delta\theta sin\theta \\ 0 \end{bmatrix}. \tag{4.21}$$

In "pinwheel" coordinates:

$$\rho' = \rho,$$

For $\rho < R_1$,

$$\theta' = \theta + \Delta\theta \left(1 - \frac{\rho'}{R_1}\right),$$

and

$$\theta = \theta' - \Delta\theta \left(1 - \frac{\rho'}{R_1}\right) = -\left\{\Delta\theta \left(1 - \frac{\rho'}{R_1}\right) - \theta'\right\} = -u'.$$

Substituting this into (4.21) gives

$$\bar{J_2} = \frac{1}{R_1\sqrt{\delta * \pi}} exp\left(-\frac{(\rho' \cos(-u'))^2}{\delta}\right) * \begin{bmatrix} R_1\rho'\sin(-u') \\ R_1\cos(-u') - \rho'\Delta\theta\sin(-u') \\ 0 \end{bmatrix}$$

$$= \frac{1}{R_1\sqrt{\delta*\pi}} exp\left(-\frac{(\rho' \cos(u'))^2}{\delta}\right) * \begin{bmatrix} -R_1\rho'\sin(u') \\ R_1 \cos(u') + \rho'\Delta\theta\sin(u') \\ 0 \end{bmatrix}, \qquad (4.22)$$

where, $u' = \left\{\Delta\theta \left(1 - \frac{\rho'}{R_1}\right) - \theta'\right\}$.

To retrieve the current in the Cartesian coordinates, it is essential to perform the inverse of the cylindrical transformation. The inverting relations are

$$x = \rho cos\theta,\ y = \rho sin\theta, \text{ and } z = z.$$

The Jacobian for this inverse transformation is:

$$A3 = \begin{bmatrix} cos\theta & -\rho sin\theta & 0 \\ sin\theta & \rho cos\theta & 0 \\ 0 & 0 & 1 \end{bmatrix},$$

where $|A3| = \rho$.

"Dropping the primes" the current in (4.22) can be written as:

$$\bar{J_2} = \frac{1}{R_1\sqrt{\delta * \pi}} exp\left(-\frac{(\rho \cos(u))^2}{\delta}\right) * \begin{bmatrix} -R_1\rho \sin(u) \\ R_1 \cos(u) + \rho\Delta\theta \sin(u) \\ 0 \end{bmatrix},$$

$$= \boldsymbol{B} * \begin{bmatrix} -R_1\rho si\, n(u) \\ R_1\, cos(u) + \rho\Delta\theta si\, n(u) \\ 0 \end{bmatrix}, \qquad (4.23)$$

where, $\boldsymbol{B} = \frac{1}{R_1\sqrt{\delta * \pi}} exp\left(-\frac{(\rho\cos(u))^2}{\delta}\right)$.

The currents can be derived as the following:

$$\bar{\boldsymbol{J_3}} = \frac{A_3}{|A_3|}\bar{\boldsymbol{J_2}},$$

$$= \frac{1}{\rho}\begin{bmatrix} cos\theta & -\rho sin\theta & 0 \\ sin\theta & \rho cos\theta & 0 \\ 0 & 0 & 1 \end{bmatrix} * \bar{\boldsymbol{J_2}}$$

$$= \begin{bmatrix} cos\theta/\rho & -sin\theta & 0 \\ sin\theta/\rho & cos\theta & 0 \\ 0 & 0 & 1/\rho \end{bmatrix} * \bar{\boldsymbol{J_2}}$$

$$= \boldsymbol{B} * \begin{bmatrix} cos\theta/\rho & -sin\theta & 0 \\ sin\theta/\rho & cos\theta & 0 \\ 0 & 0 & \frac{1}{\rho} \end{bmatrix} * \begin{bmatrix} -R_1\rho\sin(u) \\ R_1\cos(u) + \rho\Delta\theta\sin(u) \\ 0 \end{bmatrix}$$

$$= \boldsymbol{B} * \begin{bmatrix} \left(\frac{cos\theta}{\rho}\right)(-R_1\rho\sin(u)) + (-sin\theta)(R_1\cos(u) + \rho\Delta\theta\sin(u)) + 0 \\ (sin\theta/\rho)(-R_1\rho\sin(u)) + (cos\theta)(R_1\cos(u) + \rho\Delta\theta\sin(u)) + 0 \\ 0 + 0 + 0 \end{bmatrix}$$

$$= \boldsymbol{B} * \begin{bmatrix} \alpha \\ \beta \\ 0 \end{bmatrix} \tag{4.24}$$

where, $\alpha = \left(\frac{cos\theta}{\rho}\right)(-R_1\rho\sin(u)) + (-sin\theta)(R_1\cos(u) + \rho\Delta\theta\sin(u))$ and $\beta = (sin\theta/\rho)(-R_1\rho\sin(u)) + (cos\theta)(R_1\cos(u) + \rho\Delta\theta\sin(u))$.

Now,

$$\alpha = \left(\frac{cos\theta}{\rho}\right)(-R_1\rho\sin(u)) + (-sin\theta)(R_1\cos(u) + \rho\Delta\theta\sin(u)),$$

$$= -R_1\sin(u)cos\theta - R_1\cos(u)sin\theta - \rho\Delta\theta sin\theta\sin(u),$$

$$= -R_1(\sin(u)cos\theta + \cos(u)sin\theta) - \rho\Delta\theta sin\theta\sin(u),$$

$$= -R_1(\sin(u+\theta) - \rho\Delta\theta sin\theta\sin(u),$$

$$= -R_1(\sin(u+\theta) + \rho\Delta\theta sin\theta\sin(-u). \tag{4.25}$$

Now,

$$u = \left\{\Delta\theta\ \left(1 - \frac{\rho}{R_1}\right) - \theta\right\},$$

$$-u = \ -\left\{\Delta\theta\ \left(1 - \frac{\rho}{R_1}\right) - \theta\right\} = -\Delta\theta\left(-\frac{\rho}{R_1} + 1\right) + \theta = \Delta\theta\left(\frac{\rho}{R_1} - 1\right) + \theta.$$

Substituting this in (4.25) results in:

$$\alpha = -R_1\left(\sin(u + \theta) + \rho\Delta\theta sin\theta \sin\left(\Delta\theta\left(\frac{\rho}{R_1} - 1\right) + \theta\right)\right.$$

Again,

$$\beta = (sin\theta/\rho)(-R_1\rho\sin(u)) + (cos\theta)(R_1\cos(u) + \rho\Delta\theta\sin(u)),$$

$$= -R_1\sin(u)\,sin\theta + R_1\cos(u)\,cos\theta + \rho\Delta\theta\,\sin(u)\,cos\theta,$$

$$= R_1\left(\cos(u)\,cos\theta - \sin(u)\,sin\theta\right) + \rho\Delta\theta\sin(u)cos\theta,$$

$$= R_1\cos(u + \theta) + \rho\Delta\theta cos\theta\sin(u). \qquad (4.26)$$

So, (4.24) can be written as the following, which represents the transformed current distribution in the Cartesian coordinates

$$\bar{\boldsymbol{J_3}} = \frac{1}{R_1\sqrt{\delta * \pi}} exp\left(-\frac{(\rho\cos(u))^2}{\delta}\right) * \begin{pmatrix} -R_1\left(\sin(u + \theta) + \rho\Delta\theta sin\theta\sin(\Delta\theta\left(\frac{\rho}{R_1} - 1\right) + \theta)\right. \\ R_1\cos(u + \theta) + \rho\Delta\theta cos\theta\sin(u) \\ 0 \end{pmatrix}, \quad (4.27)$$

where $u = \ \Delta\theta\left(1 - \frac{\rho}{R_1}\right) - \theta$, $\rho = \sqrt{x^2 + y^2}$, and $\theta = \tan^{-1}\frac{y}{x}$.

The current distribution for the "pinwheel" antennas in the transformed array is $\boldsymbol{I'_n} = \bar{\boldsymbol{J_3}}.e^{i(n-1)\emptyset}$, where $n = 1,2 \ldots N$ and $\emptyset$ is the phase between the adjacent "pinwheel" antenna elements. It is important to note that the transformations do not affect the fundamental antenna quantities such as complex power and impedance [68]. It is desired that the "pinwheel" shape antenna has a radiation field pattern similar to the dipole antenna, but its impedance and complex power will be preserved under the "pinwheel" transformations. Now, the material parameters from (4.14) and the transformed current from (4.27) were used to transform each element of the "reference array" into a "pinwheel" antenna element and realize the linearly transformed

"pinwheel" antenna array, as shown in Figure 4.1b. The dimensions and edge-to-edge distance between the array elements were kept the same in the transformed "pinwheel" antenna array as in the "reference" linear dipole array. It is worth noting that while designing the "pinwheel" antenna elements of the transformed array, the current distribution from (4.27) and the material parameters from (4.14) were translated as the coordinates were no longer at the origin. The coordinates of the "pinwheel" elements changed along the y-direction, and the coordinates remained constant in the x-direction ($x_n = 0$).

To demonstrate the accuracy of the proposed theoretical model of the linear "pinwheel" antenna array, numerical simulations were performed in the commercially available finite-element analysis (FEA) software COMSOL Multi- physics®. The transformation electromagnetics/optics (TE/TO) approach often results in anisotropic, non-homogeneous, and complex material parameters in matrix form. COMSOL Multiphysics has the capability to validate works related to transformation electromagnetics/optics, as it allows the specification of material anisotropy and continuous inhomogeneity, as found in [55, 56] and [62 -66]. The work presented here adopts the validation process presented in [55, 56] and [62 -66] by comparing theory with COMSOL results. In the "pinwheel" transformation, along with the transformed current source from (4.27) and transformed material parameters from (4.14), the "pinwheel" shaped antenna geometry is also a function of the proposed transformation.

COMSOL Multiphysics has a unique functionality, which allows the definition of the complex "pinwheel" shaped geometry and material, as opposed to other commercially available full-wave tools. First, the single element, as shown in Figure 4.1a, was simulated to verify the transformed current from (4.27) and the transformed media from (4.14). Simulation results from a half-wave ($\lambda/2$) dipole antenna in free-space are shown in Figure 4.5a. A frequency of 10 GHz

was chosen. If the dipole is twisted by an angle of 180^0 without proper material compensation from (4.14), the field pattern changes significantly, which is demonstrated in Figure 4.5b. The field pattern is recovered outside the transformation media once the correct material is used from (4.14), which is illustrated in Figure 4.5c. The fields from the dipole in Figure 4.5a and the transformed "pinwheel" antenna in Figure 4.5c outside the material shell are the same. This is emphasized in Figure 4.5d, which shows almost no field distribution outside the transformation media when the difference between the two fields is taken. This also confirms that the current distribution in (4.14) is conserved under the "pinwheel" coordinate transformation in (4.27). It is also important to note that the meshing method used for the simulation is free-triangular. The mesh used in the simulation has over 45,000 elements to ensure convergence and accurate results and also to effectively approximate the continuous profiles given by equation (4.14). The minimum meshing element quality is 0.2694, the average element quality is 0.9154, and the element area ratio is 0.001049. The total mesh vertices are 22,555.

Figure 4.6 demonstrates the verification of the proposed transformed antenna array design. Figure 4.6a represents the electric field of the reference dipole antenna array as described in Figure 4.1b. The phase difference between any two adjacent elements is set to 90^0 to scan the beam at an angle $\theta_s = 22.5^0$. For a fair comparison, Figure 4.6b demonstrates the electric field distribution radiated by the transformed "pinwheel" linear array, where the "pinwheel" antenna elements are not enclosed by the material parameters defined by (4.14). The fields in Figure 4.6b are significantly different from that radiated by the original linear dipole array in Figure 4.6a. Figure 4.6c shows the electric field distribution radiated by the proposed "pinwheel" antenna array, where each antenna element is enclosed by the transformation medium from (4.14) and the current distribution is given by (4.27).

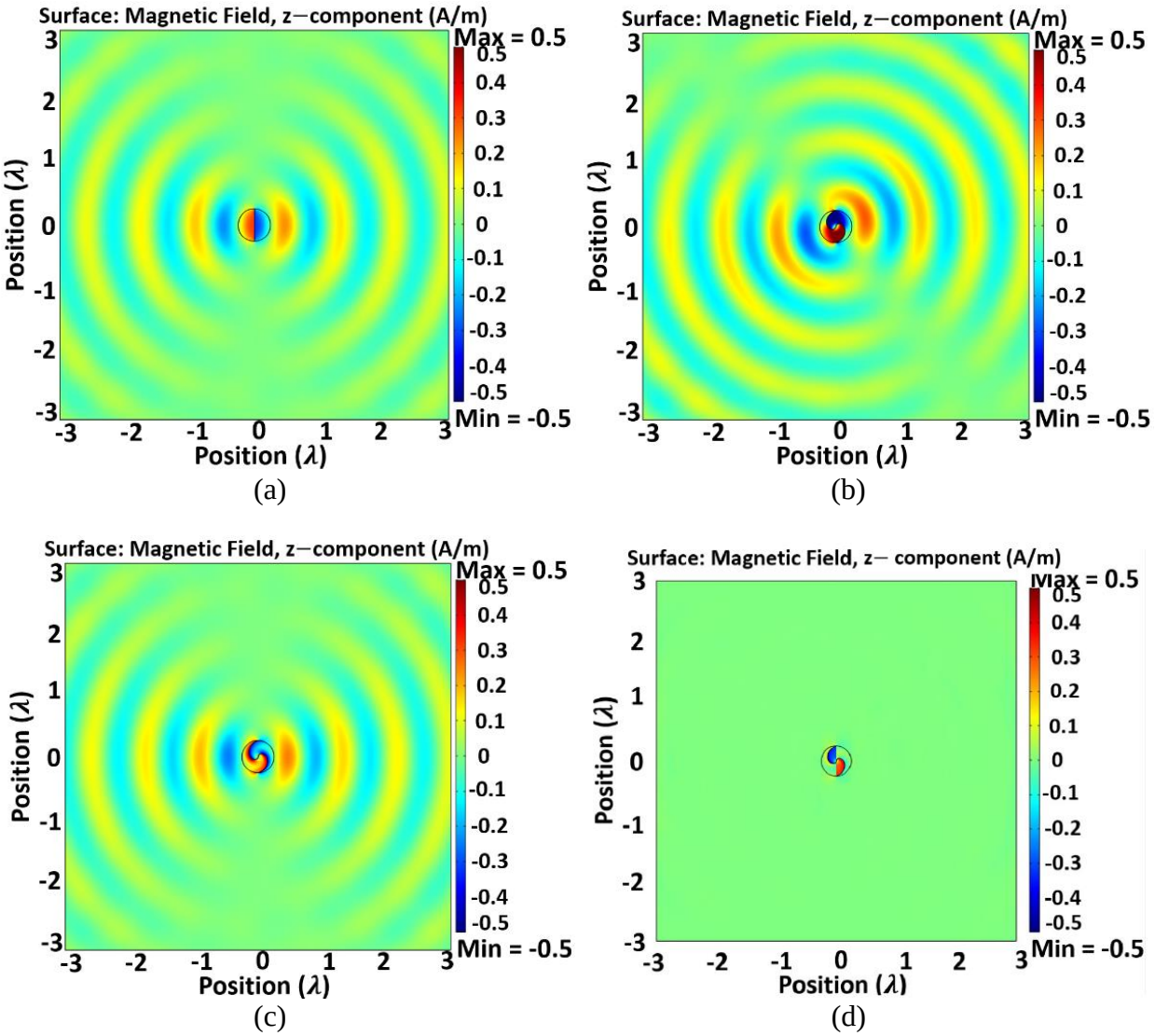

Figure 4.5. The z-component of the magnetic field of single antenna element from: (a) dipole antenna of length $L = \lambda/2$ in free-space; (b) dipole that has undergone a "pinwheel" rotation of $\Delta\theta = 180^0$ without any material compensation from equation (4.14); (c) dipole that has undergone a "pinwheel" rotation of $\Delta\theta = 180^0$ with proper material compensation from equation (4.14); and (d) the difference between the fields (a, c).

The phase difference between any two adjacent "pinwheel" elements is kept the same as the "reference array". The simulation results show that the radiated fields by the transformed "pinwheel" linear array (Figure 4.6c) and the reference dipole array (Figure 4.6a) are virtually identical. To further verify the design, the difference between the two fields is shown in Figure

4.6d, which clearly shows that there is almost zero field distribution around the array after subtraction of field in Figure 4.6c from the field in Figure 4.6a.

Furthermore, the far-fields of the "reference dipole array" and the transformed "pinwheel" array are simulated and illustrated in Figure 4.7. As shown in Figure 4.7, the normalized radiation patterns of the reference array and the transformed "pinwheel" array are almost the same when each element of the "pinwheel" array is enclosed by the transformed medium, however are different when the elements are not compensated with proper material parameters. Figure 4.7b shows the normalized radiation pattern at a scan angle $\theta_s = 11.25^0$. The phase difference between any two adjacent elements is set to 45^0, as set in the original dipole array.

Metamaterials are good candidates for realizing the non-homogeneous and anisotropic material parameters from (4.14) to implement the proposed "pinwheel' array. In metamaterial realizations, losses may be a restraining factor in practical implementation [64–66]. Considering the losses in practical materials, numerical simulations were performed introducing different values of loss tangents ($\tan\delta$) for a scan angle $\theta_s = 22.5^0$, as shown in Figure 4.8. Loss was incorporated in the simulations by replacing ε_{yy} with $(\varepsilon_{yy} - j|\varepsilon_{yy}|tan\,\delta)$ [65, 66, 69]. Similar modifications were made to other material tensor parameters. Figure 4.8 shows that the antenna performance degrades with the increase of loss factor. With the loss tangent reduced to only 0.1, the effect of loss is almost unnoticeable. No significant differences were observed in the range $tan\,\delta \leq 0.01$. With loss tangents of 0.1, 03, and 0.5, the lossy material is still effective, excepting for the reduction of the electric field magnitude.

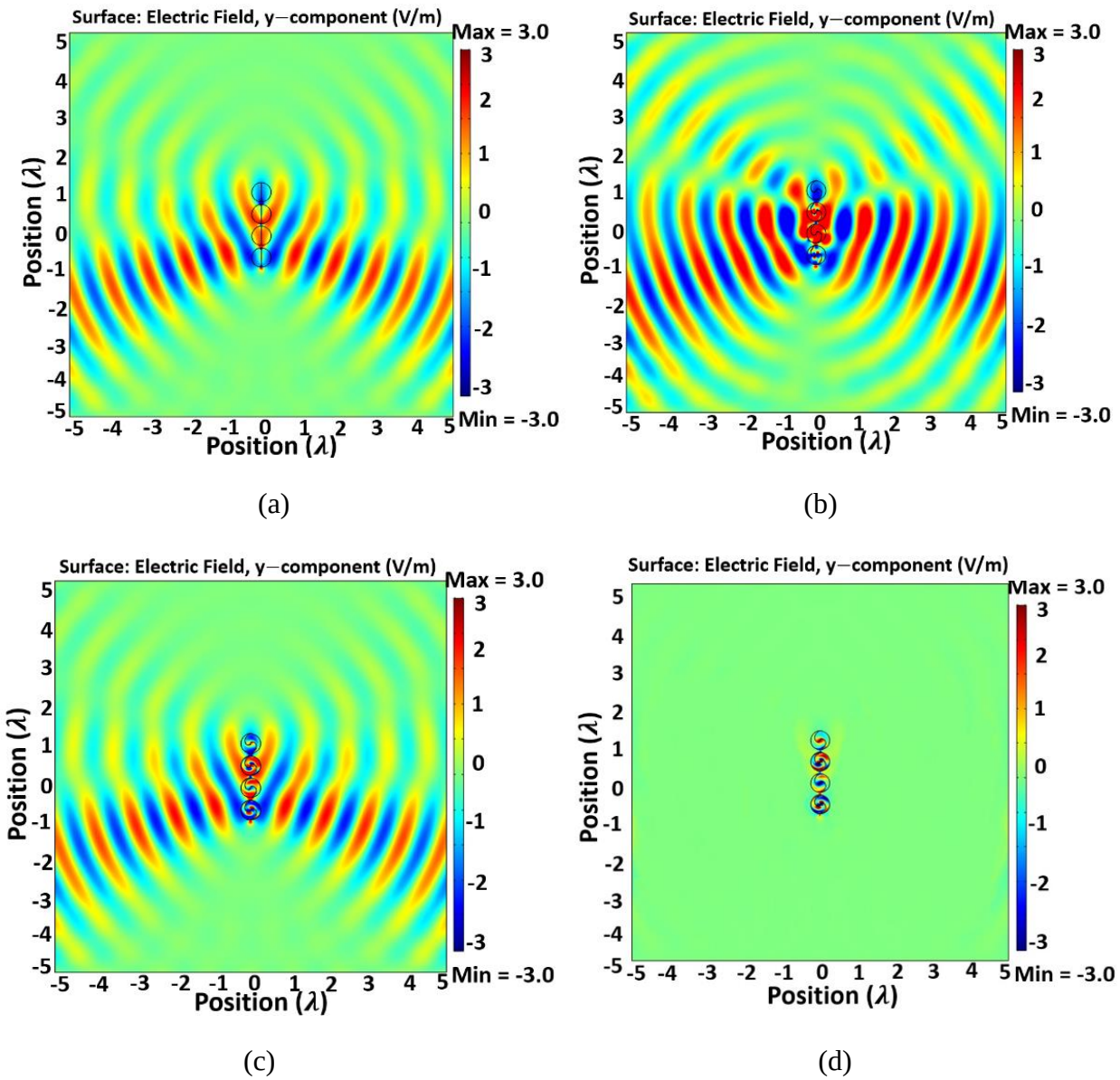

Figure 4.6. Total electric field distributions for three different array configurations for a scan angle of $\theta_s = 22.5^0$ for (a) reference/original dipole antenna linear array, (b) "pinwheel" antenna array without any material compensation, (c) material-embedded "pinwheel" shaped antenna linear array, and (d) difference between the electric fields in (a) and (c).

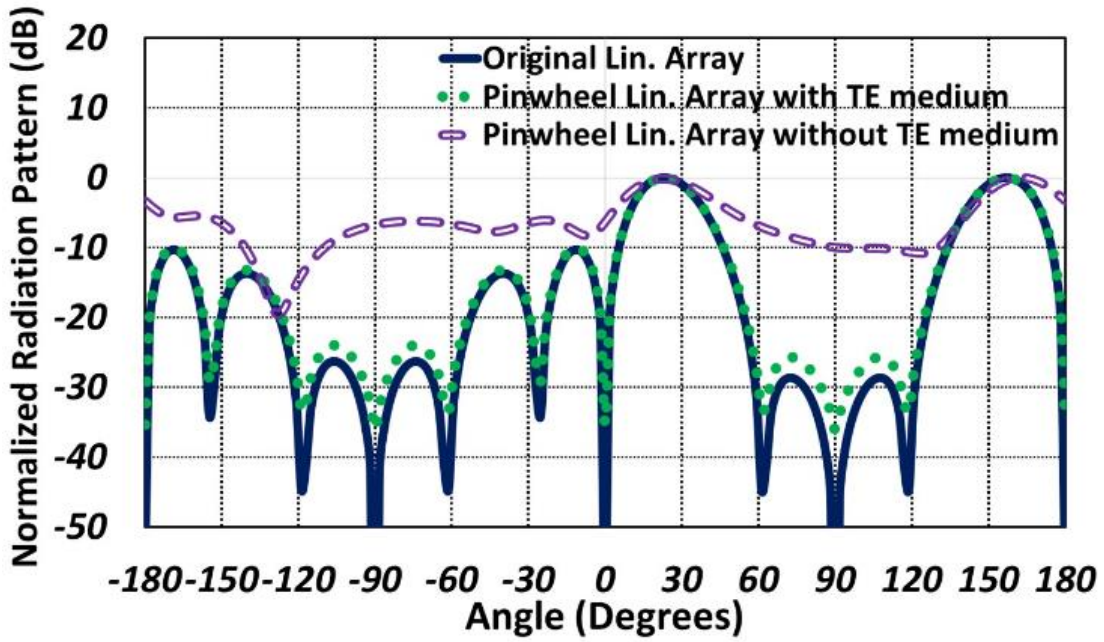

(a)

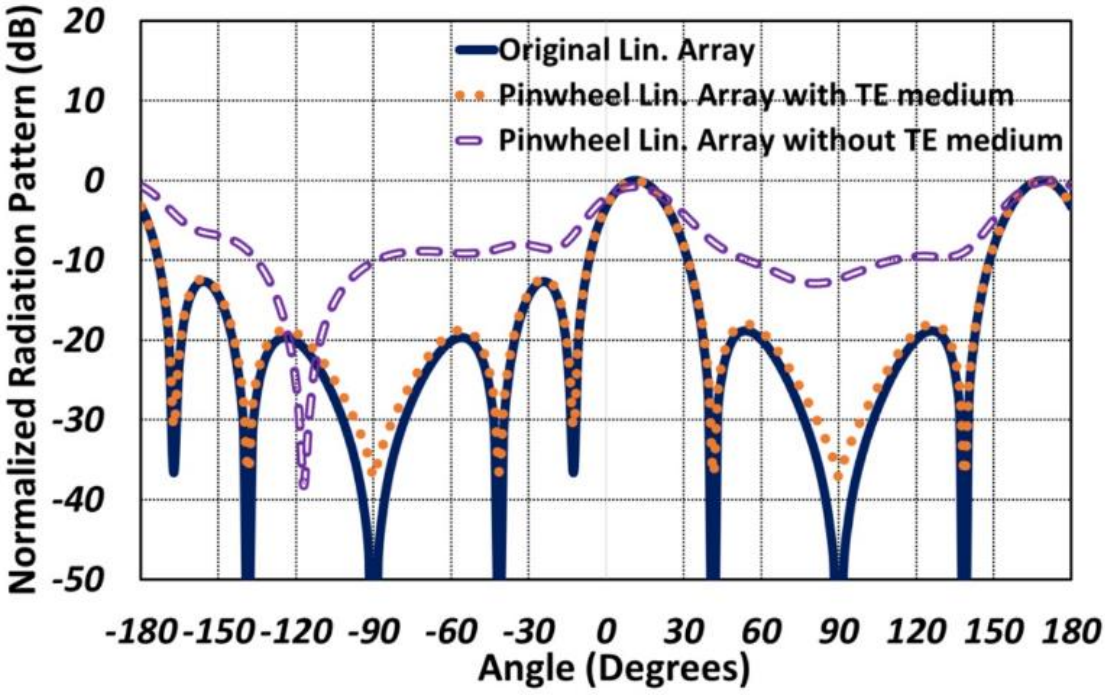

(b)

Figure 4.7. Far-field radiation patterns for three different array configurations at scan angles of (a) $\theta_s = 22.5^0$ and (b) $\theta_s = 11.25^0$.

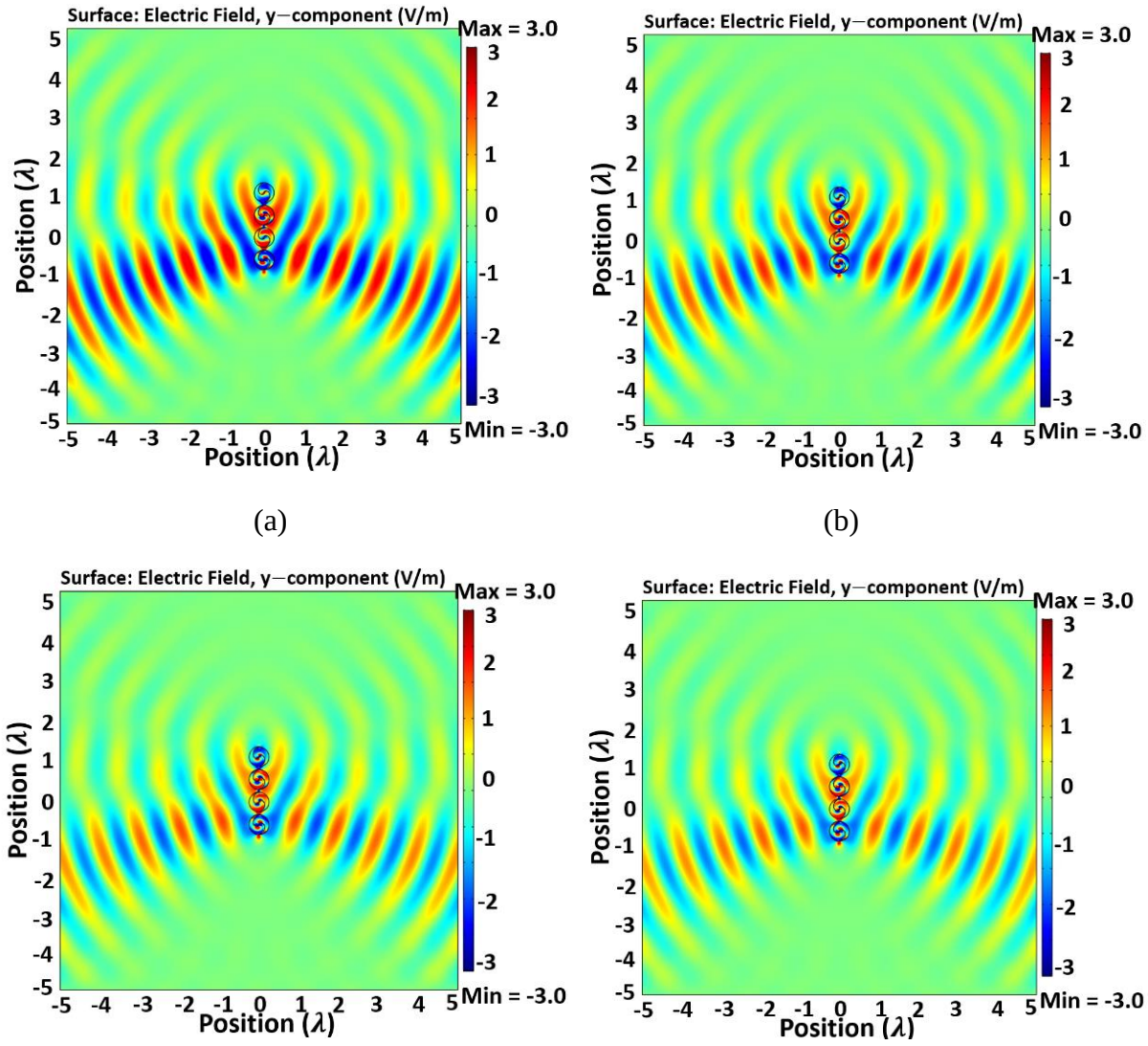

Figure 4.8. The electric fields for the proposed TO-based "pinwheel" array for different values of loss factor ($tan\,\delta$) (**a**) $tan\,\delta = 0.01$; (**b**) $tan\,\delta = 0.1$; (**c**) $tan\,\delta = 0.3$; (**d**) $tan\,\delta = 0.5$.

Overall, it has been shown how the transformation electromagnetics/optics technique can be employed to transform a linear dipole array into an array of complex geometry antennas, where the individual elements of the transformed array are "pinwheel"-shaped antennas transformed from dipole antenna elements. The transformed parameters are derived, and through full-wave simulations, it is shown that the original linear dipole array and the transformed "pinwheel" linear array have the same behaviors in some specified region, verifying the correctness and effectiveness

of the proposed array. It is believed that the proposed array will have tremendous potential for future applications in structurally integrated and conformal phased arrays for wireless communications, radars, and sensing where structural and mechanical constraints do not align with antenna performance.

5. COORDINATE TRANSFORMATIONS-BASED ANTENNA ELEMENTS EMBEDDED IN A METAMATERIAL SHELL WITH SCANNING CAPABILITIES

In this chapter, the TE/TO technique has been employed to realize a non-homogeneous, anisotropic material-embedded beam-steerer using both a single antenna element and an antenna array without phase control circuitry. Initially through theory and validation with numerical simulations it is shown that beam-steering can be achieved in an arbitrary direction by enclosing a single antenna element with the transformation media. Then, this is followed by an array with fixed voltages and equal phases enclosed by transformation media. This enclosed array is scanned and the proposed theory is validated through numerical simulations. Furthermore, through full-wave simulations it is shown that a horizontal dipole antenna embedded in a metamaterial can be designed such that the horizontal dipole performs identically to a vertical dipole in free-space. Similarly, it is also shown that a material-embedded horizontal dipole array can perform as a vertical dipole array in free-space, all without the need of a phase shifter network. These methods have applications in scanning for wireless communications, radars, beam-forming, and steering.

As it is well established that the concepts of transformation optics (TO) [13, 14] have been used to control the propagation characteristics of electromagnetic (EM) fields in interesting and useful ways by using regions of non-homogeneous, anisotropic materials. The TO technique leads to implementation of unconventional electromagnetic devices [69 - 76] using novel wave-matter interactions computed with coordinate transformations that exhibit unconventional and unusual propagation characteristics. Phased array antennas have garnered significant interest in wireless communications applications due to their capability of changing the shape and direction of the radiation pattern without physically moving the antennas. This technique is often referred to as beam-steering and can be accomplished by rotating the antenna elements or changing the relative

phases of the radio-frequency (RF) signals driving the elements. Beam-steering of a phased array antenna is often a challenging task because it involves synthesis of multiple antenna elements and integration of control circuits, including solid-state phase shifters [35] and beam-forming networks [36], to control or guide the beam in a desired direction, as shown in Figure 5.1a. Recently, researchers showed that the TO technique could be useful to control the beam in a specific direction using coordinate transformation-based non-homogeneous material regions. Rahm *et al* [29] showed how to design a beam shifter using TO. Utilizing a similar idea, researchers in [51, 74] proposed a set of beam-shifters to avoid obstacles in the beam path. In [75], researchers experimentally showed a TO- based lens for beam control at microwave frequencies. This pioneering research paved the way for beam-steering of antennas using the TO technique. The concepts of TO were later expanded to design unique antennas [55, 56] and phased array antennas for different conformal applications [64 - 66]. In [76], it is shown the techniques of TO can be utilized to manipulate EM fields and rotate them in a specified direction.

This approach can thus be used to control radiation characteristics of an antenna element (as shown in Figure 5.1b), or an antenna array in free-space and to rotate it in a desired direction, hence realizing a beam-steerer using TO-based media. This specific TO approach results in material properties which require active tuning to achieve beam-steering, but significant advancements and attention given to reconfigurable material properties, specifically in tunable constitutive parameters (permittivity and permeability), could in the future allow for practical implementation of novel beam-steering techniques [77 – 80]. Misra *et al* [77] demonstrated electrically tunable permittivity in $BaTiO_3$ under DC bias conditions. In [78], researchers showed the influence of DC bias and temperature on the dielectric permittivity to achieve switchable dielectric permittivity in a semifluorinated azobenzene. Significant research has been done also to

control the permeability of materials. In [79] researchers proposed microfluidic split-ring resonators inside a flexible elastomeric material to achieve reconfigurable effective permeability. Agarwal *et al* [80] demonstrated the preparation of adaptive hybrid capsules with microgel/SiO_2 composite walls with tunable shell permeability.

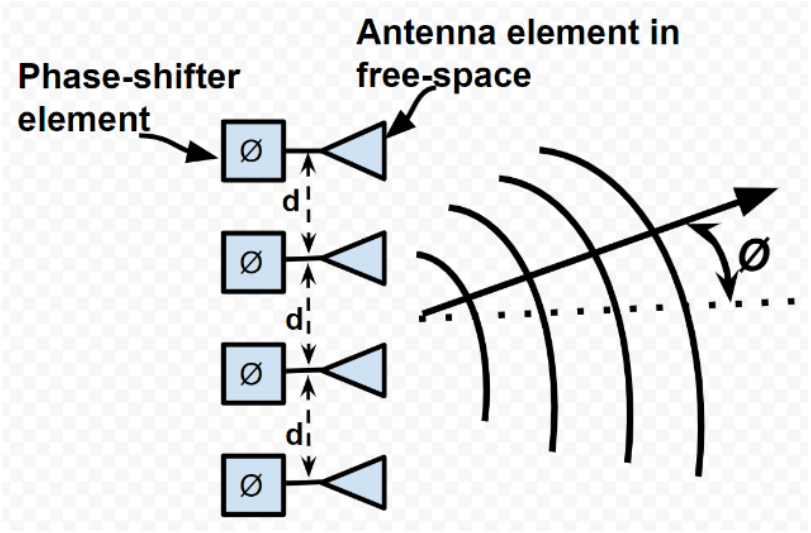

(a)

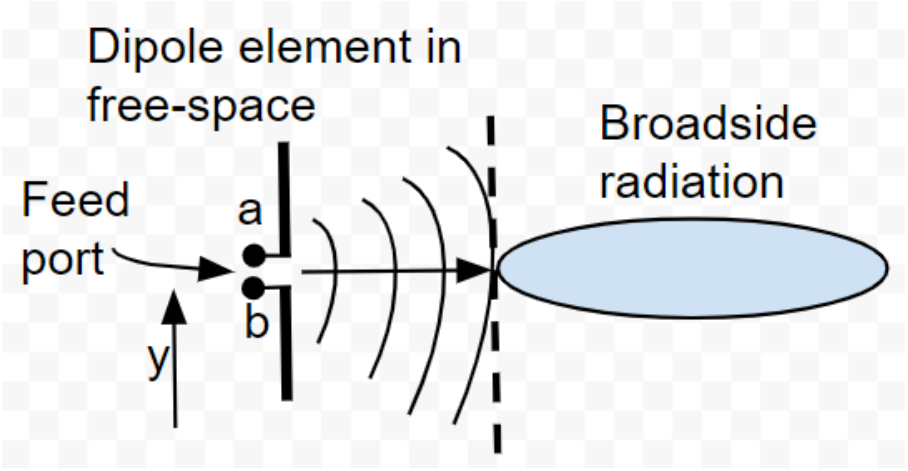

(b)

Figure 5.1. (a) A typical phased array antenna for beam-scanning, (b) A dipole antenna element along y-direction in free-space.

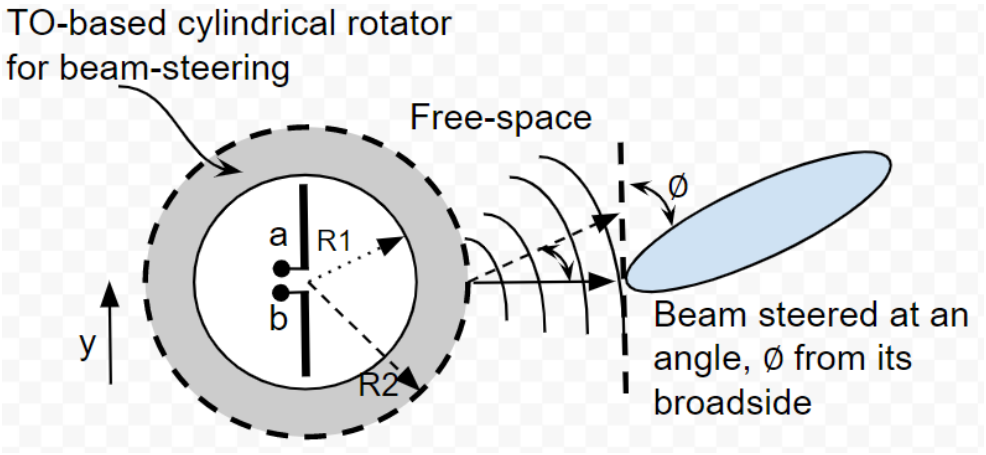

(a)

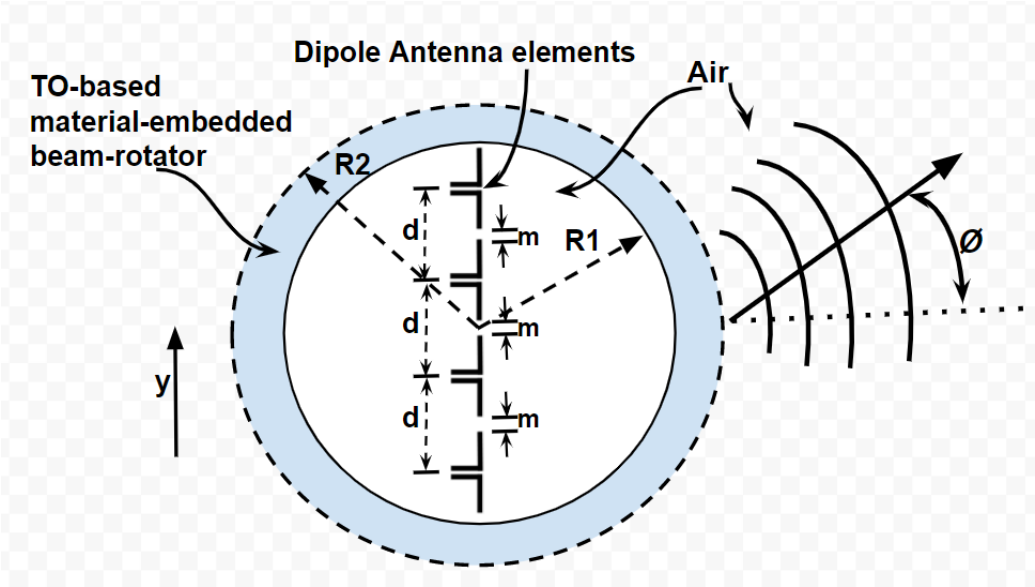

(b)

Figure 5.2. Metamaterial based cylindrical beam-steerer using TO (a) Proposed TO-based cylindrical beam-steerer enclosing a single dipole element, (b) Material-embedded cylindrical beam-steerer using TO enclosing a co-linear vertical dipole array.

Therefore, the objective of this chapter is to present a design and application of a TO-based cylindrical rotator for beam-steering, where a *single* dipole antenna element (as shown in Figure 5.2a) and an antenna *array* (as shown in Figure 5.2b) are enclosed by a TO-based non-homogeneous, anisotropic material shell designed using the transformation introduced in [76] (shown by the dotted ring in Figure 5.2). Through numerical simulations, beam- steering of the

TO-based single element and the antenna array is demonstrated without using any phase control circuitry. Then, the same TO-based cylindrical beam-rotator is applied to a vertical dipole antenna in free-space to design a horizontal dipole antenna. It is shown that the horizontal dipole element embedded in a metamaterial radiates in a similar manner as the vertical dipole element in free-space. Similarly, the TO-based cylindrical beam-rotator is also applied to a co-linear vertical array in free-space to design a horizontal co-linear array, where through numerical simulations it is shown that the material-embedded horizontal array radiates as the vertical array in free-space. Finite element method based full-wave simulations via COMSOL Multiphysics ® are used to numerically analyse and demonstrate the performance of the proposed TO-based beam-scanning technique. It should be noted that the theory being validated by COMSOL Multiphysics is similar to the approaches taken by previous works and reported in [55, 56], [64-66], and [76].

5.1. TO-Based Single Element Cylindrical Beam-Steerer

Next, consider the dipole element positioned in free-space along the y-axis represented in Figure 5.1b. The dipole is of λ length, where λ is the free-space wavelength at which the dipole antenna is designed to operate. The current distribution of the dipole in Figure 5.1b along $x = 0$ was chosen to be [55, 56]:

$$\bar{\boldsymbol{J}} = \begin{bmatrix} 0 \\ \frac{1}{\sqrt{\sigma * \pi}} . e^{-\frac{x^2}{\sigma}} \\ 0 \end{bmatrix}, \tag{5.1}$$

where σ is much smaller than the length of the dipole. The current distribution model is a way of handling sheet current as the limit of a volumetric current density which is suggested in [55, 56]. The σ parameter is set to be infinitesimally small relative to the length of the dipole and the limit $\sigma \to 0$ can be taken to approximate the current distribution on a thin wire at $x = 0$ [55, 56]. The intent is to introduce a TO- based material shell (again as illustrated as the grey ring in Figure 5.2a)

to control the radiation characteristics of the dipole element to steer its beam to a desired direction. Starting with the basic transformation media approach, the associated permittivity and permeability tensors of transformation media are given by table 2.1 and equations (2.8) and (2.9):

$$\boldsymbol{\varepsilon}' = \boldsymbol{\mu}' = \frac{A\varepsilon A^T}{det\, A}, \tag{5.2}$$

where $A = \partial(x', y', z')/\partial(x, y, z)$ is the Jacobian matrix and A^T is transpose of the Jacobian. The mapping between the original (r, θ, z) and the transformed (r', θ', z') cylindrical coordinate systems are [76]:

$$r' = r, \tag{5.3}$$

$$\theta' = \begin{cases} \theta + \beta, & r < R_1 \\ \theta + \frac{\beta(R_2 - r)}{R_2 - R_1}, & R_1 \le r < R_2, \\ \theta, & r \ge R_2 \end{cases} \tag{5.4}$$

$$z' = z, \tag{5.5}$$

where β is the angle of rotation in the region between radii R_1 and R_2 in Figure 5.2. By controlling the rotation angle β, it is possible to control the radiation characteristics, hence the amount of beam-steering in a desired direction using a single antenna element and the array without phase control circuitry and multiple antenna elements, as shown in Figure 5.2. The transformation equation (5.2) yields the permittivity and permeability tensors of the material between $r = R_1$ and $r = R_2$ as [76]:

$$\boldsymbol{\varepsilon}' = \boldsymbol{\mu}' = \begin{pmatrix} 1 + 2df + d^2 sin^2\theta & -d^2 f - dg & 0 \\ -d^2 f - dg & 1 - 2df + d^2 cos^2\theta & 0 \\ 0 & 0 & 1 \end{pmatrix}, \tag{5.6}$$

where $d = \frac{\beta * r}{R_2 - R_1}$, $f = cos\theta sin\theta$, $g = cos^2\theta - sin^2\theta$, and $\varepsilon' = \mu' = I$ in other regions in Figure 5.2. The derivation of the material parameters closely follows the methods outlined in chapter 4.

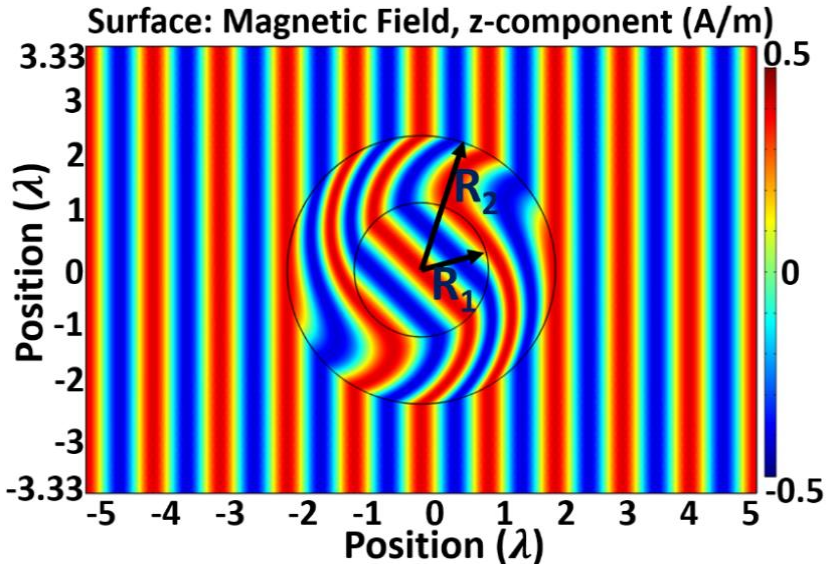

(a)

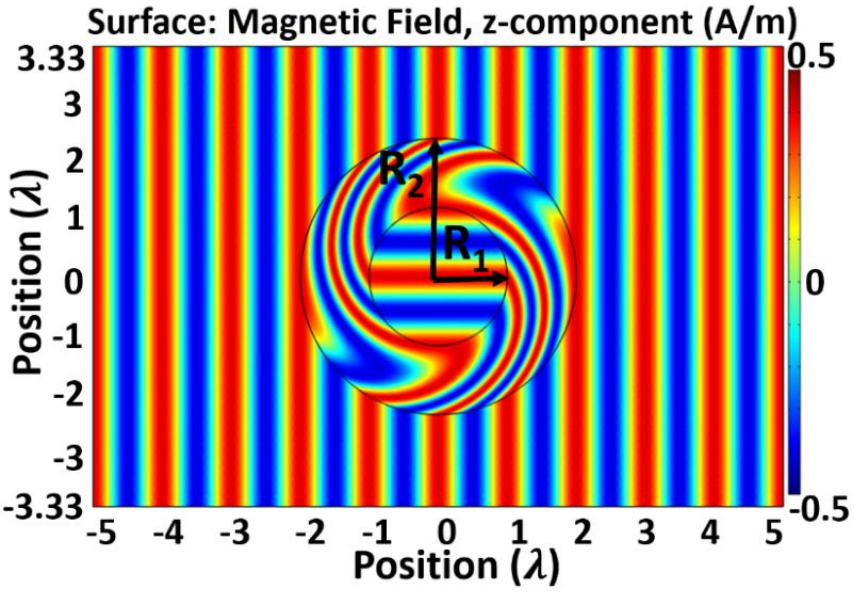

(b)

Figure 5.3. Verification of material parameters for TO-based cylindrical rotator showing perfect TEM wave with no scattering at the boundaries of material region and free-space (a) at rotation angle $\beta=45^0$, (b) at rotation angle $\beta=90^0$.

Equation (5.6) results in anisotropic and inhomogeneous permittivity and permeability tensors for the spherical shell. Note that the results lead to a perfect impedance matching with no reflection at the boundaries of the material region and free-space which is shown in Figure 5.3.

Such an anisotropic and inhomogeneous transformation medium can be realized by discrete metamaterials and structures such as periodic split ring resonators (SRRs) [67]. The theoretical material parameters in (5.6) were validated using full-wave simulations in the finite element solver COMSOL Multiphysics ®, as shown in Figure 5.3. An incident TE Plane wave of 10 GHz frequency was used from left to right along the x-direction. The inner radius $R_1 = 1.1\lambda$, and the outer radius $R_2 = 2\lambda$. The radii R_1 and R_2 of the metamaterial coating were chosen by closely following the similar works reported in [69] and [76]. As in this case, the dipole element was full-wave ($L = \lambda$), it was necessary to choose the inner radius R_1 of the metamaterial coating bigger than the length of dipole, so that it follows the transformation rule from (5.4). The metamaterial coating is located in the radiative near field region, as $0.62\sqrt{\frac{D^3}{\lambda}} < \text{metamaterial coating} < \frac{2D^2}{\lambda}$, where D= L= maximum linear dimension of the antenna, and λ = wave-length of the EM wave. The material parameters were calculated using (5.6) for different angle of rotations (β). Numerical simulations were also done to see the spatial variation of the constitutive material parameters, as shown in Figure 5.4 and it was observed that the material parameters were well within the range of material properties (permittivity and permeability) mentioned in [77 – 80]. The rotation angle β was chosen to be 45^0 for the simulations.

Next, a full-wave (λ) dipole antenna element was placed in the region $r < R_1$ and the material parameters from (5.6) were used to design the cylindrical beam-steerer in the region $R_1 \leq r < R_2$ to control the radiation characteristics of the dipole element in a desired direction, as shown in Figure 5.2a. The beam-steering angle ϕ of the dipole antenna element is controlled by the rotation angle β. Equations (5.4) and (5.6) show that it is possible to rotate the EM fields in an arbitrary direction, which makes the beam-rotator capable of steering the beam.

The objective of this research is to exploit the concepts of transformation electromagnetics/optics (TE/TO) for realizing a beam-steering technique using a rotation mapping introduced in [76]. For simplicity and ease of coordinate transformation, here no transformation was considered along z-direction. As a result a 2D transformation media was chosen which resulted in material parameters in (5.6). An experimental realization of the rotation coating requires building blocks that have anisotropic dielectric functions and the similar theory of this kind of rotation mapping could be extended to 3D instead of a 2D one. In that case, we will have permittivity and permeability tensors in (5.6) due to variations along z-direction.

The performance of the proposed single element TO-based beam-steerer, as shown in Figure 5.2a, was demonstrated through numerical solutions in the finite-element simulation software COMSOL Multi-physics ®. Figure 5.5 presents the y-component of the electric field of the proposed single element beam-rotator verifying the transformed media from (5.6). Figure 5.5a shows the simulation results from a full-wave ($L = \lambda$) dipole antenna in free-space along the y-direction (Figure 5.1b). This will be called the "vertical dipole". A frequency of 10 GHz was chosen. Now, to control the radiation characteristics of the dipole element in a desired direction, the transformation media from (5.6) was used as the beam-steerer around the dipole and the rotation angle β in (5.4) was controlled to steer the beam of the dipole antenna element in the desired direction.

A rotation angle $\beta = 22.5^0$ was chosen to rotate the fields pattern of the vertical dipole at an angle of 22.5^0, as a result the beam was steered at an angle $\phi = 22.5^0$, as shown in Figure 5.5b. Similarly, rotation angle $\beta = 45^0$ was chosen to steer the beam of the vertical dipole to an angle $\phi = 45^0$ (Figure 5.5c). Figure 5.5d shows electric field radiation of a full-wave ($L = \lambda$) dipole antenna in free-space along the x-direction. This is denoted as "horizontal dipole" antenna. The current

distribution from (5.1) was re-defined for the horizontal dipole as the location of the dipole changed to y = 0 from x = 0. Now, the TO-based beam-rotator was used and a rotation angle β = 90^0 was chosen to transform the horizontal dipole into the vertical dipole, as shown in Figure 5.5e. The fields from the vertical dipole in Figure 5.5a and the transformed horizontal dipole antenna in Figure 5.5e outside the material shell are the same. Figure 5.5f verifies that the difference between the two fields is negligible and there is almost no field distribution outside the transformation media.

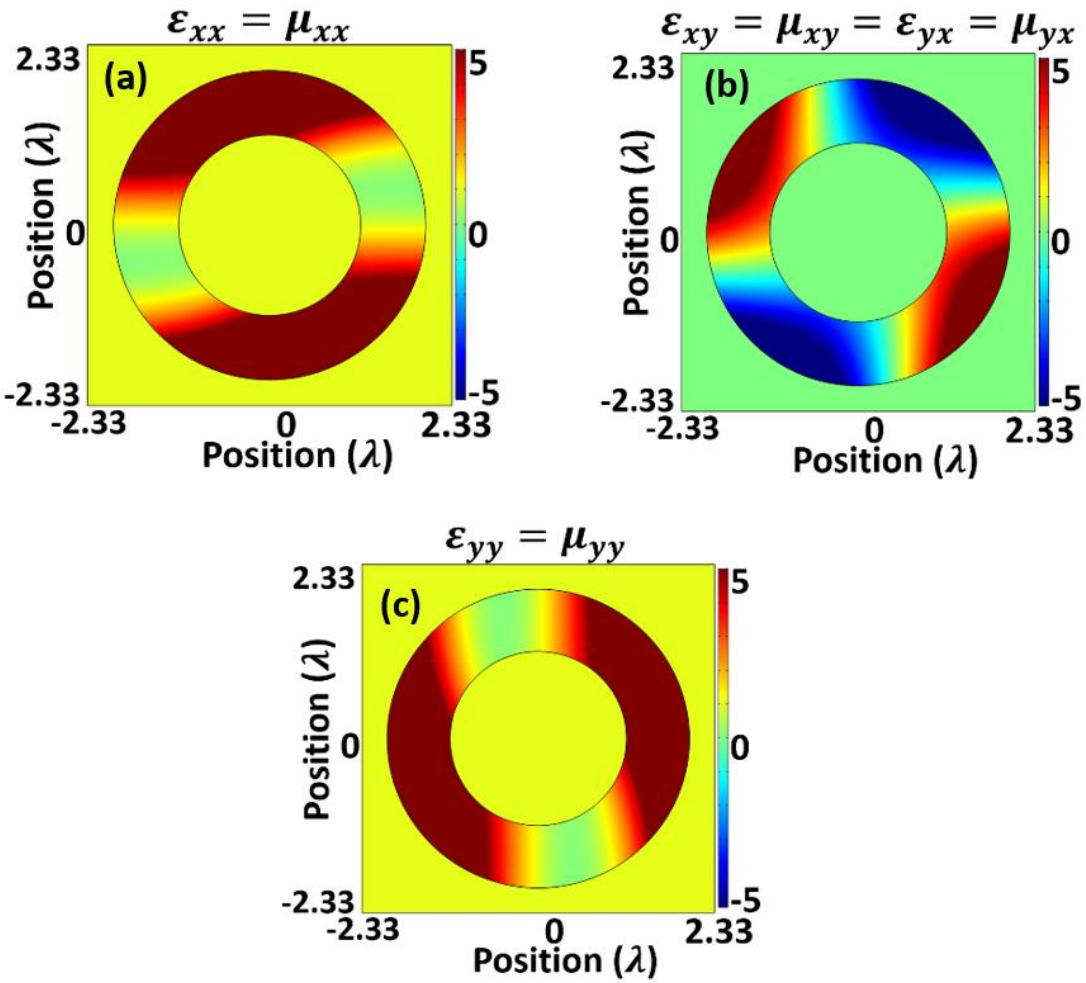

Figure 5.4. Spatial variation of material parameters inside the TO-based rotator shell. The dimensions of the rotator are given by $R_1 = 1.17\lambda$ and $R_2 = 2\lambda$. The material parameters ε_{xy}, μ_{xy}, ε_{yx}, and μ_{yx} are equal.

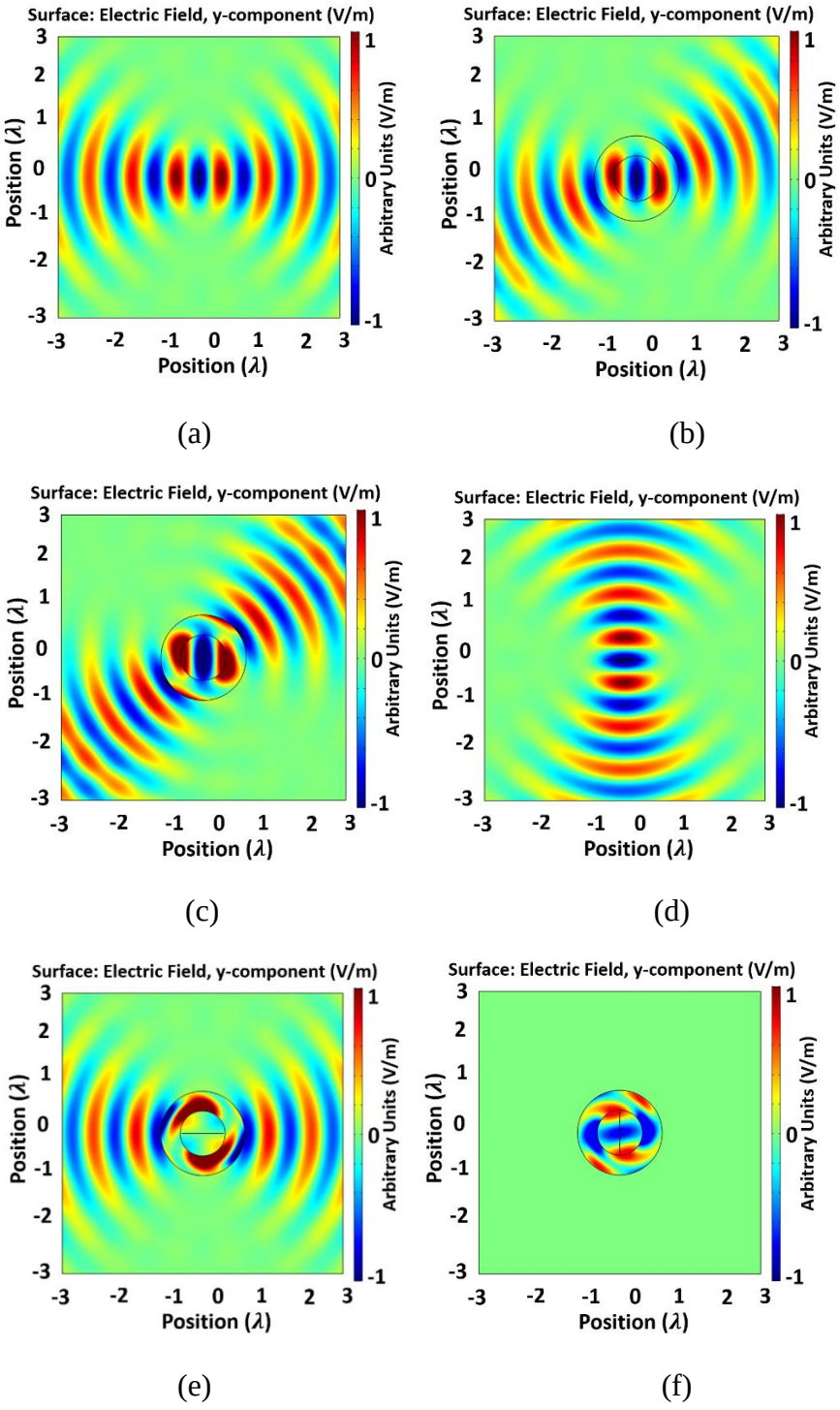

Figure 5.5. The y-component of the electric field of proposed TO-based single element beam-steerer (a) dipole antenna of length L = λ in free-space along y-direction (vertical); (b) the fields of vertical dipole that has undergone a rotation of $\beta = 22.5^0$; (c) the fields of vertical dipole that has undergone a rotation of $\beta = 45^0$; (d) dipole antenna of length L = λ in free-space along x-direction (horizontal); (e) the fields of horizontal dipole that has undergone a rotation of $\beta = 90^0$; (f) difference between the magnetic fields in (a) and (e).

Furthermore, the far-field radiation patterns of the TO-based beam-rotator using a single antenna element were simulated and are illustrated in Figure 5.6. As shown in Figure 5.6a, the transformation media from (5.6) was used to rotate the beam of the vertical dipole in free-space to an angle ϕ = 22.5^0 and ϕ = 45^0 by setting the rotation angle $\beta = 22.5^0$ and $\beta = 45^0$ in transformation media from (5.6), respectively. Moreover, Figure 5.6b shows that the radiation pattern of the vertical dipole in free-space is similar to the radiation pattern of the horizontal dipole, when the horizontal dipole is enclosed by the transformation media and is rotated by $\beta = 90^0$, but is different if the horizontal dipole is not enclosed by the transformed medium and is not rotated by an angle $\beta = 90^0$.

Moreover, considering that losses exist in practical materials, numerical simulations were performed incorporating different values of loss tangents ($\tan\delta$), as shown in Figure 5.7. Loss was incorporated in the simulations by replacing ε_{xx} with $(\varepsilon_{xx} - j|\varepsilon_{xx}|tan\ \delta)$ [65, 66]. Other tensor parameters were also modified similarly. A rotation angle $\beta = 22.5^0$ was chosen to steer the beam at 22.5^0. Figure 5.7 shows that while the antenna's radiated field strength degrades with the increase of loss factor, its overall steering capability remains unchanged. With the loss tangent reduced to only 0.1, the effect of loss is almost unnoticeable. No significant differences were observed in the range $\tan\delta \leq 0.01$.

5.2. Antenna Array Enclosed by TO-Based Cylindrical Beam-Steerer

The same TO technique from section 5.1 can be utilized to realize a cylindrical beam-rotator enclosing an antenna array with the TO-based non-homogeneous, anisotropic media. Next, consider the N-element co-linear dipole array along the y-axis represented in Figure 5.2b. Each of the elements in the array are equally spaced with the edge-to-edge distance between the elements of $m = \lambda/15$, where λ is the free-space wavelength at which the phased array is designed to

operate. A two-dimensional (2D) space is considered to illustrate the proposed array. The current distribution of each of the dipole elements in the array is approximated as the current distribution of a thin wire along $x = 0$ and is defined by equation (5.1). In this case, an array of 4 elements is chosen to validate the proposed beam scanning method. Each of the dipoles in the array is of $\lambda/2$ length spanning over a distance of 2.2λ. There was no phase difference considered between the adjacent dipole elements. Here, a TO-based material shell enclosing the dipole array to control the radiation characteristics of the array and steer its beam to a desired direction as shown in Figure 5.2b is introduced.

Next, the 4-element dipole antenna array was placed in the region $r < R_1$ and the material parameters from equation (5.6) were used to design the cylindrical beam-steerer in the region $R_1 \leq r < R_2$ enclosing the array to control the radiation characteristics of the antenna array in a desired direction, as shown in Figure 5.2b. The beam-scanning angle $\emptyset_s$ of the dipole antenna array will be controlled by the rotation angle β from (5.6). From equations (5.4) and (5.6), it is shown that it is possible to rotate the EM fields in an arbitrary direction, which makes the beam-rotator capable of steering the dipole antenna array pattern in a desired direction, thus enabling antenna array scanning.

The performance of the proposed phased array antenna enclosed by TO-based material-embedded cylindrical beam-steerer, as shown in Figure 5.2b, was demonstrated through numerical solutions in the commercially available finite-element simulation software COMSOL Multiphysics ®. Figure 5.8 presents the y-component of the electric field of the proposed beam-rotator for scanning of the phased array antenna verifying the transformed media from (5.6). Figure 5.8a demonstrates the simulation results from the dipole antenna array in free-space along the y-direction (as shown in Figure 5.2b). For reference, it will be called the "vertical array". A frequency

of 10 GHz was chosen. To control the radiation characteristics of the dipole antenna array in a desired direction, the transformation media from (5.6) was used as the beam-steerer around the array and the rotation angle β in (5.4) was controlled to steer the beam of the dipole antenna array in the desired direction.

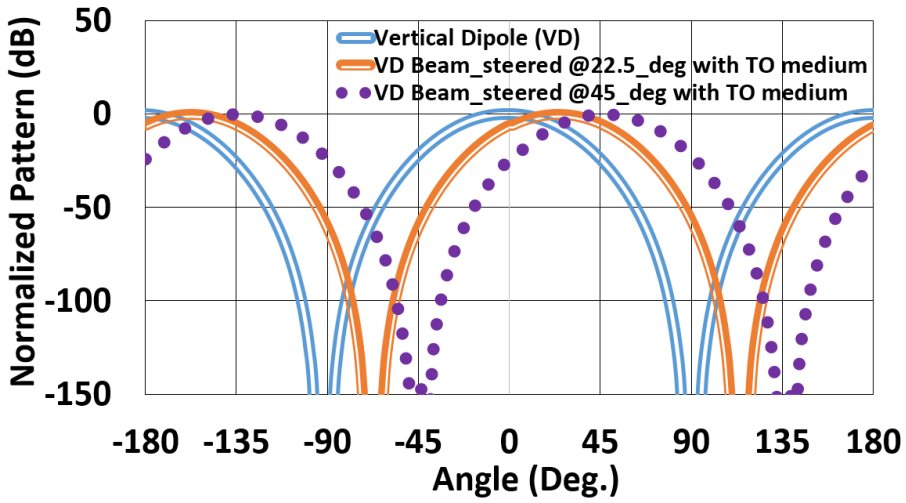

(a)

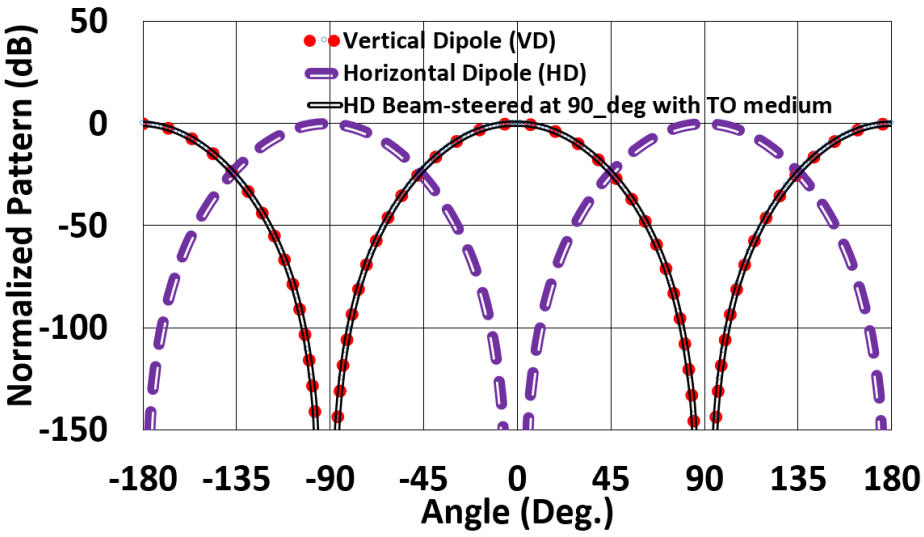

(b)

Figure 5.6. Far-field radiation pattern of proposed TO-based single element beam-steerer (a) beam-steering of the virtual dipole at $\phi = 22.5^0$ and $\phi = 45^0$; (b) beam-steering of the horizontal dipole at $\phi = 90^0$.

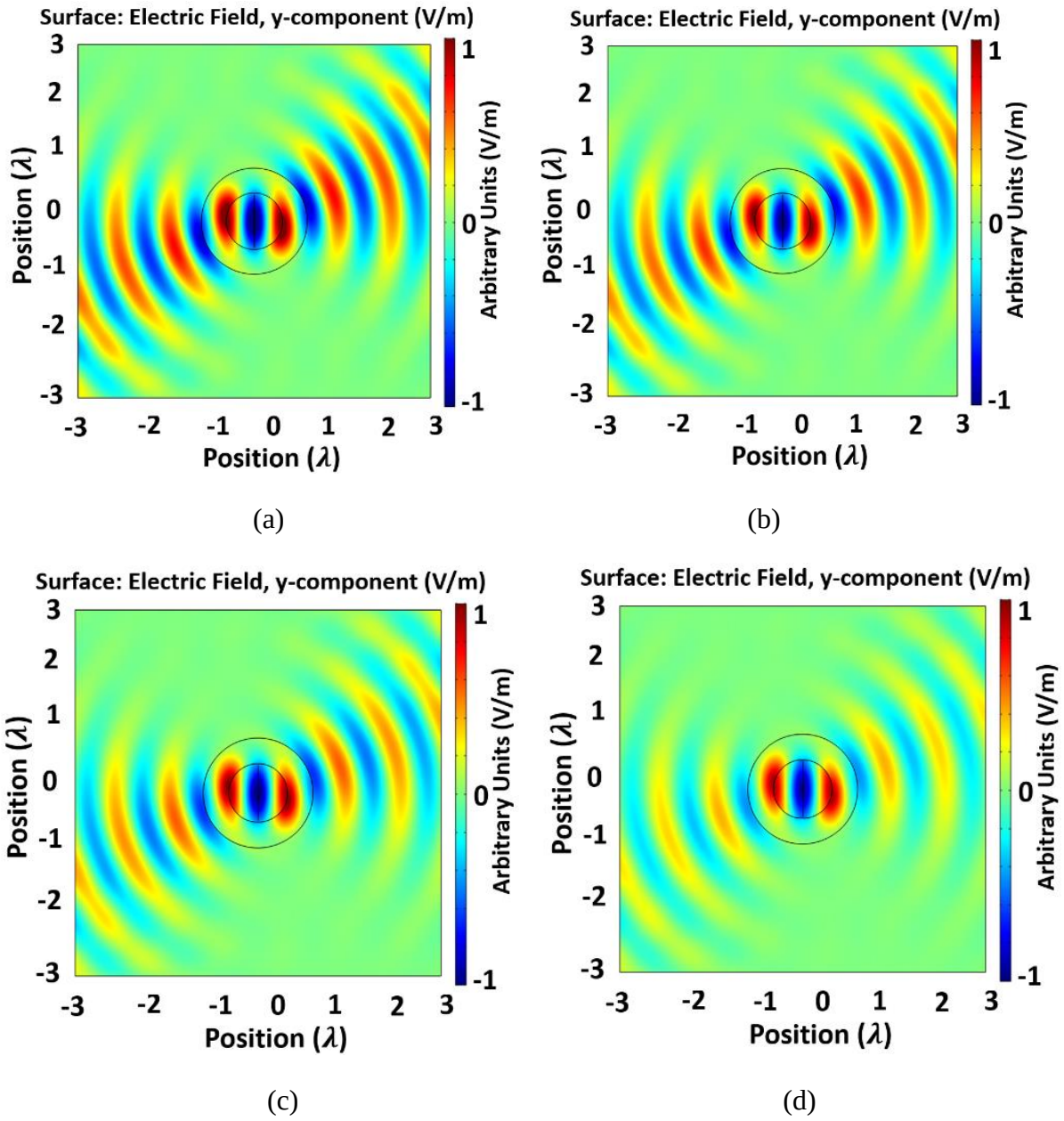

Figure 5.7. The electric fields for the proposed TO-based single element beam-steerer for different values of loss factor $(\tan\delta)$ (a) $\tan\delta = 0.0$; (b) $\tan\delta = 0.01$; (c) $\tan\delta = 0.1$; (d) $\tan\delta = 0.3$ (continued).

A rotation angle $\beta = 22.5^0$ was chosen to rotate the field patterns of the "vertical array" at an angle of 22.5^0, as a result a beam-scanning of the "vertical dipole array" occurred at an angle $\emptyset_s = 22.5^0$, as shown in Figure 5.8b. Similarly, rotation angle $\beta = 45^0$ was chosen to scan the "vertical dipole array" beam to an angle $\emptyset_s = 45^0$ (as demonstrated in Figure 5.8c).

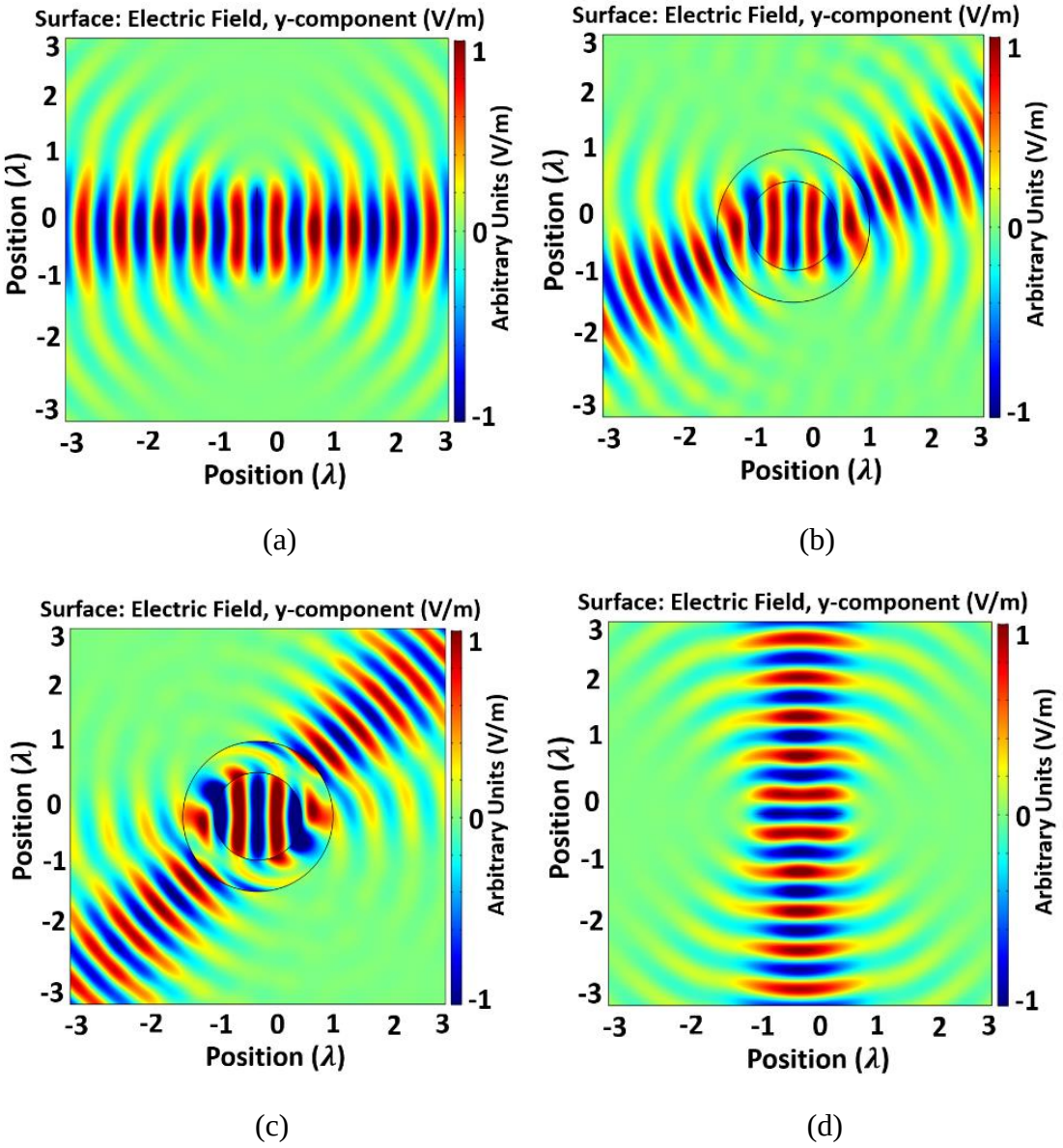

Figure 5.8. The electric fields of the proposed array antenna enclosed by TO-based material-embedded cylindrical beam-rotator for beam-scanning (a) dipole antenna array in free-space along y-direction (vertical array); (b) the fields of vertical dipole array enclosed by TO-based material shell and scanned at $\emptyset_s = 22.5^0$; (c) the fields of vertical dipole array enclosed by TO-based material shell and scanned at $\emptyset_s = 45^0$; (d) dipole antenna array in free-space along x-direction (horizontal array); (e) the fields of horizontal dipole array enclosed by TO-based material shell and that has undergone a rotation of $\emptyset_s = 90^0$; (f) difference between the electric fields in (a) and (e).

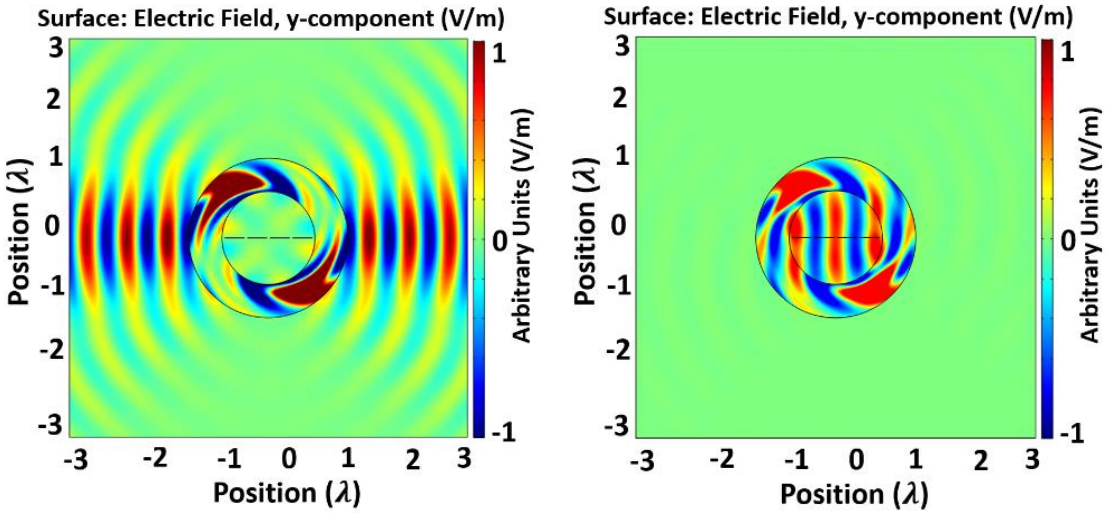

(e) (f)

Figure 5.8. The electric fields of the proposed array antenna enclosed by TO-based material-embedded cylindrical beam-rotator for beam-scanning (a) dipole antenna array in free-space along y-direction (vertical array); (b) the fields of vertical dipole array enclosed by TO-based material shell and scanned at $\emptyset_s = 22.5^0$; (c) the fields of vertical dipole array enclosed by TO-based material shell and scanned at $\emptyset_s = 45^0$; (d) dipole antenna array in free-space along x-direction (horizontal array); (e) the fields of horizontal dipole array enclosed by TO-based material shell and that has undergone a rotation of $\emptyset_s = 90^0$; (f) difference between the electric fields in (a) and (e) (continued).

Figure 5.8d presents the electric field radiation of a dipole antenna array in free-space along the x-direction. For reference, it is denoted as the "horizontal array". The current distribution from (5.1) was adjusted for each of the elements of the "horizontal array" as the location of each dipole element changed to $y = 0$ from $x = 0$. Now, the "horizontal array" was enclosed by the proposed TO-based beam-rotator and a rotation angle $\beta = 90^0$ was chosen to transform the "horizontal dipole array" into the "vertical dipole array", as shown in Figure 5.8e. The fields from the "vertical dipole array" in Figure 5.8a and the transformed "horizontal dipole array" in Figure 5.8e outside the material shell are the same. This is emphasized in Figure 5.8f, which shows almost no field distribution outside the transformation media when the difference between the two fields is taken, validating the results further.

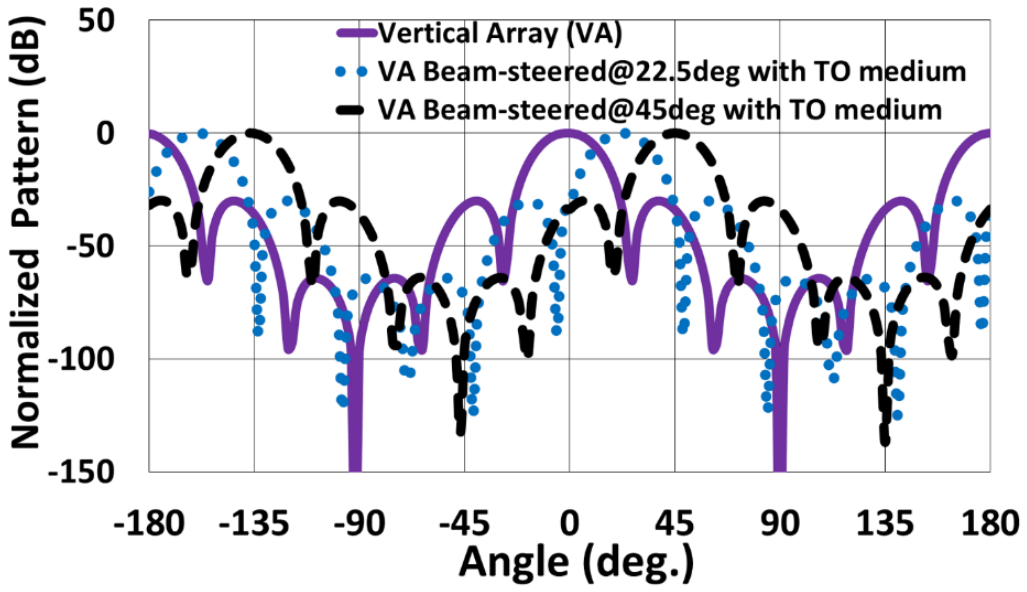

(a)

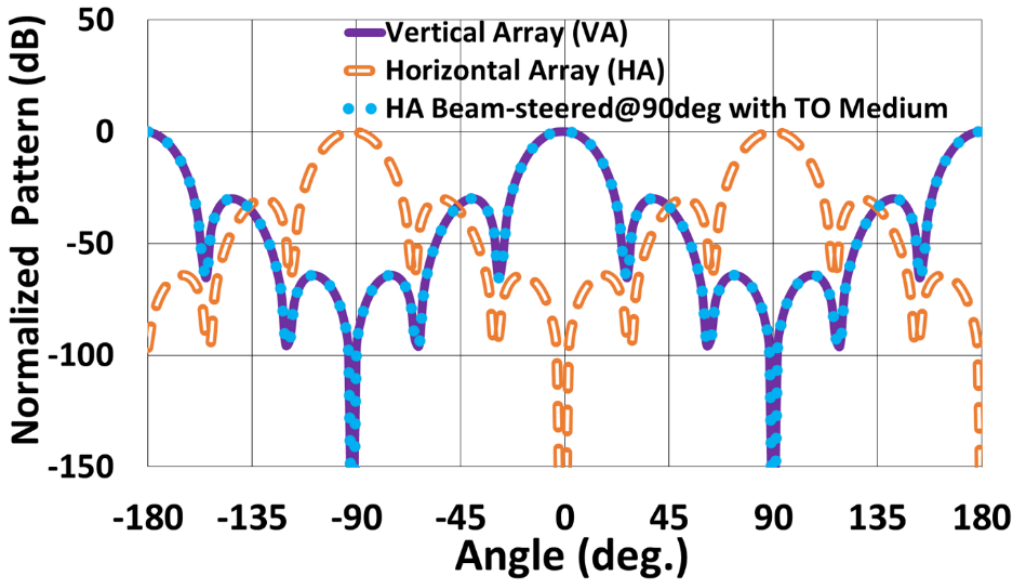

(b)

Figure 5.9. Far-field radiation pattern of proposed antenna array enclosed by TO-based material-embedded cylindrical beam-rotator (a) beam-scanning of the "virtual array" at $\emptyset_s = 22.5^0$ and $\emptyset_s = 45^0$; (b) beam-scanning of the "horizontal array" at $\emptyset_s = 90^0$.

Moreover, the far-field patterns of the proposed array enclosed by the TO-based material-embedded cylindrical beam-rotator were simulated and are illustrated in Figure 5.9. As shown in Figure 5.9a, the transformation media from (5.6) was used to rotate the beam of the "vertical array"

in free-space to an angle $\emptyset_s$= 22.5^0 and $\emptyset_s$= 45^0 by setting the rotation angle $\beta = 22.5^0$ and $\beta = 45^0$ in transformation media from (5.6), respectively.

Moreover, Figure 5.9b shows that the radiation pattern of the "vertical array" in free-space is similar to the radiation pattern of the "horizontal array", when the "horizontal array" is enclosed by the transformation media and is rotated by $\beta = 90^0$, but is different if the "horizontal array" is not enclosed by the transformed medium and is not rotated by an angle $\beta = 90^0$.

Furthermore, since practical metamaterial designs have losses, finite- element full-wave simulations were performed adding different values of loss tangent ($\tan\delta$). For a scan angle $\emptyset_s$ = 90^0, the normalized radiation patterns of the TO-based "horizontal array" for different values of loss tangent ($\tan\delta$) are compared in Figure 5.10. Loss was incorporated in the simulations by replacing ε_{xx} with ($\varepsilon_{xx} - j|\varepsilon_{xx}|tan\ \delta$) [65, 66]. Similar modifications were made in other tensor material parameters. As loss is increased, the antenna's radiated field strength degrades, but its overall steering capability remains unchanged, which is shown in Figure 5.10. With the loss tangent reduced to only 0.1, the effect of loss is almost insignificant. No noticeable differences were observed in the range $\tan\delta \leq 0.01$.

Dispersion exists in all materials and systems, natural or manufactured. There are many ways to implement the needed material properties needed given the frequency regime, application, environmental considerations etc. Dispersion along with other fundamental properties such as loss, noise etc. should be taken into consideration to meet a specific application or system requirement. This being said, several research works [81] - [83] have been performed to explore and analyze the limitations of specific implementations of TO devices due to dispersive materials. To this end, a TO-based beam-steering technique is proposed which results in an anisotropic, non-homogeneous material. Keeping the practical implementation of metamaterials and its dispersive

nature in mind, numerical simulations are presented in Figures 5.7 and 5.10 by incorporating losses to see how the losses in the material parameters in (5.6) affect the performances of the proposed beam-rotator. It is anticipated that the material parameters from (5.6) will demonstrate the dispersive nature while being practically implemented.

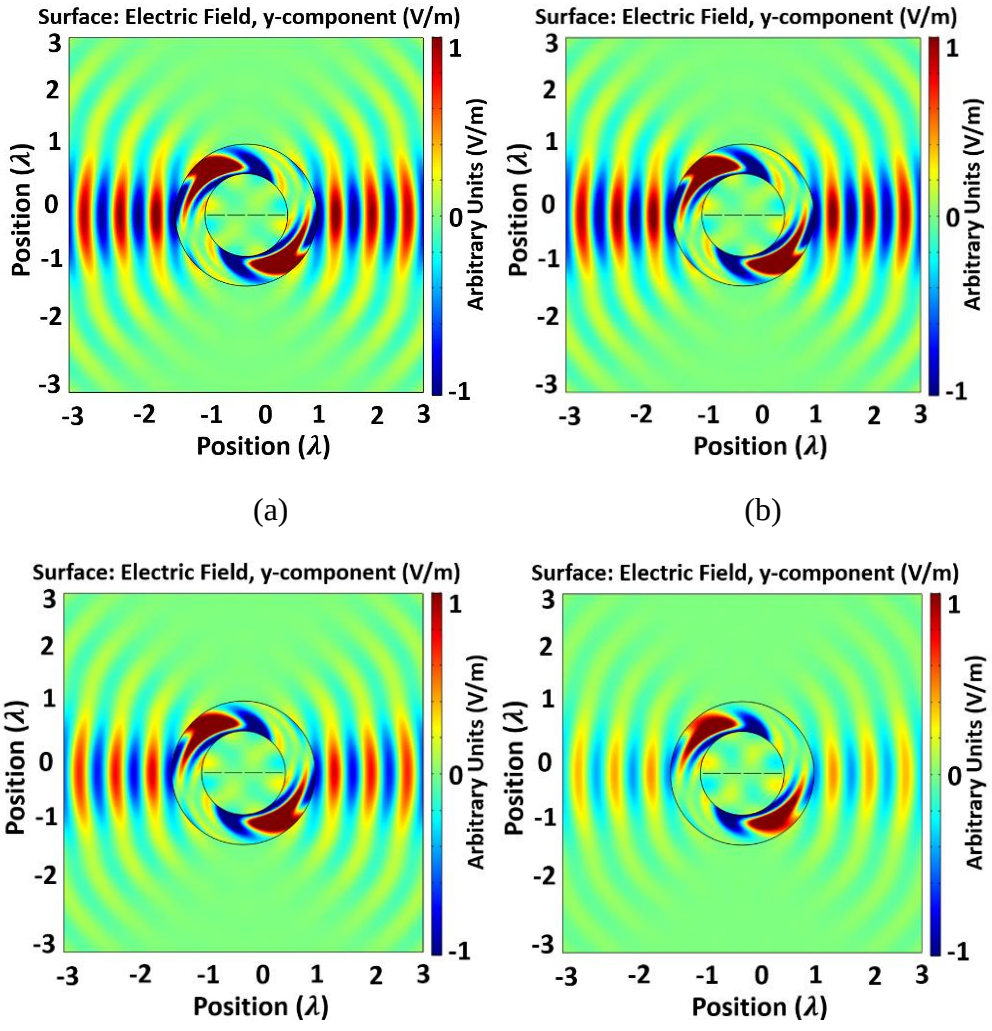

Figure 5.10. The electric fields for the proposed TO-based "horizontal array" for different values of loss factor ($\tan\delta$) (a) $\tan\delta = 0.0$; (b) $\tan\delta = 0.01$; (c) $\tan\delta = 0.1$; (d) $\tan\delta = 0.3$.

5.3. TO-Based Square Rotator

The coordinate transformation approach from [71] was later extended to design a TO-based square rotator to control the radiation characteristics of end-fire scanning arrays [64]. Based on similar motivation, here, the coordinate transformations based TO approach has been applied to a vertical dipole element in free space to design a material-embedded horizontal dipole antenna, as shown in Figure 5.11. Specifically, it is shown that a horizontal dipole element can be embedded inside a coordinate transformation-based thin rectangular material such that the horizontal dipole radiates the same as of a vertical dipole antenna in free-space. Next, consider the vertical dipole antenna positioned in free- space along the y-direction, as shown in Figure 5.11. The dipole is of λ length, where λ is the free-space wavelength at which the dipole antenna is designed to operate. The current distribution of the dipole is approximated as the current distribution of a thin wire along the *z* – axis ($x = 0$) and is defined by taking the limit of a volume current to arrive at a sheet current density [55]. The intent is to design a horizontal antenna embedded inside a square rotator. The rotator region was bounded by two squares with the inner and outer sides equal to *2c* and *2d*, respectively, where $c = 1.3\lambda$ and $d = 1.8\lambda$. An appropriate coordinate transformation needs to be defined. Two separate mappings can be defined for this purpose and the transformation regions can be divided into two regions, as denoted as T_1 and T_2 (separated by dotted lines as shown in Figure 5.11). Transformation for the region T_1 is defined as [69]:

$$x' = -y + \frac{2d}{d-c}(x - c), \tag{5.7}$$

$$y' = x, \tag{5.8}$$

and

$$z' = z. \tag{5.9}$$

The following transformation is employed for region T_2 [69]:

$$x' = x, \tag{5.10}$$

$$y' = y - \frac{2c}{d-c}(x - d), \tag{5.11}$$

and

$$z' = z. \tag{5.12}$$

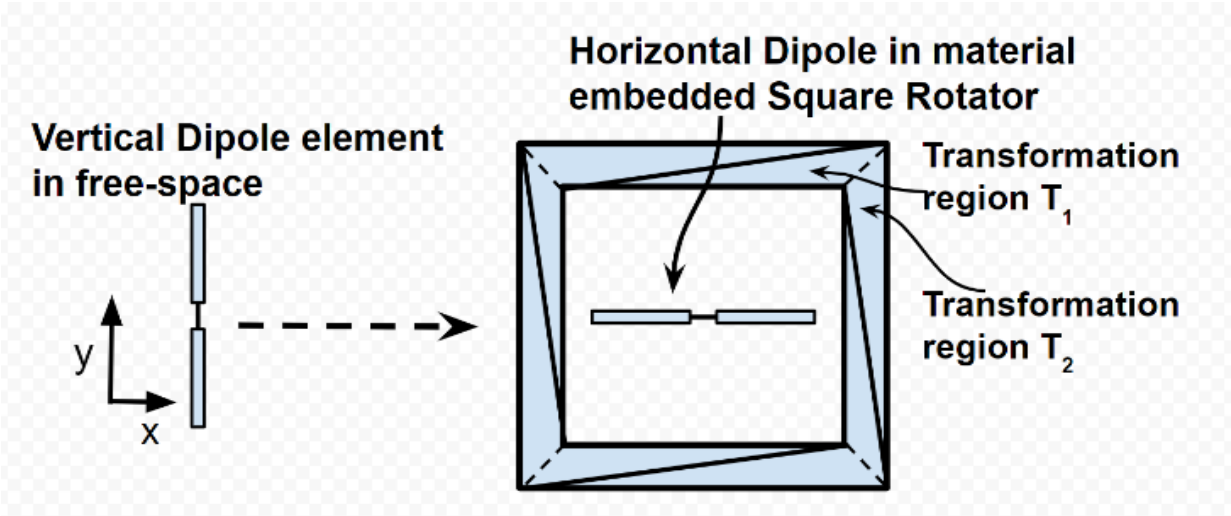

Figure 5.11. A TO-based thin rectangular material-embedded horizontal dipole antenna radiating like a vertical dipole antenna in free-space.

Using the above transformations and (2.8) and (2.9) the permittivity and permeability tensors of the material can be computed as [69]. For brevity, it is not shown here. After the transformation, the region inside the inner boundary of the rotator is simply the original region rotated by 90^0. The current distribution from (5.1) was re-defined for the horizontal dipole as the location of the dipole changed to $y = 0$ from $x = 0$.

The performance of the proposed horizontal dipole antenna embedded inside a TO-based square rotator medium was demonstrated through numerical simulations in COMSOL Multiphysics ®. Figure 5.12 represents the y-component of the electric field of the proposed TO-based material embedded horizontal dipole verifying the transformations. Figure 5.12(a) demonstrates the simulation results from a full-wave ($L = \lambda$) dipole antenna in free-space along

the y-direction (as shown in Figure 5.11). For the reference, it will be called the “vertical dipole”. A frequency of 10 GHz was chosen. Figure 5.12(b) demonstrates the simulation results from a full-wave ($L = \lambda$) dipole antenna in free-space along the x-direction. For the reference, it will be called the “horizontal dipole”. The electric field radiation of the “horizontal dipole” is shown in Figure 5.12(c), when it is embedded inside the TO-based square rotator medium. The fields from the “vertical dipole” in Figure 5.12(a) and the material-embedded “horizontal dipole” in Figure 5.12(c) outside the material shell are the same, which is shown in Figure 5.12(d) for validation, where it represents the difference between the two fields and shows that there is almost no field distribution outside the transformation media. Furthermore, the far-field radiations of the proposed TO-based material-embedded horizontal dipole were simulated and illustrated in Figure 5.13, which shows that the material-embedded horizontal dipole element radiates as same as the “vertical dipole” element in free-space, which further validates the proposed technique.

Here, it has been shown how transformation optics can be utilized to steer a beam in an arbitrary direction from a single antenna element and an antenna array without using phase control circuitry and beam-forming networks. The proposed beam-steerer is a TO-based non-homogeneous, anisotropic material shell theoretically computed using coordinate transformations. The transformed parameters are derived, and through full-wave simulations, the beam-steering performances of the TO-based beam-steerer are demonstrated. Additionally, the TO-based beam-rotator is applied to the vertical dipole antenna in free-space to design a horizontal dipole antenna, and through numerical simulations it is shown that the material-embedded horizontal dipole element radiates as a vertical dipole element in free-space, verifying the design. Similarly, the TO-based beam-rotator is applied to a vertical dipole array to design a TO-based material-embedded horizontal dipole array, which behaves like a vertical dipole array in free-space. While currently,

we present numerical verification, in practice, this TO approach requires actively tuned material parameters. To this end, significant advancements have been made to realize actively tunable constitutive material parameters, which could enable practical implementation of this TO-based beam-steering technique.

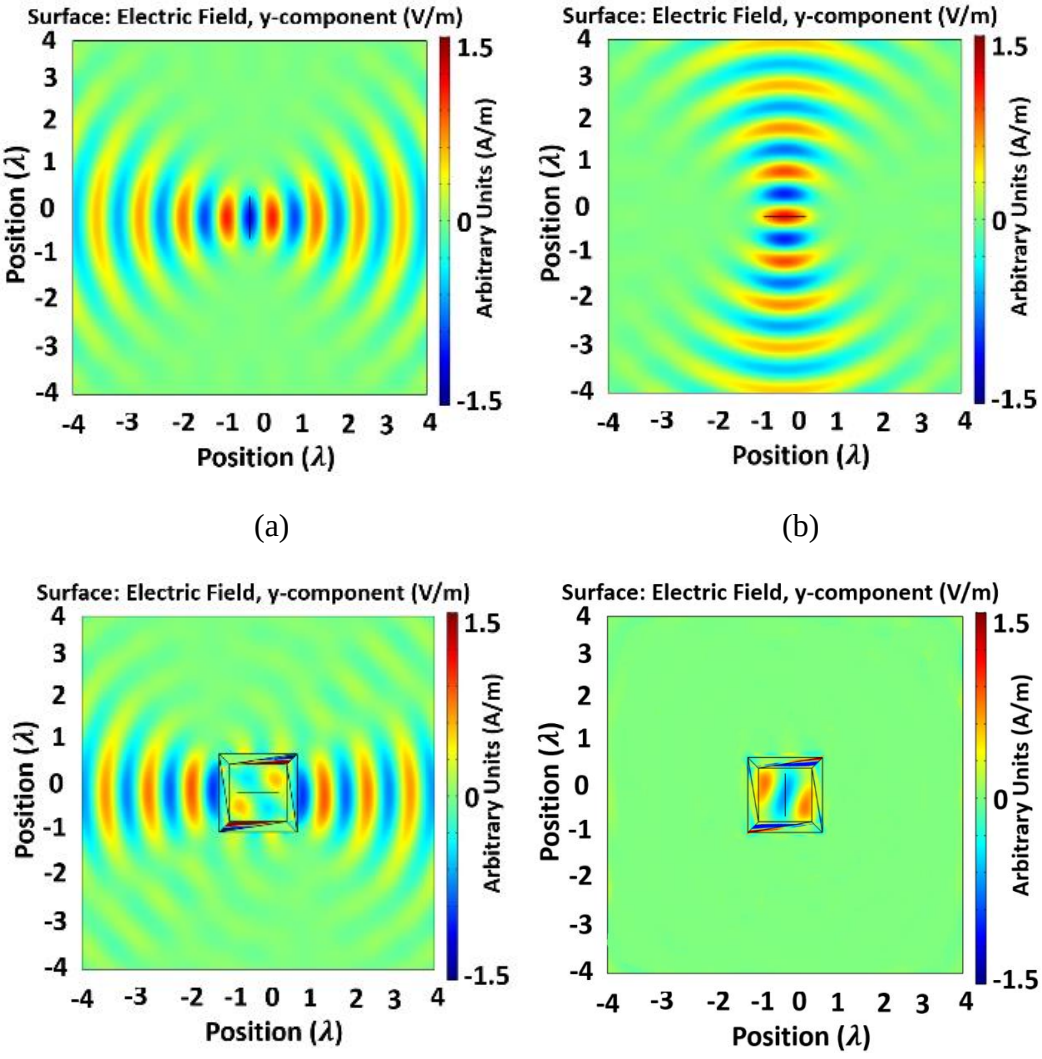

Figure 5.12. The y-component of the electric field of the dipole antenna element from: (a) vertical dipole antenna of length L = λ in free-space, (b) horizontal dipole antenna of length L = λ in free-space (c) the horizontal dipole embedded inside the TO-based square rotator medium, and (d) the difference between the fields (a) and (c).

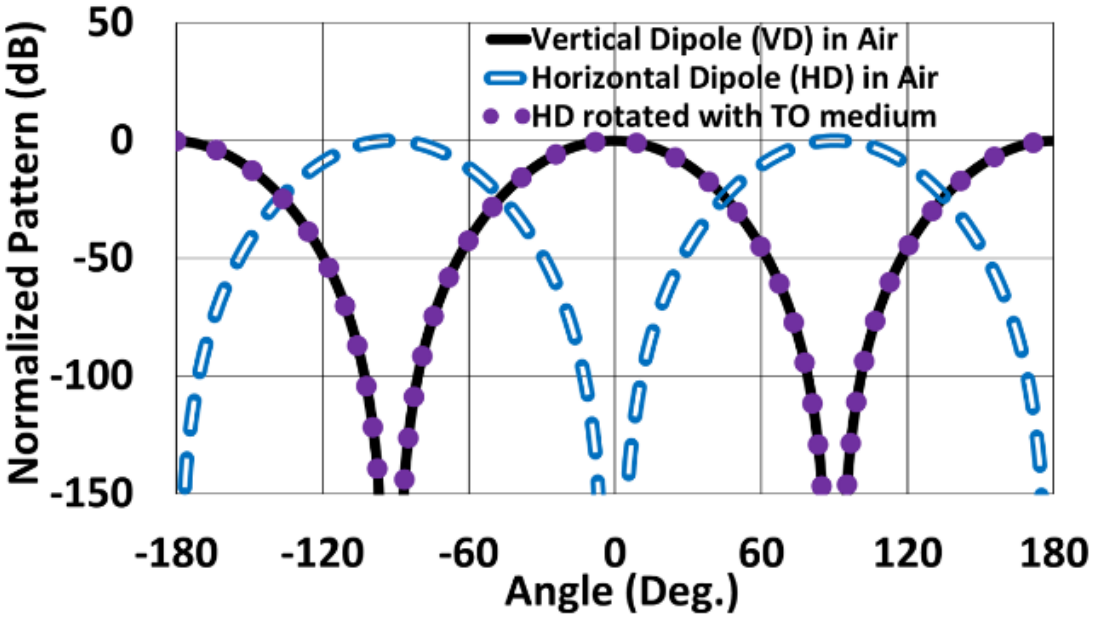

Figure 5.13. Far-field radiation patterns of the three different dipole antenna configurations.

6. SUMMARY AND CONCLUSION

Complex artificial or engineered materials, namely, metamaterials strongly interact with light and can be utilized to manufacture electromagnetic structures which imitate material response that is not found in nature. Recently, a coordinate transformation based approach, known as transformation electromagnetics/optics (TE/TO) gained much popularity among the scientific community, which results in complex, non-homogeneous, and anisotropic constitutive material parameters using an appropriate coordinate transformation to design unique and seemingly-impossible electromagnetic devices. This research focused on the theoretical and mathematical background of the transformation electromagnetics/optics (TE/TO) technique and demonstrated some examples of how to use the TE/TO technique to design unique and unconventional electromagnetic devices through full-wave finite element simulations in an instructive manner.

Based on the understanding of TE/TO concepts, a phased array antenna was proposed using the electromagnetic source transformation, where an appropriate coordinate transformation was used to transform a linear dipole antenna array into a linear complex-geometry antenna array without perturbing its electromagnetic radiation behavior. The complex-geometry antenna array was a “pinwheel” shaped antenna transformed from dipole antenna element. The transformed constitutive material parameters and the current distribution for the “pinwheel” shaped antenna elements were derived and validated through full-wave numerical simulations in COMSOL Multiphysics. It is believed that the proposed array will have tremendous potential for future applications in structurally integrated and conformal phased arrays for wireless communications, radars, and sensing where structural and mechanical constrains do not align with antenna performance.

Moreover, the techniques of TE/TO were adopted to design a beam-steerer to steer or scan a beam at an arbitrary direction from a single antenna element and an array without using phase control circuitry. The proposed beam-steerer is a TO-based non-homogeneous, anisotropic material shell theoretically computed using coordinate transformations. Through full-wave simulations in COMSOL Multiphysics the beam-scanning performances of the TO-based beam-rotator was demonstrated and validated. Additionally, it was shown that a material-embedded horizontal dipole element behaves as a vertical dipole element in free-space using the same coordinate transformations-based beam-rotator. Similar approach was also applied to a vertical dipole array, and through full-wave simulations it was shown that a material-embedded horizontal dipole array radiates as a vertical dipole array in free-space, verifying the effectiveness and correctness of the proposed design.

Overall, transformation of passive space led to the development of unique electromagnetic devices using the TE/TO concepts. The concepts of TE/TO have been extended to regions containing sources and that will open the door to several unique applications of electromagnetic waves, known as source transformations. Here, the concepts of source transformations have been explored to array antennas with new elements where antenna performance is a function of structural and mechanical constraints, a TO-based beam-steerer which enables beam-scanning with a single antenna element and an antenna array without using phase control circuits. Using this approach the radiating element surrounded by a transformation media can be optimized to achieve the desired performance of the overall system. Since practical metamaterial designs have losses, and while currently, numerical verification is presented, in practice, this TO-approach will require actively tunable material parameters. To this end, significant advancements have been made by material scientists to design tunable materials using different approaches, which could enable the

implementation of the TO-based antenna designs. Future designs could incorporate a cylindrical geometry which can be fabricated with available methods, starting with simulation and optimization of the individual components, then fabrication of radiating elements surrounded by TE/TO-based transformation media, and finally measurement of the device and overall system performances. The overall contributions from this dissertation are reported in [74], [84], [85], and [86].

REFERENCES

1. J. C. Maxwell, *A treatise on electricity and* magnetism Vol I, Oxford: Clarendon Press, 1873.

2. J. C. Maxwell, *A treatise on electricity and magnetism* Vol II, Oxford: Clarendon Press, 1873.

3. A. A. Huurdeman, *The Worldwide History of Telecommunications*, Wiley, 2003.

4. V. Mukherji, Jagadish C. Bose, second edition, Builders of Modern India series, Publications Division, Ministry of Information and Broadcasting, Government of India, 1994.

5. C. W. Bernard, *Tesla: Inventor of the Electrical Age*, Princeton University Press, 2013.

6. S. Hong, *Wireless: From Marconi's Black-Box to the Audio*, Cambridge, Mass.: MIT Press, 2001.

7. Customising and optimising antannas with materials science and manufacturing techniques, [Online] Available: www.avnet.com.

8. N. Kundtz, "Advances in Complex Artificial Electromagnetic Media," Duke University, PhD Dissertation 2009.

9. V. Browning and S. Wolf. (2001) DARPA. [Online]. www.darpa.mil.

10. V.G. Veselago, "The electrodynamics of substances with simultaneously negative values of ε and μ," Soviet Physics Uspekhi, 10(4):509, 1968.

11. D. R. Smith, W. J. Padilla, D. C. Vier, S. C. Nesat-Nasser, and S. Schultz, "Composite medium with simultaneously negative permeability and permittivity," *Phys. Rev. Lett*., 84(18): 4184-4187, May 2000.

12. R. A. Shelby, D. R. Smith, and S. Schultz, "Experimental Verification of a Negative Index of Refraction," *Science*, 292 (5514): 77-79, 2001.

13. J. B. Pendry, D. Schurig, and D. R. Smith, "Controlling Electromagnetic Fields," *Science*, 312, June 2006, pp. 1780-1782.

14. U. Leonhardt, "Optical Conformal Mapping," *Science*, 312, June 2006, pp. 1777-1780.

15. U. Leonhardt and T. G. Philbin, "General Relativity in Electrical Engineering," *New Journal of Physics*, 8, October 2006, pp. 247/1-18.

16. E. J. Post, *Formal Structure of Electromagnetics*. Dover Publications, Inc., New York, 1962.

17. J. Plebanski, “Electromagnetic waves in gravitational fields”, *Phys. Rev.*, 118:1396-1408, 1960.

18. A. J. Ward and J. B. Pendry, “Refraction and geometry in Maxwell’s equations,” *Journal of Modern Optics*, vol. 43, pp. 773-793, 1996.

19. D. Schurig, J. J. Mock, B. J. Justice, S. A. Cummer, J. B. Pendry, A. F. Starr, and D. R. Smith, “Metamaterial electromagnetic cloak at microwave frequencies,” *Science*, 314: 997-980, 2006.

20. Cai, W., Chettiar, U., Kildishev, A. *et al.*, “Optical cloaking with metamaterials”, *Nature Photon* 1, 224–227 (2007).

21. D. P. Gaillot, C. Croënne, and D. Lippens, "An all-dielectric route for terahertz cloaking," *Opt. Express* 16, 3986-3992 (2008).

22. Y. Lai, H. Chen, Z.-Q. Zhang, and C. T. Chan, “Complementary media invisibility cloak that cloaks objects at a distance outside the cloaking shell,” *Phys. Rev. Lett.*, vol. 102, pp. 093 901/1-4, 2009.

23. C. Li and F. Li, "Two-dimensional electromagnetic cloaks with arbitrary geometries," *Opt. Express* 16, 13414-13420 (2008).

24. Y. Lai, J. Ng, H. Chen, D. Han, J. Xiao, Z.-Q. Zhang, and C. T. Chan, “Illusion optics: the optical transformation of an object into another object,” *Phys. Rev. Lett.*, vol. 102, pp. 253 902/1–4, 2009.

25. H. Chen, X. Luo, H. Ma, *et al*., “The anti-cloak”, *Opt. Express* 2008, vol. 16, no. 19, pp. 14 603–14 608.

26. T. Yang, H. Chen, X. Luo, *et al*., “Superscatterer: enhancement of scattering with complementary media”, *Optical Express* 2008, vol. 16, no.22, pp. 18545-18550.

27. J. Ng, H. Chen, and C. T. Chan, “Metamaterial frequency-selective superabsorber,” *Opt. Lett*., vol. 34, no. 5, pp. 644–646, Mar. 2009.

28. M. Rahm, S.A. Cummer, D. Schurig, *et al*., “Optical design of reflectionless complex media by finite embedded coordinate transformations”, *Phys. Rev. Lett.* 2008, vol. 100, 063903.

29. M. Rahm, D. A. Roberts, J. B. Pendry, and D. R. Smith, “Transformation-optical design of adaptive beam bends and beam expanders,” *Opt. Express*, vol. 16, no. 15, pp. 11 555–11 567, Jul. 2008.

30. B. Donderici and F. L. Teixeira, "Metamaterial Blueprints for Reflectionless Waveguide Bends," in *IEEE Microwave and Wireless Components Letters*, vol. 18, no. 4, pp. 233-235, April 2008.

31. X. Zhang, H. Chen, X. Luo, and H. Ma, "Transformation media that turn a narrow slit into a large window," Opt. Express 16, 11764-11768 (2008).

32. D. H. Kwon and D. H. Werner, "Polarization splitter and polarization rotator designs based on transformation optics," *Opt. Express* 16, 18731-18738 (2008).

33. D.H. Kwon, D.H. Werner, "Transformation optical designs for wave collimators, flat lenses and right-angle bends", *New J. Phys*. 2008, 10, 115023.

34. Y. Luo, J. Zhang, L. Ran, H. Chen, J.A. Kong, "New Concept Conformal Antennas Utilizing Metamaterial and Transformation Optics", *IEEE Antennas Wirel. Propag. Lett*. 2008, 7, 509–512.

35. D. Mitra, P. Roy, D. Dawn, "A variable gain CMOS phase shifter for phased array antenna applications", *Microw. Opt. Technol. Lett.*, 2016, vol. 59, no. 2, 324-328.

36. J.R. Sanford, "Design of a Miniature Reactive Beam Forming Network", *IEEE Intl. Symps. on Ant. Propag. and USNC-USRI Rad. Sci. Meeting*, 2019, Atlanta, GA, pp. 1357-1358.

37. S. Prasad, "Generalized array pattern synthesis by the method of alternating orthogonal projections," in *IEEE Transactions on Antennas and Propagation*, vol. 28, no. 3, pp. 328-332, May 1980.

38. C. A. Olen and R. T. Compton, in Antennas and Propagation Society International Symposium, 1990. AP-S. Merging Technologies for the 90's. Digest (1990), Vol. 2, pp. 828–831.

39. K. K. Yan and Y. Lu, "Sidelobe reduction in array-pattern synthesis using genetic algorithm," in *IEEE Transactions on Antennas and Propagation*, vol. 45, no. 7, pp. 1117-1122, July 1997.

40. D. W. Boeringer and D. H. Werner, "Particle swarm optimization versus genetic algorithms for phased array synthesis," in *IEEE Transactions on Antennas and Propagation*, vol. 52, no. 3, pp. 771-779, March 2004.

41. D. Schurig, J. B. Pendry, and D. R. Smith, "Calculation of Material Properties and Ray Tracing in Transformation Media," *Optics Express*, 14, 21, September 2006, pp. 9794-9804.

42. D. Kwon and D. H. Werner, "Transformation Electromagnetics: An Overview of the Theory and Applications," in *IEEE Antennas and Propagation Magazine*, vol. 52, no. 1, pp. 24-46, Feb. 2010.

43. G. V. Eleftheriades and M. Selvanayagam, "Transforming Electromagnetics Using Metamaterials," in *IEEE Microwave Magazine*, vol. 13, no. 2, pp. 26-38, March-April 2012.

44. Z. Ahsan, *Tensor Analysis with Applications*, Anamaya Publishers, New Delhi, India 2008.

45. P. B. Laval, “The Jacobian: Change of Variables in Multiple Integrals,” Kennesaw State University (KSU), notes for the course Math 2203 at KSU.

46. S. G. Johnson, “Coordinate Transformation and Invariance in Electromagnetism,” Massachusetts Institute of Technology, notes for the course 18.369 at MIT 2010.

47. J. W. Allen, “Application of Metamaterials to the Optimization of Smart Antenna Systems,” Duke University, PhD Dissertation 2011.

48. N. B. Kundtz, D. R. Smith and J. B. Pendry, "Electromagnetic Design With Transformation Optics," in *Proceedings of the IEEE*, vol. 99, no. 10, pp. 1622-1633, Oct. 2011.

49. D. A. Roberts, N. Kundtz, and D. R. Smith, “Optical Lens compression via transformation optics. *Opt Express*, 17(19):16535-16542, 2009.

50. COMSOL Multiphysics Inc., [Online] Available: www.comsol.com.

51. M. Y. Wang, J. J. Zhang, H. Chen, Y. Luo, S. Xi, L.-X. Ran, and J. A. Kong, "Design and Application of a Beam Shifter by Transformation Media," *Progress In Electromagnetics Research*, Vol. 83, 147-155, 2008.

52. E. Heyman and L. B. Felsen, "Gaussian beam and pulsed-beam dynamics: complex-source and complex-spectrum formulations within and beyond paraxial asymptotics," *J. Opt. Soc. Am. A* 18, 1588-1611 (2001).

53. A. Chabory, J. Sokoloff, and S. Bolioli, "Novel Gabor-Based Gaussian Beam Expansion for Curved Aperture Radiation in Dimension Two," *Progress In Electromagnetics Research*, Vol. 58, 171-185, 2006.

54. S. A. Cummer, B. I. Popa, D. Schurig, D. R. Smith, and J. Pendry. Full-wave simulations of electromagnetic cloaking structures. *Physical Review E (Statistical, Nonlinear, and Soft Matter Physics)*, 74(3):036621, 2006.

55. N. Kundtz, D. A. Roberts, J. Allen, S. Cummer, and D. R. Smith, "Optical source transformations," *Optics Express*, vol. 16, no. 26, pp. 21215-21222, December 2008.

56. J. Allen, N. Kundtz, D. A. Roberts, S. A. Cummer, and D.R. Smith, “Electromagnetic source transformations using superellipse equations,” *Applied Physics Letters*, 94(19):194101, 2009.

57. W. X. Jiang *et al*, “Arbitrarily elliptical-cylindrical invisible cloaking,” *J. Phys. D: Appl. Phys.* 41 085504, 2008.

58. D. H. Kwon and D. H. Werner, “Two-dimensional eccentric elliptic electromagnetic cloak,” *Appl. Phys. Lett*. 92, 013505, 2008.

59. T. L. Marzetta and B. M. Hochwald, "Capacity of a mobile multiple-antenna communication link in Rayleigh flat fading," in *IEEE Transactions on Information Theory*, vol. 45, no. 1, pp. 139-157, Jan. 1999.

60. P. E. Law, Jr., *Shipboard Antennas*, 2nd ed., vol. 2. Artech House, Norwood, 1986.

61. P. -. Kildal, A. A. Kishk and A. Tengs, "Reduction of forward scattering from cylindrical objects using hard surfaces," in *IEEE Transactions on Antennas and Propagation*, vol. 44, no. 11, pp. 1509-1520, Nov. 1996.

62. D. F. Kelley and W. L. Stutzman, "Array antenna pattern modeling methods that include mutual coupling effects," in *IEEE Transactions on Antennas and Propagation*, vol. 41, no. 12, pp. 1625-1632, Dec. 1993.

63. D.H. Kwon and D. H. Werner, "Restoration of antenna parameters in scattering environments using electromagnetic cloaking", *Appl. Phys. Lett.*, 92, 113507 (2008).

64. B.I. Popa, J. Allen, S.A. Cummer, "Conformal Array Design with Transformation Electromagnetics", *Appl. Phys. Lett.* 2009, 94, 244102.

65. D.H. Kwon, "Virtual Circular Array using Material-Embedded Linear Source Distributions", *Appl. Phys. Lett.* 2009, 95, 173503.

66. L. Deng, Y. Wu, W. Hong, J. Zhu, B. Peng, S. Li, "Conformal Array Design on Arbitrary Polygon Surface with Transformation Optics", *AIP Adv*. 2016, 6, 065011.

67. J.B. Pendry, A.J. Holden, D.J. Robbins, W.J. Stewart, "Magnetism from conductors and enhanced nonlinear phenomena", *IEEE Trans. Micro. Theory Tech*, 1999, 47, 2075–2084.

68. J.W. Allen, H. Steyskal, D.R. Smith, "Impedance and complex power of radiating elements under electromagnetic source transformation", *Microw. Opt. Technol. Lett.* 2011, 53, 1524–1527.

69. D.H. Kwon, C.D. Emiroglu, "Low-profile embedded design of endfire scanning arrays with coordinate transformations", *J. Appl. Phys.* 2010, 107, 034508.

70. J. Yi, P. Tichit, S.N. Burokur, *et al*., "Illusion optics: Optically transforming the nature and the location of electromagnetic emissions", *J. Appl. Phys.* 2015, 117, 084903.

71. P. Tichit, S.N. Burokur, A.D. Lustrac, "Ultradirective antenna via transformation optics", *J. Appl. Phys.* 2009, 105, 104912.

72. P. Tichit, S.N. Burokur, A.D. Lustrac, "Transformation media producing quasi-perfect isotropic emission", *Opt. Exp.* 2011, vol. 19, 20551-20556.

73. P. Tichit, S.N. Burokur, J. Yi, *et al.*, "Transformation Electromagnetics for Antennas with an Illusion on the Radiation Pattern", *IEEE Ant. and Wirel. Propag. Lett.*, 2014, vol. 13, pp. 1796-1799.

74. D. Mitra, J. Cleveland, J. Lewis, *et al*., "On the use of Multiple Beam-Shifters Developed using Transformation Electromagnetics to Control Propagation Characteristics", *IEEE Res. and Appl. of Phot. in Defense Conference (RAPID)*, Miramar Beach, FL, USA, 2020, pp. 1-2.

75. J. Yi, S.N. Burokur, A.D. Lustrac, "Experimental validation of a transformation optics based lens for beam steering", *Appl. Phys. Lett*., 2015, 107, 154101.

76. H. Chen, C.T. Chan, "Transformation media that rotate electromagnetic fields", *Appl. Phys. Lett.*, 2007, 90, 241105.

77. S. Misra, M. Kalaswad, D. Zhang, *et al*., "Dynamic tuning of dielectric permittivity in BaTiO3 via electrical biasing", *Mat. Res. Lett*., 2020, 8:9, 321-327.

78. R. Stangenberg, C. Grigoriadis, H. Butt, *et al*., "Switchable permittivity with temperature and DC-bias in a semifluorinated azobenzene derivative", *Collo. Poly. Sci*., 2014, 292, 1939-1948.

79. T.S. Kasirga, Y.N. Ertas, M. Bayindir, "Microfluidics for reconfigurable electromagnetic metamaterials", *Appl. Phys. Lett*., 2009, vol. 95, no.21, 214102.

80. G. Agarwal, A. Ulpenich, X. Zhu, *et al*., "Microgel-Based Adaptive Hybrid Capsules with Tunable Shell Permeability", *Chem. Mater*., 2014, 26, 5882-5891.

81. P. Yao, Z. Liang, X. Jiang, "Limitation of the electromagnetic cloak with dispersive material", *Appl. Phys. Lett.*, 2008, 92, 031111.

82. H. Hashemi, C.-W. Qiu, A.P. McCauley, J.D. Joannopoulos, S.G. Johnson, "Diameter-bandwidth product limitation of isolatedobject cloaking", *Phys. Rev. A*, 2012, 86, 013804.

83. M. Cassier, G.W. Milton, "Bounds on Herglotz functions and fundamental limits of broadband passive quasi-static cloaking", *J. Math. Phys.* arXiv: 1610.08592, 2017, 58, 071504.

84. D. Mitra, S. Dev, J. Lewis, J. Cleveland, M. Allen, J. Allen and B. D. Braaten, "A Phased Array Antenna with New Elements Designed Using Source Transformations," *Applied Sciences: Special Issue on Antennas and Wireless Propagation Implementing Metamaterial Structures*, vol. 11, no. 7, article 3162, Apr. 2021.

85. D. Mitra, S. Dev, M. Allen, J. Allen and B. D. Braaten, "Coordinate Transformation-based Antenna Elements Embedded in a Metamaterial with Scanning Capabilities," *Electronics: Special issue on Metamaterials and Metasurfaces*, vol. 10, no. 9, article 1081, May 2021.

86. D. Mitra, B. D. Braaten, J. Allen and M. Allen, "On the Rotation of the Field from a Dipole using Transformation Electromagnetics," accepted for presentation in the 2021 *IEEE Research and Applications of Photonics in Defense Conference (RAPID)*, Aug. 2-4, 2021, Marimar Beach, FL, USA.